Analysis of the Dynamic Behaviour of the Hangingwall Beam during a Seismic Event

by

A Daehnke
BSc Eng (Mech)

A thesis submitted in partial fulfilment of the requirements for the degree of Master of Science in Engineering.

Centre for Research into Computational and Applied Mechanics

University of Cape Town

September 1992

ABSTRACT

In a deep-level gold mine planes of weakness oriented parallel to the reef allow the hangingwall to separate from adjacent rock strata. The hangingwall then acts as a separate beam supporting only its selfweight. Mining-induced near vertical shear fractures divide the hangingwall beam into distinct blocks of relatively intact material. The objective of this study is to investigate the response of the isolated hangingwall beam during a seismic event. The study is particularly concerned with the global, resonant behaviour of the hangingwall and local shear or crushing failure of the rock at the shear fractures is not considered.

A finite element program is developed to compute the hangingwall response during seismicity. The response is normalised, thus permitting the response spectrum method to describe maximum hangingwall motions during a seismic event at various beam lengths. By comparing the response spectrum describing a single-degree-of-freedom (SDOF) system with the spectrum of the hangingwall, it is evident that, although the hangingwall response spectrum is shifted to a higher frequency and velocity domain, the shapes of the two spectra are essentially the same. The frequency and velocity shift is calculated for 15 seismic events and empirical rules are developed to quantify the spectral shift for a wide range of event magnitudes.

Unlike the spectrum describing hangingwall motions, the construction of a SDOF response spectrum is computationally cheap and is standard practice in earthquake engineering. By applying the empirical rules the seismologist can extrapolate the SDOF spectrum to estimate maximum hangingwall motions due to a seismic event and critical beam lengths which are prone to resonance.

The effect on the response of the hangingwall supported by backfill consisting of dewatered and cemented tailings is evaluated. It is shown that a fill-to-face lag of less than $5m$ reduces hangingwall motions considerably. Further, at small strains the stiffer cemented tailings provide superior support than that offered by comparatively soft dewatered tailings.

A chart is presented which correlates event magnitudes to critical beam lengths prone to resonance.

DEDICATION

To Leo and Borca for their love and support.

ACKNOWLEDGMENTS

I wish to express my appreciation to the following people and organizations:

- My supervisor, Professor JB Martin for his guidance.
- To Dr NC Gay and Ms D Hemp for detailed documentation of seven seismic events.
- The Chamber of Mines Research Organization for the motivation for the study and financial assistance.
- The Foundation for Research and Development for their financial assistance.

DECLARATION

This is to certify that the results, calculations and other work presented in this thesis are essentially my own work, and that no part of it has been submitted for a degree at any other university.

Signed by candidate

A Daehnke
September 1992

Contents

List of Figures

Chapter 1

Introduction

Among the many problems associated with deep-level mining, rockbursts are the most serious cause of loss of life as well as production. The rockburst problem in South African gold mines has become progressively more severe as the average depth of mines has increased beyond two kilometres below the surface. In a study conducted by Heunis [1] the percentage of fatal accidents due to rockbursts in a typical deep-level mine was 46% of the total fatalities. Yet for five shallow to medium depth mines the percentage of rockburst related fatalities was only 15%. It is therefore clear that as the depth of mines increases in the future, rockbursts will contribute increasingly to the major cause of fatal accidents in mines.

A rockburst, as defined by Wagner [2], is a seismic event that results in damage to mining excavation, destruction of mining equipment, and injury to and loss of life of mining personnel.

Seismic activity originates as stress concentrations induced by mining excavations. As the stresses exceed the strength of the rock seismic pulses are emitted. In most cases seismicity is associated with shear displacements on fractures or geological weaknesses (Roberts *et al.* [3]).

The gold reef in South African gold mines occurs in strong quartzite rock as flat tabular deposits. Parallel to the reef are thin planes of weakness, generally referred to as parting planes. The weak parting planes allow the stope hangingwall to separate from adjacent layers, essentially forming a beam supporting only its selfweight. Near vertical shear fractures are the most important mining-induced fractures, since these, together with the parting planes, divide the hangingwall beam into distinct blocks.

The objective of this study is to investigate the stability of the isolated hangingwall beam segmented into blocks by vertical shear fractures. In particular, an understanding

of the *global* response of the hangingwall beam during seismicity is sought. An attempt is made to correlate the ground motion parameters of a seismic event to the amplified motions of a resonating hangingwall beam. The investigation concentrates on the global motion of the hangingwall beam, and does not consider localised crushing or shearing failure of rock. Such failure, which might result in individual hangingwall blocks falling into the stope, needs to be controlled by local support and is not modelled in this study.

The report is structured as follows. Chapter 2 reviews the stope geometry and fracture patterns in the stope vicinity induced by the mining excavation. Numerical modelling techniques using the finite element suite ABAQUS and program BLKBEAM developed by the author are presented in Chapter 3. A brief account of seismicity in mines is given in Chapter 4, whilst Chapter 5 considers the response of the hangingwall beam subjected to seismic events. Chapter 6 illustrates a technique to predict the hangingwall response given the ground motion histories of a mine tremor. In Chapter 7 the effect of stope support is briefly addressed and finally design recommendations and conclusions are drawn in Chapter 8.

Chapter 2

Review of the Stope Geometry

Gold mining in South Africa takes place at depths of up to $3500m$ below the surface where the gravitational stress can exceed $100MPa$ (Snyman and Martin [4]). The gold bearing reef is excavated in narrow tabular stopes approximately $1m$ high. The removal of this highly stressed rock causes complicated fracture patterns in the rock mass surrounding the stope. The sedimentary gold reefs are often surrounded by thin planes of weakness, known as parting planes, which are oriented parallel to the reef plane.

A study of the fracture pattern and the parting planes which occur in the stope vicinity is important to provide an insight into the hangingwall structure. This chapter discusses the pattern of fracturing, highlights features of the hangingwall, and reviews past work pertaining to the hangingwall beam.

2.1 Pattern of Fracturing

A fracture pattern believed to be representative of most stopes has been presented by Brummer [5] and is illustrated in Figure 2.1. The features shown in Figure 2.1 can be classified according to the following categories:

1. Primary or shear fractures.
2. Secondary or extension fractures.
3. Parting planes.

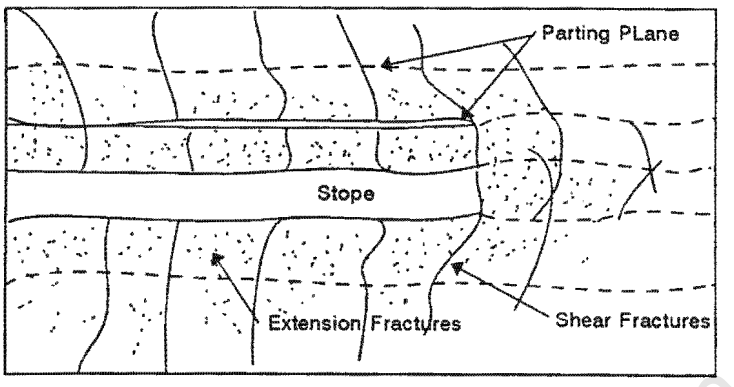

Figure 2.1: Fracture pattern in the stope vicinity of a deep mine.

2.1.1 Shear fractures

Shear fractures are associated with highly stressed rock, and thus are only found in deep-level mines. The fractures initiate $6m$ to $8m$ ahead of the advancing stope face and separate the rock into blocks of relatively intact material. They are oriented approximately parallel to the stope face and are regularly spaced at about $1m$. Shear fractures usually occur in conjugate pairs in the hangingwall and footwall.

2.1.2 Extension fractures

Extension fractures initiate slightly ahead of the stope face and are smaller than shear fractures. They form after the shear fractures have propagated and are truncated by the parting planes. Extension fractures are spaced at intervals of between $5mm$ and $30mm$.

2.1.3 Parting planes

Parting planes are thin planes of weakness observed parallel to the reef plane. The fairly smooth and flat planes consist of shaley material, which provides little cohesion and low frictional resistance between the rock strata. These properties allow layers of rock above the stope to separate from adjacent layers. Each layer then acts as a separate beam supporting only its selfweight. Parting planes in South African deep-level gold mines are generally spaced at approximately $1m$ intervals.

2.2 The Hangingwall Beam

The rock stratum immediately above the stope is of particular importance, since it is from this region that most rock falls occur. This layer can be considered to behave like a two dimensional plane strain beam, and is referred to as the *hangingwall beam.*

Various authors have investigated the stability of the hangingwall by isolating the hangingwall beam from surrounding rock. In most studies it is assumed that, since mining progresses through near vertical shear fractures which form ahead of the face, the beam is made up of rectangular blocks. Thus, to remain structurally intact, the hangingwall beam may not support tensile stresses.

Evans [6] has attributed the stability of the hangingwall beam to a voussoir arch mechanism. His work included experiments on voussoir beams in which he supported up to 50 building bricks placed face to face.

The voussoir arch model analysed by Brady *et al.* [7] is based on the work by Evans and is illustrated in Figure 2.2. The section of the beam transmitting the lateral compressive force is approximated by the parabolic arch traced on the beam span.

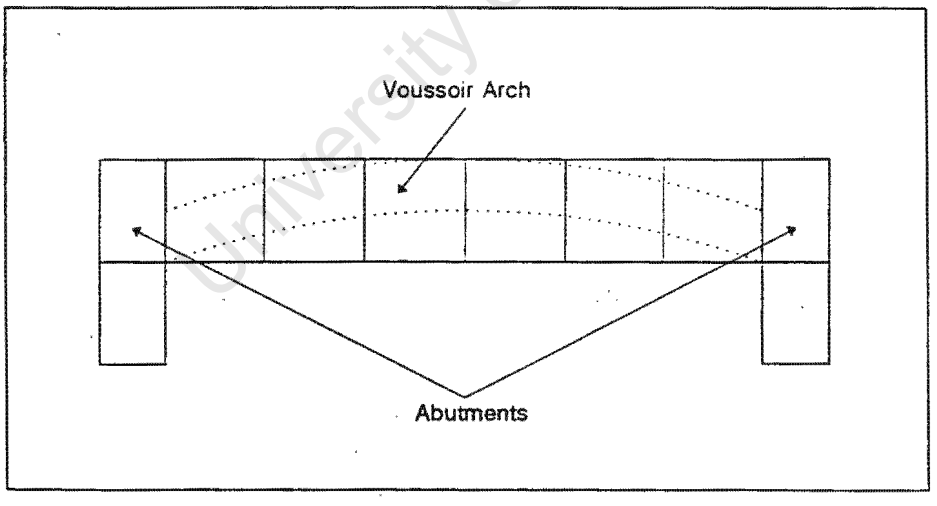

Figure 2.2: Voussoir beam model as analysed by Brady.

Brady *et al.* proposed the following three possible failure modes for the voussoir beam geometry indicated in Figure 2.2.

1. Shear at the abutment when the shear resistance is less than the required abutment vertical resistance.

2. Crushing of the rock at the hinges active in the top centre section of the beam and the lower abutment contact.

3. Buckling of the roof beam which leads to the beam becoming a 'snap-through' mechanism.

De Villiers [8] used the finite element method to model the hangingwall beam made up of rectangular blocks which were allowed to separate, but relative sliding was prevented. This work showed that the hangingwall beam behaviour consists of two regimes. Firstly, a shallow voussoir arching mechanism develops through the depth and spanning across the length of the beam. The beam is relatively stable, but will eventually become unstable and snap through when the vertical displacement at the centre of the beam reaches a distance which is of the same order of magnitude as the depth of the beam. For a $1m$ deep beam this occurs at a halfspan of about $30m$. Secondly, once the hangingwall and footwall beams come into contact, a stable steady state regime can be established, with the contact point following the advance of the face.

Sepher and Strimpson [9] used a non-linear finite element model to determine the maximum deflection of vertical jointed beams. The mechanism of stability was determined to be the formation of a voussoir arch. The compressive zone induced by the voussoir arch was concluded to play a major role in the overall stability of beam roofs over underground openings.

In a study by Pender [10] the significance of prefailure joint dilatancy was investigated by means of an analysis of a single span beam. The beam was modelled as a number of discrete blocks separated by vertical joints. The joints, which had dilatant shear behaviour, generated an axial thrust which suppressed the tensile forces due to bending effects.

Joughin [11] considered the dynamic response of the hangingwall beam to a seismic input. His work concentrated on the interaction between the hangingwall beam and the overlying rock mass. Joughin did not consider the effect of the vertical shear fractures and modelled the hangingwall beam as a continuous, elastic beam.

Hall *et al.* [12] and Fenves *et al.* [13] used the finite element method to determine the response of jointed arches excited by earthquakes. They used a jointed arch model to analyse the stability of concrete arch dams during seismicity. Arch dams are often built with vertical contraction joints which cannot transmit tensile stresses. Therefore, as is the case with the fractured hangingwall beam, a linear elastic analysis does not correctly represent loading conditions in segmented dam arches.

The work by Brady and the authors mentioned above leads to the formulation of the following broad principles regarding hangingwall beam behaviour.

1. The hangingwall cannot be modelled by continuous, elastic beams or plates, since the behaviour is dominated by the blocks generated by mining-induced near vertical shear fractures.

2. The hangingwall beam stability is determined by the axial thrust generated by the deflection, under gravity loading, of the voussoir beam against the confinement of the abutments.

3. For a voussoir beam with a low span to thickness ratio, the most likely failure mode is shear failure at the abutments.

4. For a hangingwall beam with high span to thickness ratio, the beam stability is limited by the possibility of buckling or 'snap-through' of the beam.

5. A hangingwall with low rock strength may fail by crushing at the hinges of the central or abutment blocks.

Crushing of rock at beam hinges and the shear failure mode can be considered as local failure. However, this investigation seeks an understanding of the global hangingwall response. Thus the hangingwall beam model in this study only represents the buckling or 'snap-through' failure mode.

As parting planes are generally spaced at approximately $1m$ intervals, the hangingwall beam considered in this study is taken to be $1m$ deep.

2.3 Summary

This chapter has summarised the stope geometry and fracture patterns characteristic of South African deep-level gold mines. Work by various authors pertaining to hangingwall beam behaviour has been discussed and principles governing the stability of the beam have been formulated. Emphasis is placed on the fact that this study attempts to model global hangingwall behaviour. Thus the only failure mode considered is buckling or 'snap-through' of the beam; local shear or crushing failure is not modelled.

Chapter 3

Numerical Modelling of the Hangingwall

In this chapter a numerical model of the isolated hangingwall beam is presented. The beam is modelled using the general nonlinear finite element suite ABAQUS and the program BLKBEAM, which was developed to analyse the response of the hangingwall beam. To verify the program, analyses generated by BLKBEAM are compared with those produced by ABAQUS. The three shear fracture model considered up to this stage is extended to a four and five shear fracture model.

3.1 The Hangingwall Beam Model

The typical pattern of fracturing in a deep-level gold mine was described in Section 2.1. The stope and fracture configuration is further simplified to formulate a basic yet representative hangingwall beam model. Figure 3.1 illustrates the simplified stope geometry. Three near vertical shear fractures and the parting planes parallel to the reef plane have segmented the hangingwall into two rectangular blocks. Due to gravity the hangingwall beam has displaced into the stope and the shear fractures have hinged open. The objective of this study is not to model local shear or crushing failure, but the global hangingwall beam response. Therefore only the hinging action of the hangingwall blocks at the shear fractures is modelled; relative sliding of the blocks is prohibited.

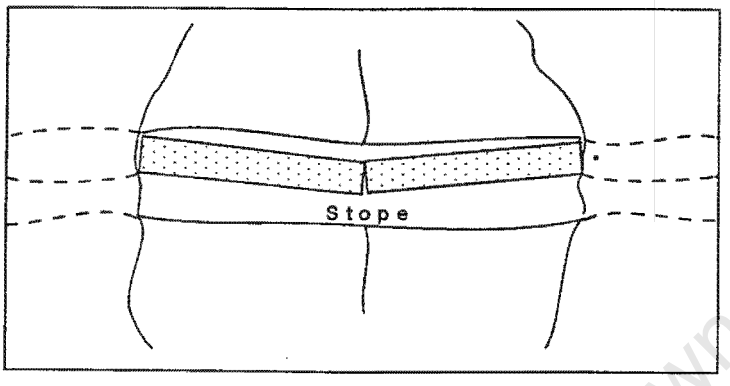

Figure 3.1: Simplified schematic of hangingwall beam in stope.

The hangingwall beam is separated from the excavation area shown in Figure 3.1. The isolated three shear fracture hangingwall beam illustrated in Figure 3.2 depicts the beam geometry used in the numerical analyses. The rectangular beam blocks can rotate at the shear fractures, however relative sliding is not permitted. The abutments of the beam are constrained to move only in the vertical direction as prescribed by the vertical displacement history of the earthquake. Horizontal movement of the abutments is prohibited.

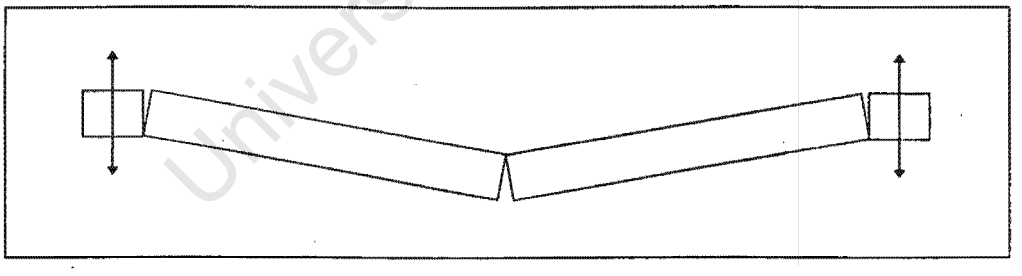

Figure 3.2: Geometry of isolated hangingwall beam used for numerical analyses.

Histories of ground motion due to earthquakes are usually obtained in two orthogonal horizontal directions and one vertical direction (Newmark and Rosenblueth [14]). In a two dimensional study, the horizontal component propagating along the length of the hangingwall and the vertical earthquake component need to be considered. The numerical beam model is excited only by the vertical ground motion component, i.e. the horizontal earthquake component is excluded, since, as outlined previously, an understanding of the global hangingwall beam response is sought. Local failure resulting in individual blocks falling into the stope is not considered. The shock waves due to the horizontal earthquake component propagating along the stope, could momentarily reduce the com-

pressive stresses in the hangingwall beam to zero. This would culminate in local failure in terms of individual blocks dropping into the stope.

Roberts *et al.* [3] determined the typical wavelength of the primary seismic wave to be $600m$. This wavelength is much larger than the longest hangingwall beam length ($23m$ halfspan) modelled in this study. Thus the assumption is made that the two beam abutments move simultaneously according to the same vertical displacement history. This allows the numerical hangingwall beam model to be modelled symmetric about the beam centre, thereby reducing the computational effort.

The hangingwall is modelled as a plane strain beam $1m$ deep and $1m$ wide. The following table presents the typical South African deep-level mine rock properties which are used by the numerical analyses:

Young's modulus	$E = 70.0 * 10^9 N/m^2$
Poisson's ratio	$\upsilon = 0.2$
Density	$\rho = 2700 kg/m$

The finite element method is used as the numerical tool to analyse the dynamic behaviour of the hangingwall beam. Sections 3.2 and 3.3 describe the finite element models using ABAQUS and program BLKBEAM. To verify and compare results computed by the two finite element programs, results presented in this chapter represent the response of a hangingwall beam with a constant halfspan length of $20m$. In all analyses the beam is excited by a sinusoidal displacement function applied to the beam abutments.

3.2 Finite Element Modelling using ABAQUS

ABAQUS is used to model the unfractured section of the hangingwall beam with four and eight noded plane strain elements. Shear fractures are modelled with slidelines which permit opening and closing of the joints, and relative sliding is prohibited. ABAQUS stipulates that the elements bordering the slidelines are four noded.

The analyses are completed in two steps. The beam is first gravity loaded, then the sinusoidal displacement function is applied to the abutments.

In an attempt to compute the dynamic beam response as efficiently as possible, the model was analysed using an implicit and explicit time stepping scheme. Results given by a pre-release version of the new explicit code ABAQUS/Explicit [15] were compared with those obtained by the implicit solver of the standard ABAQUS [16] program (Version 4.8). The explicit scheme was not computationally more efficient and coding bugs were

encountered in the pre-release version, and therefore the implicit time stepping scheme was utilised.

Five mesh configurations were tested: three designs use only four noded elements, whilst two other mesh designs incorporated eight noded elements for the unfractured section of the beam and four noded elements as slideline borders. The mesh configuration deemed most suitable to model the hangingwall beam consists of 4×42 four noded plane strain reduced integration elements. Although this configuration computes results which differ by a maximum of 25% when compared with the solution of a well refined mesh (4×40 eight noded elements in the unfractured beam section combined with 4×8 four noded elements at the shear fractures), the refined mesh is computationally five times as expensive. The chosen mesh is considered as the best compromise between accuracy and computational cost and is indicated in Figure 3.3.

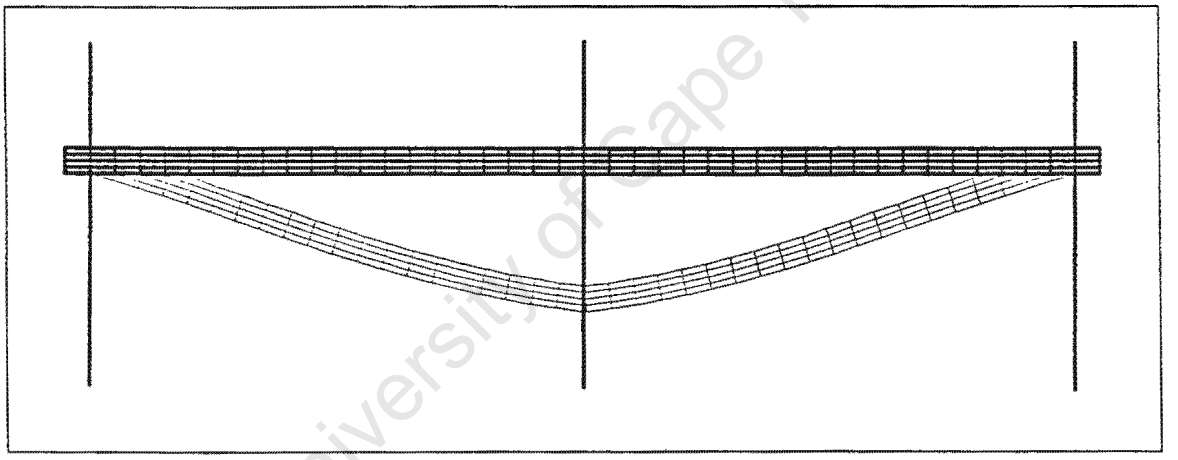

Figure 3.3: ABAQUS mesh used to model hangingwall beam. The slidelines are indicated by the three vertical lines.

The dynamic analysis of the hangingwall beam remains computationally expensive. The dynamic bending behaviour of the unfractured section of the beam could be analysed accurately with fewer elements than utilised by the chosen mesh design. Yet the slidelines need to be discretised with at least four elements along the depth of the beam to model the shear fractures adequately. In an attempt to reduce the degrees of freedom, the mesh was refined locally along the length of the slidelines. However, multiple point constraints necessary for the mesh refinement cancel the computational benefit associated with reduced degrees of freedom.

The ABAQUS analyses are computationally expensive, because a large number of degrees of freedom are solved for. To construct a single response spectrum (the response spectra

are presented in Chapter 5) the beam response has to be evaluated between 20 and 60 times. ABAQUS is not a viable tool to run so many analyses, and therefore a special purpose finite element program was developed to model the hangingwall beam. This program uses far fewer degrees of freedom and is computationally 30 to 50 times faster than ABAQUS.

3.3 Finite Element Modelling using BLKBEAM

Program BLKBEAM is coded in Fortran and utilises six-degree-of-freedom two noded beam elements. BLKBEAM models the unfractured section of the beam using four beam elements with mass lumped at the nodes. The shear fractures are represented by beam elements which are permitted to rotate at the contact point. Depending on the direction in which the shear fractures open, the interface beam elements are orientated so that beam sections cannot penetrate each other. This technique is illustrated in the following diagram.

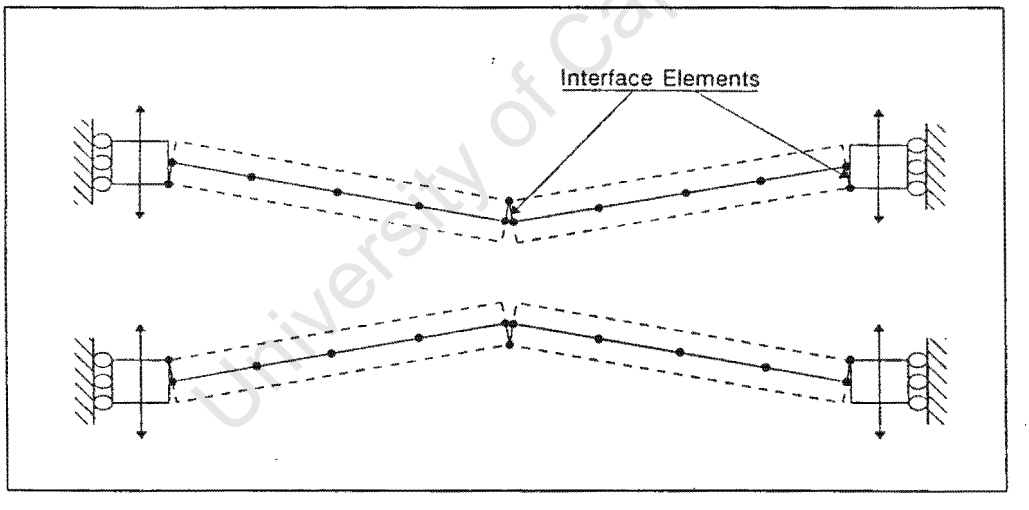

Figure 3.4: Orientation of interface beam elements depending on geometry of beam.

3.3.1 Description of program BLKBEAM

Details of the program are discussed with reference to the flow chart shown at the end of this section in Figure 3.7.

Input of model parameters
This is the control routine and calls the worker modules in the order listed below. The

excitation data, beam properties and initial conditions are specified. The dynamic analysis is completed in two load steps; the initially horizontal, unloaded beam is first gravity loaded and upon reaching equilibrium in its deflected position the second load step – the seismic excitation – is applied. The routine ensures that the beam is in equilibrium before the second load step is applied by continually checking whether the acceleration and velocity at the beam centre are less than $10^{-6}m/s^2$ and $10^{-10}m/s$ respectively. As soon as the beam centre motion is less than both tolerances, the beam is considered to be stationary in its gravity loaded position and the second load step commences. To attain the equilibrium position as rapidly as possible, the beam is 60% damped during the first load step.

1. Checking status of shear planes

Throughout the analysis the program assumes that the shear fractures are open. This module checks at each time increment whether the shear fractures have closed and in that case sets a flag to recycle the increment with the appropriate boundary conditions.

2. Formation of stiffness matrix

This routine calculates the element stiffness matrices and assembles these into the global stiffness matrix. Non-linear geometric effects are taken into account and the element stiffness matrices are recalculated at the beginning of each time increment. The interface elements are oriented correctly to prevent the beam sections penetrating each other. As indicated by Figure 3.5, the six degrees of freedom of the beam elements represent rotation as well as vertical and horizontal displacements at the nodes.

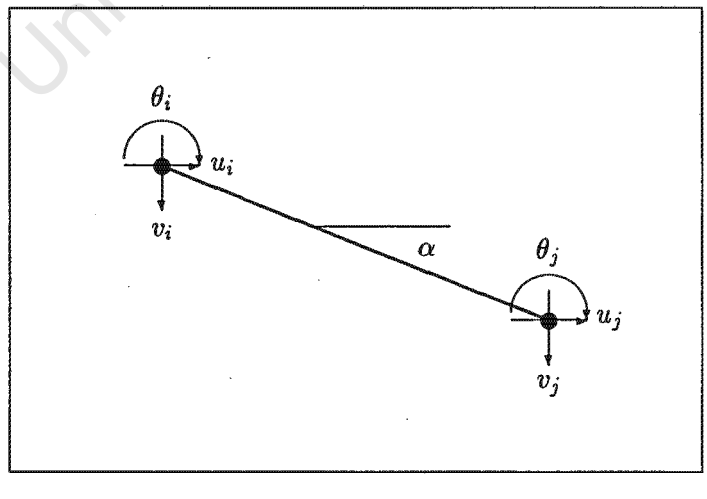

Figure 3.5: Beam element used by BLKBEAM.

The element stiffness matrix used in this study (Dawe [17]) is computed according to

the orientation of the element co-ordinate system relative to the global reference frame and is given by the following matrix:

$$
\mathbf{k}^e = \begin{array}{c}
\begin{matrix} u_i & v_i & \theta_i & u_j & v_j & \theta_j \end{matrix} \\
\begin{bmatrix}
\frac{AE}{l}e^2 + 12\frac{EI_z}{l^3}f^2 & & & & & \\
(\frac{AE}{l} - 12\frac{EI_z}{l^3})ef & \frac{AE}{l}f^2 + 12\frac{EI_z}{l^3}e^2 & & & \textit{Symmetric} & \\
-6\frac{EI_z}{l^2}f & 6\frac{EI_z}{l^2}e & 4\frac{EI_z}{l} & & & \\
-\frac{AE}{L}e^2 - 12\frac{EI_z}{l^3}f^2 & (-\frac{AE}{l} + 12\frac{EI_z}{l^3})ef & 6\frac{EI_z}{l^2}f & \frac{AE}{l}e^2 + 12\frac{EI_z}{l^3}f^2 & & \\
(-\frac{AE}{l} + 12\frac{EI_z}{l^3})ef & -\frac{AE}{l}f^2 - 12\frac{EI_z}{l^3}e^2 & -6\frac{EI_z}{l^2}e & (\frac{AE}{l} - 12\frac{EI_z}{l^3})ef & \frac{AE}{l}f^2 + 12\frac{EI_z}{l^3}e^2 & \\
-6\frac{EI_z}{l^2}f & 6\frac{EI_z}{l^2}e & 2\frac{EI_z}{l} & 6\frac{EI_z}{l^2}f & -6\frac{EI_z}{l^2}e & 4\frac{EI_z}{l}
\end{bmatrix}
\end{array}
$$

where A is the cross-sectional area of the element, E is the Young's modulus and I_z is the second moment of area about the z axis. Factors e and f are given by

$$e = \cos\alpha = \frac{x_j - x_i}{l}$$

and

$$f = \sin\alpha = \frac{y_j - y_i}{l} \ ,$$

where α is the orientation of the element relative to the global co-ordinate system, and $x_{i,j}$ and $y_{i,j}$ are the co-ordinate positions of the element nodes in the global system. The length of the element is given by l and is calculated by

$$l = \sqrt{(x_j - x_i)^2 + (y_j - y_i)^2} \ .$$

The elements along the length of the hangingwall have the second moment of area of a beam $1m$ deep and $1m$ wide. The second moment of area of the interface elements is governed by a function which, at each time increment, calculates I_z according to how far the shear fractures have hinged open. This is necessary to compensate for the reduced contact area at the shear fractures of an actual hangingwall as the cracks open. Local deformation of the rock at the fractures depends on the contact area and, since the numerical model always hinges at a point, the I_z of the interface elements needs to be modified as the fractures open. The function governing I_z of the interface beam elements was determined as follows. Using ABAQUS, the static deflection at the centre of the hangingwall beam for

various gravity load cases was computed. The different loading cases span a wide range of degrees of shear fracture opening. The function defining the second moment of area of the interface elements is tuned, such that program **BLKBEAM** computes deflections for the various gravity load cases which agree with those calculated by **ABAQUS**.

As illustrated by Figure 3.4, the end blocks representing the beam abutments are not modelled by beam elements. Hence the second moment of area of the interface elements representing the two outermost shear fractures is half that of any other shear fractures.

3. Application of boundary conditions
This module applies the essential boundary conditions. The following diagram indicates how, depending on the status of the shear fractures, the relevant boundary conditions are applied to the interface elements.

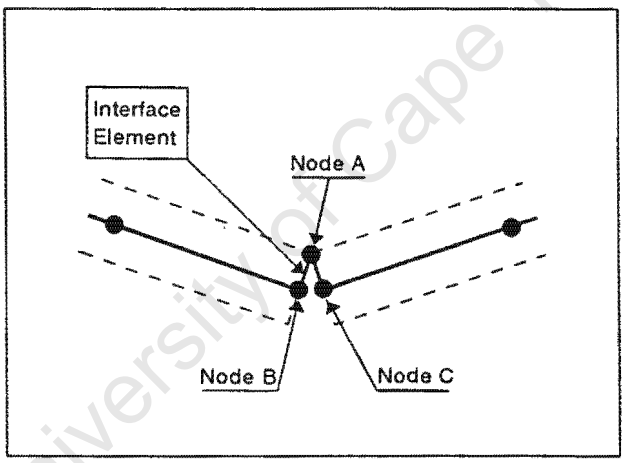

Figure 3.6: Position of the interface beam element nodes.

At all times, the interface elements indicated in Figure 3.6 are permitted to rotate relative to each other about node A. As soon as the interface elements have rotated such that the horizontal displacement of node B exceeds the displacement of node C, the shear fractures are closed and the time increment is recycled with nodes B and C constrained to have equal rotation and horizontal displacement. During the next time increment the constraints of node B and C are relaxed; however, should the fractures remain closed the increment is again recycled with the appropriate boundary conditions. Thus, whilst any shear fracture is closed, the program recycles every second time increment.

This routine also calls the static condensation routine. The static condensation routine was taken from Paz [18] and is utilised to condense out all massless degrees of freedom. The degrees of freedom to be reduced are identified as dependent coordinates and are expressed in terms of the independent degrees of freedom. The relation between the

dependent and independent degrees of freedom is found by establishing the static relation between them, hence the name static condensation. In general this method of reducing the dynamic problem is not exact and introduces errors. However, no errors are introduced in condensing massless degrees of freedom (Paz). The benefits of using the condensation routine are twofold. Firstly, the system matrix dimensions are reduced and consequently the program is computationally more efficient. Secondly, fewer degrees of freedom imply a reduced maximum eigenvalue, and therefore the explicit solution scheme can solve the equations using a larger time step. For the three shear fracture model the number of degrees of freedom are reduced from 19 to 8. In the case of a $20m$ halfspan beam the static condensation procedure therefore reduces the largest eigenvalue by 85%. This permits the largest stable time step for the explicit solver to be increased 2.5 times from $0.36ms$ to $0.90ms$. The small computational penalty incurred by the program looping through the static condensation routine at each time increment is far outweighed by the larger time step which (in the case of a $20m$ halfspan beam) permits the solution to proceed 2.5 times faster.

4. Formation of mass matrix

This routine forms the lumped mass matrix and, if required, calls an eigenvalue extraction routine developed by Bathe and Wilson [19] to compute the eigenvalues and eigenvectors of the system. The eigenvalues are utilised to calculate the maximum stable time step used by the explicit solution scheme and to determine the natural frequencies of vibration of the hangingwall beam.

5. Formation of damping and force vectors

The program makes use of a Rayleigh damping scheme. Extra damping is added to the damping matrix such that the shear fractures are critically damped. The damping matrix is formulated according to

$$[\mathbf{C}] = \alpha[\mathbf{K}] + \beta[\mathbf{M}] \,,$$

where **[C]**, **[K]** and **[M]** are the damping, stiffness and mass matrices respectively. The coefficients α and β are determined by the relationships [20]

$$\alpha = \frac{2(\zeta\omega_2 - \zeta\omega_1)}{\omega_2^2 - \omega_1^2} \,,$$

$$\beta = \frac{2\omega_1\omega_2(\zeta\omega_2 - \zeta\omega_1)}{\omega_2^2 - \omega_1^2}$$

in which case ζ is the fraction of critical damping and ω_1 and ω_2 are respectively the lowest and highest natural frequencies of the system.

The damping matrix is lumped [21]; this is necessary when solving the system equations using an explicit solution scheme. The matrix is lumped by adding in each row of [C] all the terms together and placing them on the diagonal. Thus, denoting the lumped

damping matrix by $[\mathbf{C^L}]$, its components are:

$$\mathbf{C^L}_{ii} = \sum_{j=1}^{n} \mathbf{C}_{ij} \quad i = 1, 2, \ldots, n$$

$$\mathbf{C^L}_{ij} = 0 \quad i \neq j$$

This module also calculates the force vector which applies the gravity loading and the seismic displacement function.

If required this module calls another routine to incorporate the effect of backfill. The backfill stiffness is multiplied by the relative displacement between the hangingwall beam and the footwall to provide a force at the supported nodes. The force vector is then modified to include the nodal forces due to the backfill support and the pressure of the overlying rock mass. The numerical model used to evaluate the effect of backfill is discussed in Chapter 7.

6. Explicit time integration scheme

A central difference time stepping scheme is used to solve the system equations. This is a two-step method involving three instants: t_{n-2}, t_{n-1} and t_n. The system equations

$$[\mathbf{M}]\ddot{a}_{n-1} + [\mathbf{C}]\dot{a}_{n-1} + [\mathbf{K}]a_{n-1} = \{\mathbf{F}\}_{n-1} \tag{3.1}$$

are evaluated at the central time, t_{n-1}. The velocity and acceleration are approximated by the central difference expression and it is assumed that both time steps are of the same length ($\Delta t = t_n - t_{n-1} = t_{n-1} - t_{n-2}$). The velocity and acceleration are given by:

$$\{\dot{a}\}_{n-1} = \frac{\{a\}_n - \{a\}_{n-2}}{2\Delta t}$$

$$\{\ddot{a}\}_{n-1} = \frac{\{a\}_n - 2\{a\}_{n-1} + \{a\}_{n-2}}{\Delta t^2} \tag{3.2}$$

Substituting Equations 3.2 into Equation 3.1 and placing all known terms on the right-hand side yields the central difference recurrence relation:

$$\left(\frac{1}{\Delta t^2}[\mathbf{M}] + \frac{1}{2\Delta t}[\mathbf{C}]\right)\{a\}_n =$$

$$\{\mathbf{F}\}_{n-1} - \left([\mathbf{K}] - \frac{2}{\Delta t^2}[\mathbf{M}]\right)\{a\}_{n-1} - \left(\frac{1}{\Delta t^2}[\mathbf{M}] - \frac{1}{2\Delta t}[\mathbf{C}]\right)\{a\}_{n-2} \tag{3.3}$$

Equation 3.3 is a system of linear algebraic equations with an effective stiffness matrix

$$[\mathbf{K_{eff}}] = \frac{1}{\Delta t^2}[\mathbf{M}] + \frac{1}{2\Delta t}[\mathbf{C}]$$

in which case $[\mathbf{K_{eff}}]$ is diagonal as both [M] and [C] are lumped and thereby the equations are uncoupled, making the method explicit.

The explicit central difference method is computationally fast. However, the method is conditionally stable and the scheme becomes unstable if the time step, Δt, is larger than the critical time step, Δt_{crit}. The critical time step is related to the largest eigenvalue by the following relation:

$$\Delta t \leq \Delta t_{crit} = \frac{2}{\sqrt{\lambda_{max}}}$$

The value of λ_{max} is calculated by the eigenvalue extraction routine. Due to the computational cost of looping through the eigenvalue routine, λ_{max} is only calculated at the beginning of analysis. To ensure a stable solution path, the calculated critical time step is reduced a further 20%, thereby safeguarding against the possibility of the largest eigenvalue becoming larger than λ_{max}.

The solution scheme solves for the displacements, velocities and accelerations of the nodes and, if the increment is not recycled, steps to the next time increment.

Finally the `OUTPUT` routine post-processes the results at the end of the analysis and writes solutions to a file.

Program `BLKBEAM` has been coded to compute many consecutive analyses. This permits one run to perform many analyses of varying beam lengths or different frequencies of the sinusoidal excitation function. Thus the tedious task of running many individual analyses of varying parameters is avoided. The powerful IBM 560 RISC System/6000 is utilised to perform the numerical simulation.

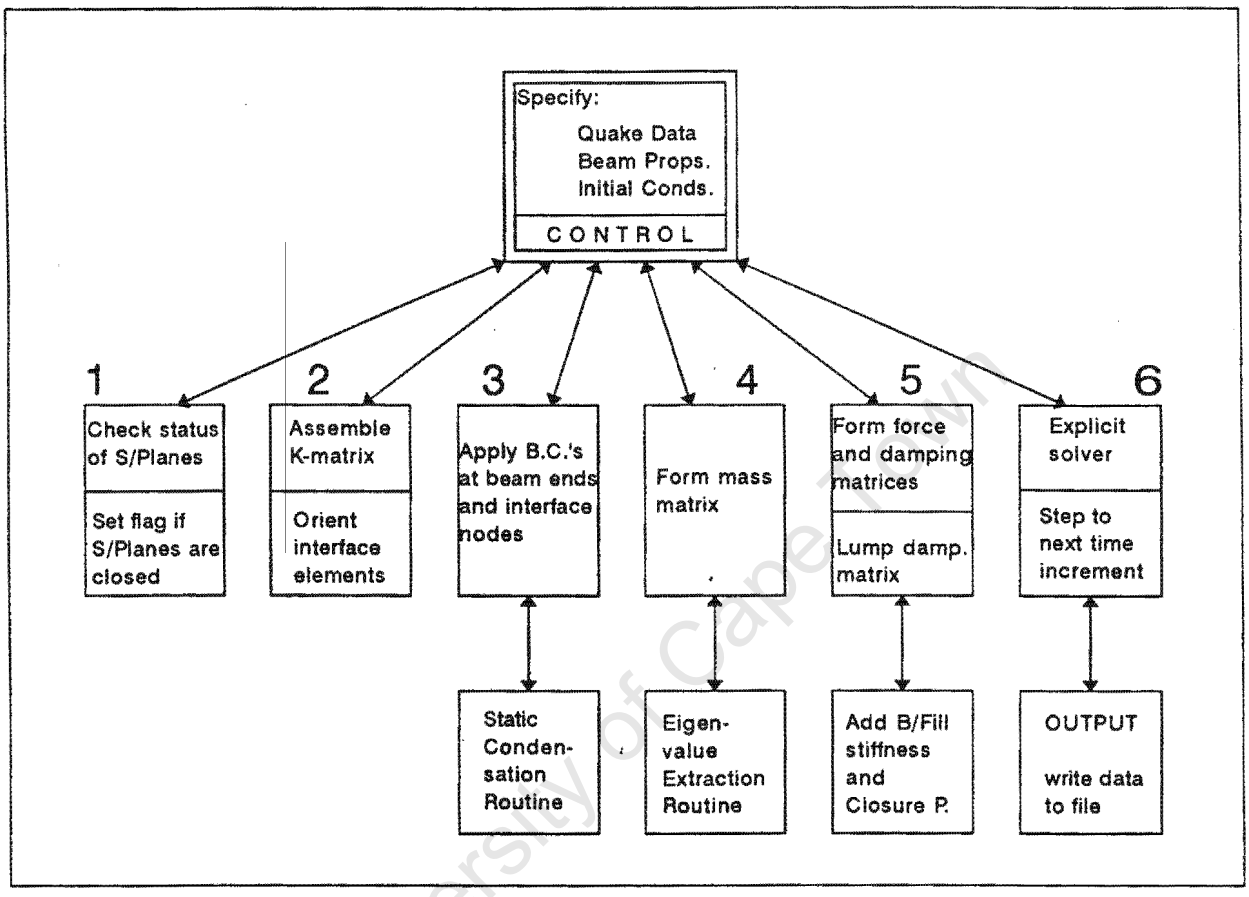

Figure 3.7: Flow chart of program BLKBEAM.

3.4 Verification of Program BLKBEAM

To verify the program, solutions computed by program BLKBEAM are compared with those given by ABAQUS. Both finite element programs analyse numerical hangingwall beam models excited by a sinusoidal displacement function applied to the beam abutments.

A $20m$ halfspan beam with three shear fractures is excited by a sinusoidal displacement function with an amplitude of $0.05m$. The analysis is repeated with frequencies of the displacement function ranging from $0.25Hz$ to $30Hz$. The beam is first gravity loaded and, upon reaching equilibrium, the sinusoidal excitation function is applied for a sufficiently long time period to record the maximum beam response (typically 6 seconds). For each analysis the dynamic displacement magnification factor is calculated. The factor is defined as the maximum relative displacement between the beam centre and the displacement

function divided by the amplitude of the displacement function ($0.05m$).

A graph displaying the dynamic magnification factor for excitation frequencies ranging from $0Hz$ to $30Hz$ is given in Figure 3.8. The magnification factor determined by BLKBEAM is compared with the factor computed by ABAQUS. The peaks of the chart indicate frequencies where the beam resonates, and in the regions where the dynamic magnification factor is larger than 12, resonance generates such large motions that the beam buckles or 'snaps through'.

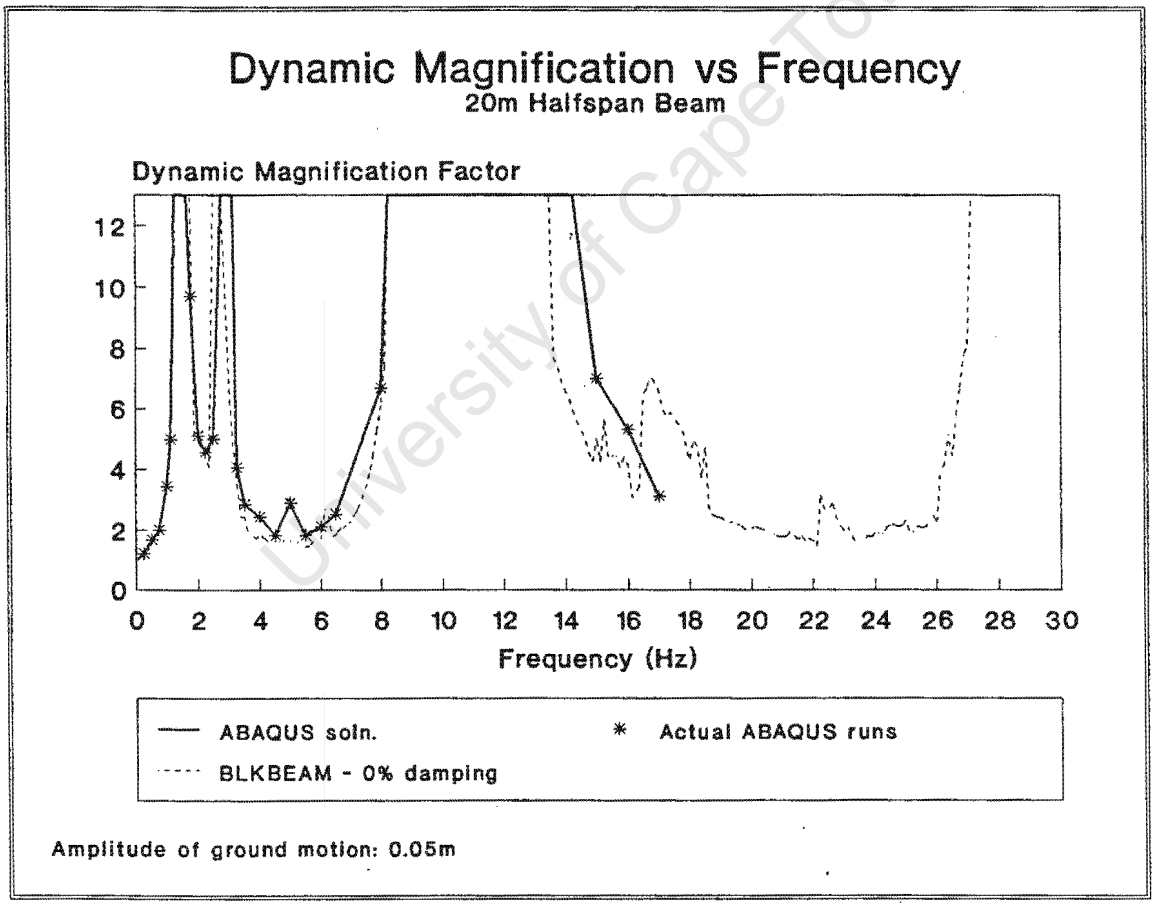

Figure 3.8: Graph comparing dynamic magnification results obtained by BLKBEAM and ABAQUS.

As indicated by Figure 3.8, the response calculated by program BLKBEAM corresponds well with the response computed by ABAQUS. The first two peaks at $1.5Hz$ and $3Hz$ represent frequencies the beam resonates in its first mode of vibration. During the following peak between $8Hz$ and $15Hz$ the beam resonates in its third mode and above $27Hz$ the beam is resonating in its fifth mode. As the hangingwall beam is modelled symmetrically about its centre, the even modes of vibration are not excited.The first, third and fifth modes of vibration are determined with the aid of the eigenvalue extraction routine and are indicated in Figure 3.9. Eigenvalues and eigenvectors can be calculated at any time during the dynamic analysis, thus permitting the natural frequencies and mode shapes to be determined for various beam deflections and combinations of open and closed shear fractures.

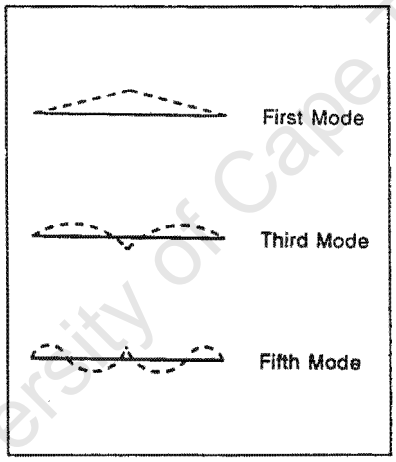

Figure 3.9: First, third and fifth modes of three shear fracture hangingwall beam.

Unlike in the case of a linear system, the natural frequencies of the non-linear hangingwall beam are not constant. The natural frequencies depend on the amount the beam deflects and how many shear fractures are open. These two aspects governing the natural frequencies are now examined in more detail.

- The fundamental frequency of the three shear fracture beam is linearly dependent on the deflection of the beam. Under gravity load the three shear fractures of the $20m$ halfspan beam are open and the fundamental frequency is $1.8Hz$. As the beam deflects further, the fundamental frequency decreases linearly. When the centre of the beam is deflected by the height of the beam ($1m$ in this case), the beam becomes a mechanism and 'snaps through'. At this point the fundamental frequency is zero. The third and fifth natural frequencies are less dependent on the beam deflection than the fundamental frequency. When the hangingwall is on the verge of buckling,

the third natural frequency of the beam vibrating in its third mode is approximately 20% greater then that of the gravity loaded beam.

- At any point in time during the dynamic analysis, the hangingwall beam geometry will consist of a combination of open and closed shear fractures. By calculating the natural frequencies of various beam geometries, an insight is gained into why the $20m$ halfspan beam resonates at the frequencies indicated by Figure 3.8.

  The fundamental frequency of the gravity loaded three shear fracture beam (all three shear fractures are open) is $1.8Hz$. As indicated by Figure 3.8, first mode resonance occurs at approximately $1.5Hz$. Since the fundamental frequency decreases linearly as the beam deflects, the 'mean' fundamental frequency during resonance is $1.5Hz$. The second first mode peak is due to the fundamental frequency of a $20m$ halfspan beam with all three shear fractures closed. Thus, whilst being excited with a sinusoidal function at approximately $3.3Hz$, the beam resonates whenever the three shear fractures are closed.

  The third natural frequency of the gravity loaded beam with all shear fractures open is $8.4Hz$. The corresponding natural frequency of the gravity loaded beam with the centre shear fracture constrained such that it cannot hinge open is $14.0Hz$. These two frequencies mark the border of the region shown in Figure 3.8 where the beam resonates in its third mode.

  The fifth natural frequency of the gravity loaded beam with all shear fractures open is $29.0Hz$. This marks the beginning of the graph region where the beam resonates in its fifth mode.

  Other features of the graph can be explained by considering the third natural frequency of the beam with all shear fractures closed. This frequency, $17.6Hz$, is represented on the graph as a peak between 16.5 and $18.5Hz$.

Further program verification involved plotting a 'safe bound' graph for a $20m$ halfspan beam. This graph is shown in Figure 3.10 and indicates the maximum amplitude of the sinusoidal excitation function at which the beam remains intact. The beam 'snaps through' in the region above the curve, whereas below the curve the beam is considered to remain structurally intact. The curve demarcating the regions is calculated by `BLKBEAM` and is compared to solutions given by `ABAQUS`. Figure 3.10 indicates that, for a wide range of load cases, the response calculated by `BLKBEAM` compares favourably with that determined by `ABAQUS`.

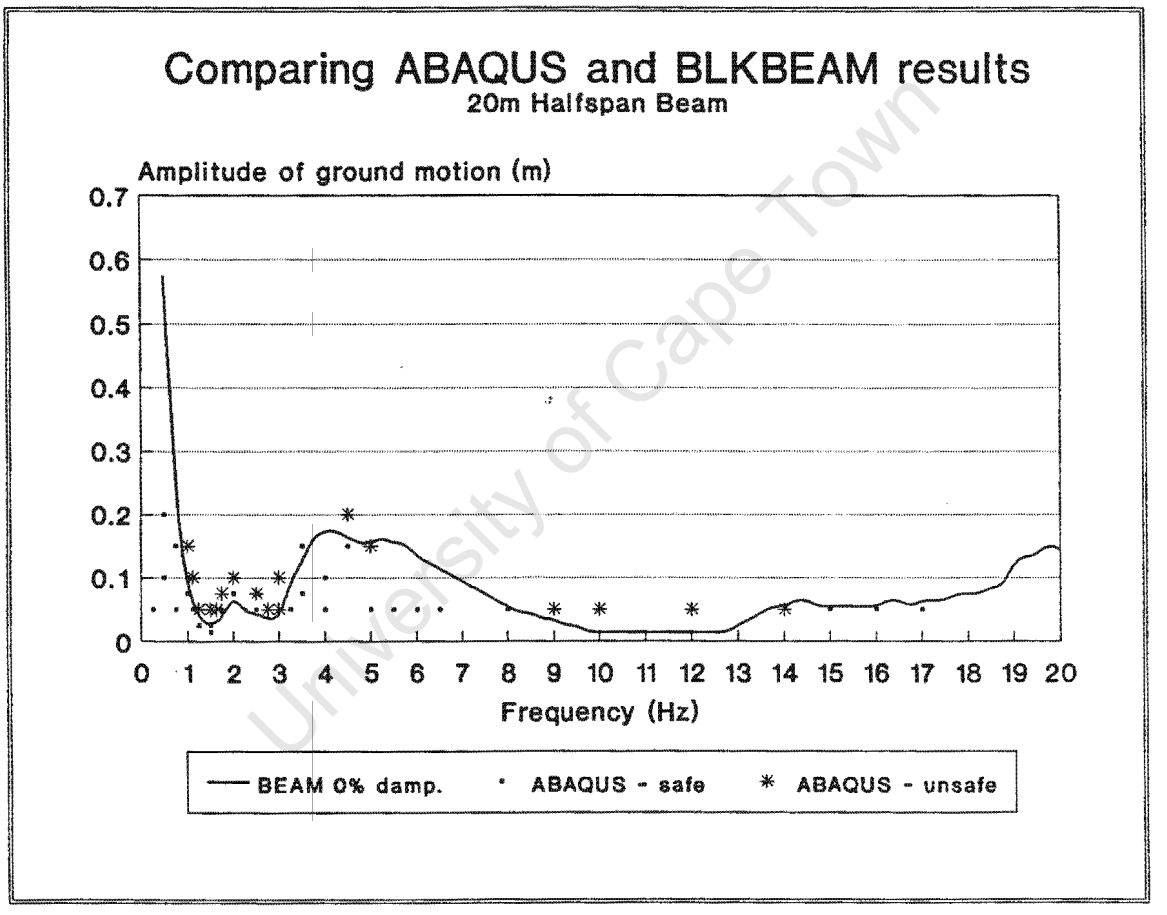

Figure 3.10: Safe bound plot of a hangingwall beam with a halfspan of $20m$.

3.5 The Five Shear Fracture Model

The three shear fracture model is adequate to represent the first mode of vibration of a fractured hangingwall beam. Even though additional shear fractures may be present in the unfractured hangingwall sections, the bending moment during the first mode of vibration is too small to prise the additional shear fractures open.

However, should the beam resonate in its third mode, the bending moment in the centre of the unfractured section is significant. To accurately model the third mode of vibration of a fractured hangingwall beam requires a further two shear fractures. Program `BLKBEAM` was extended to incorporate two additional shear fractures in the centre of the unfractured section of the three shear fracture model. Figure 3.11 displays the five shear fracture model.

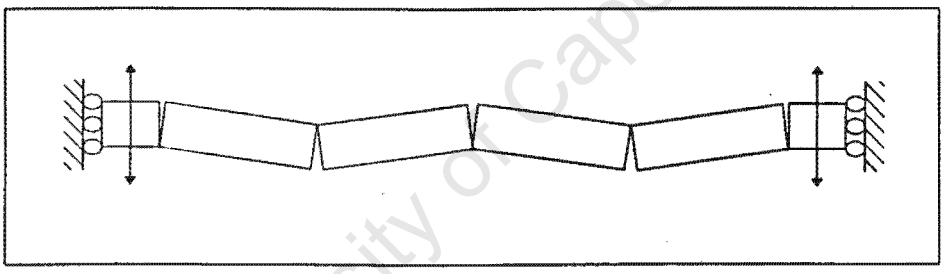

Figure 3.11: Geometry of the five shear fracture hangingwall beam model.

Figure 3.12 compares the dynamic magnification of the three shear fracture model with the five shear fracture model for 0% and 10% damping. As expected, in the first mode of vibration the two models yield very similar results. For the third and fifth mode the resonating frequencies of the five shear fracture model are shifted approximately $1.5Hz$ lower then the corresponding frequencies of the three shear fracture model. The response of the 10% damped hangingwall beam is lower than the 0% damped case. This is especially apparent during the first mode of vibration.

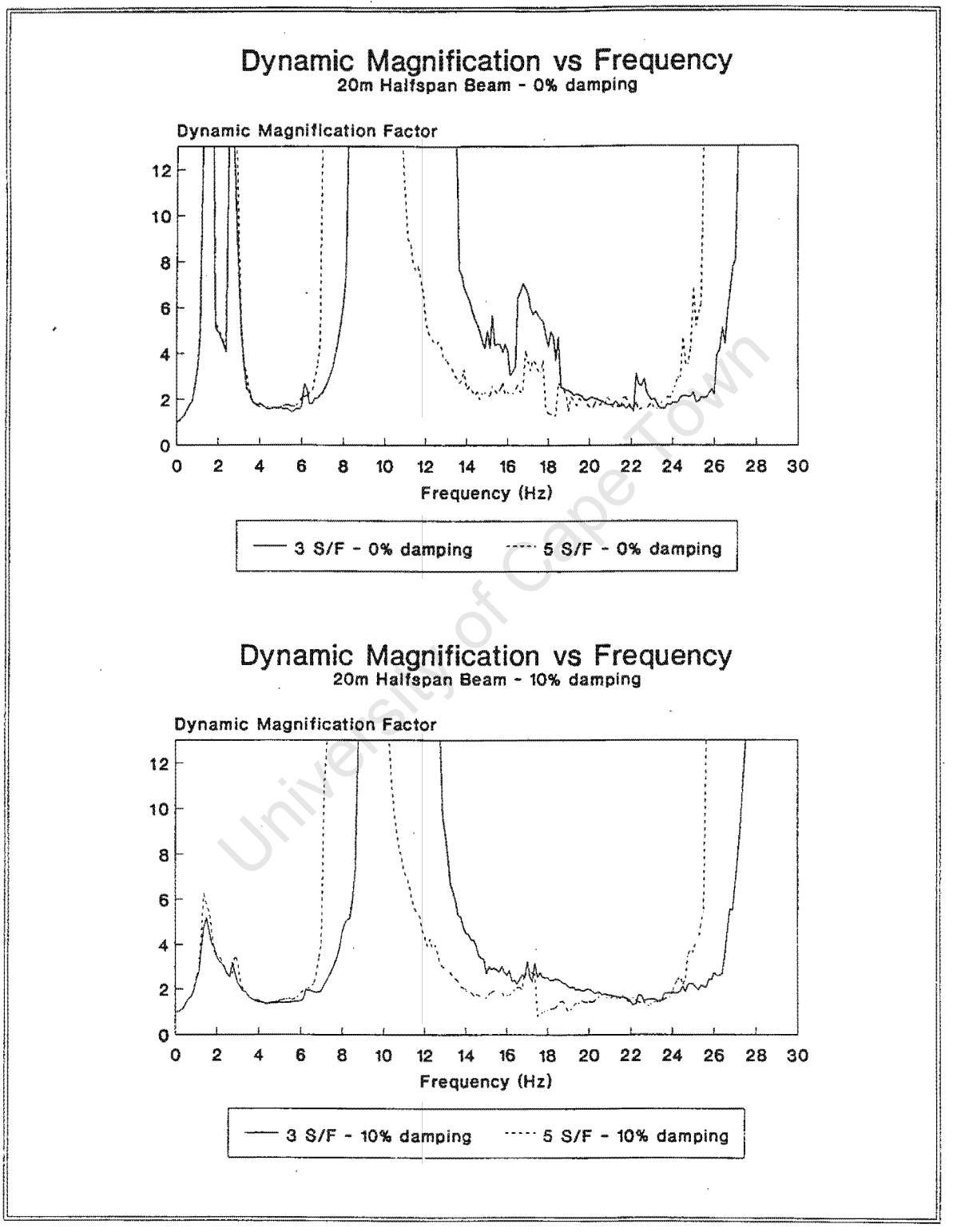

Figure 3.12: Comparison of the three and five shear fracture models.

3.6 The Four Shear Fracture Model

The centre fracture of the five shear fracture model can be constrained to prevent opening, thereby creating a four shear fracture model. The code is flexible enough to permit the centre section of the four shear fracture model to assume any length. The four shear fracture model is indicated in the following diagram.

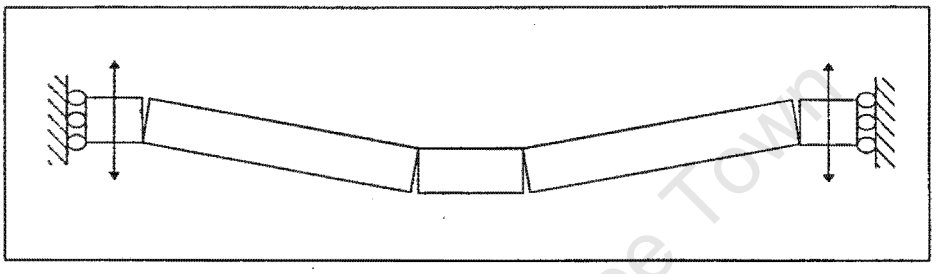

Figure 3.13: Geometry of the four shear fracture hangingwall beam model.

The code modelling the four shear fracture beam is essentially the same as for the five shear fracture model. It is thus deemed unnecessary to verify the four shear fracture model by comparing the response to the three or five shear fracture beam response, or to the response predicted by ABAQUS. The response of the four shear fracture model due to seismic excitation is given in Chapter 5.

3.7 Summary

This chapter has formulated a simple yet representative hangingwall beam model. The numerical model is analysed by the finite element suite ABAQUS and program BLKBEAM. Program BLKBEAM is computationally efficient and computes the beam response accurately. The three shear fracture model was extended to a four and five shear fracture model.

Thus the numerical tools have been developed to analyse the dynamic response of a fractured hangingwall beam. Subsequent chapters concentrate on the dynamic behaviour of the hangingwall beam during a seismic event.

Chapter 4

Seismicity in Mines

The virgin state of stress in the earth's crust is disturbed by mining excavations which result in stress concentrations in the rock. When the stresses approach the strength of the rock, seismic pulses are emitted (Cook [22]). Various studies have concluded that most seismic events result from shear failure on pre-existing faults, dykes and mining-induced fractures (Roberts *et al.* [3], McGarr [23] [24], Cook [25], Potgieter *et al.* [26], Ortlepp [27], Rourke *et al.* [28], Antwerpen *et al.* [29], Curtis [30] and Spottiswoode [31]). Elastic waves generated by the dynamic fault slip propagate through the rock mass. Upon encountering a mining excavation, a rock burst might occur. The extent and severity of damage to underground excavation is closely linked to high ground velocities, and velocities in excess of $2m/s$ are considered particularly dangerous (Wagner [2]).

The first section of this chapter presents graphs relating the acceleration, velocity, frequency and tremor duration to the tremor magnitude. Section 4.2 reviews the response spectrum method, and Section 4.3 summarises salient features of actual seismic events used to excite the numerical hangingwall beam model.

4.1 Ground Motion Characteristics

N.C. Joughin [32] analysed over 3100 seismic events in the Harmony gold mine and classified the events according to two distinct groups. The first group consists of 95% of the events, whose focal point was positioned within $100m$ above the reef plane. Of these events 85% were above advancing faces and 10% above worked-out areas. The second group, consisting of the remaining 5%, occurred in a confined area near a dolorite sill at an elevation of approximately $800m$ above the reef plane. McGarr [33] concluded from a study at East Rand Proprietary Mines that most tremors are located within $100m$ of

active mining faces. These statistics reveal that the hypocentral distances of the majority of seismic events in a deep mine are extremely short.

Due to the short hypocentral distances, ground motion in the stopes can attain high velocities and accelerations. Peak ground accelerations and velocities versus hypocentral distance are given in Figure 4.1 (McGarr *et al.* [34]). The ground acceleration and velocities are plotted for seismic events ranging in magnitude from 0 to 5 relative to the Richter scale. Figure 4.1 clearly illustrates the rapid attenuation of the ground motion as the hypocentral distance increases.

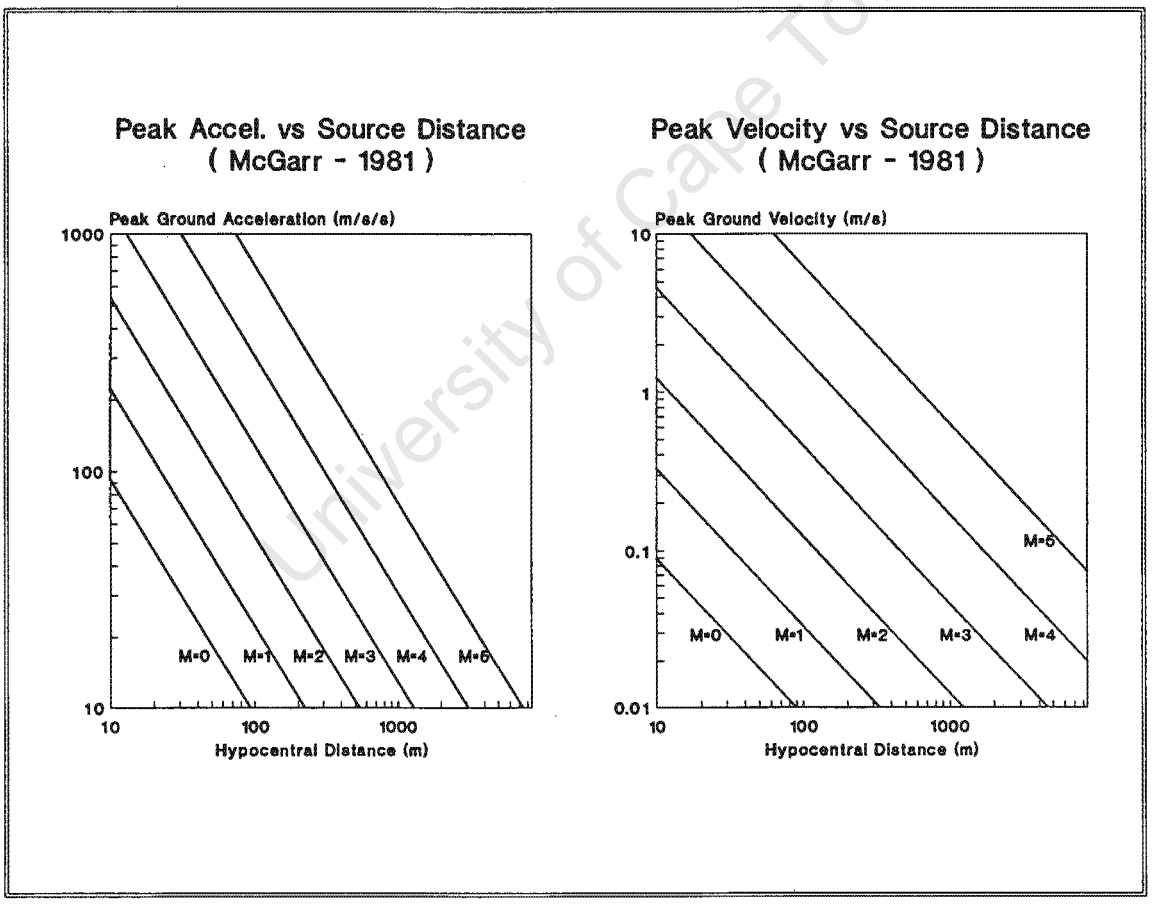

Figure 4.1: Ground accelerations and velocities for mine tremors of varying magnitude.

The corner frequency of a seismic event can be defined as the frequency with the maximum seismic energy. A structure is likely to resonate when excited by a seismic event with a corner frequency of the same order of magnitude as a natural frequency of the system. A relationship established by Spottiswoode *et al.* [35] relating the corner frequency to tremor magnitude is given in Figure 4.2. Also shown in Figure 4.2 is a plot defined by Deliac *et al.* [36] associating the duration of the event to the tremor magnitude.

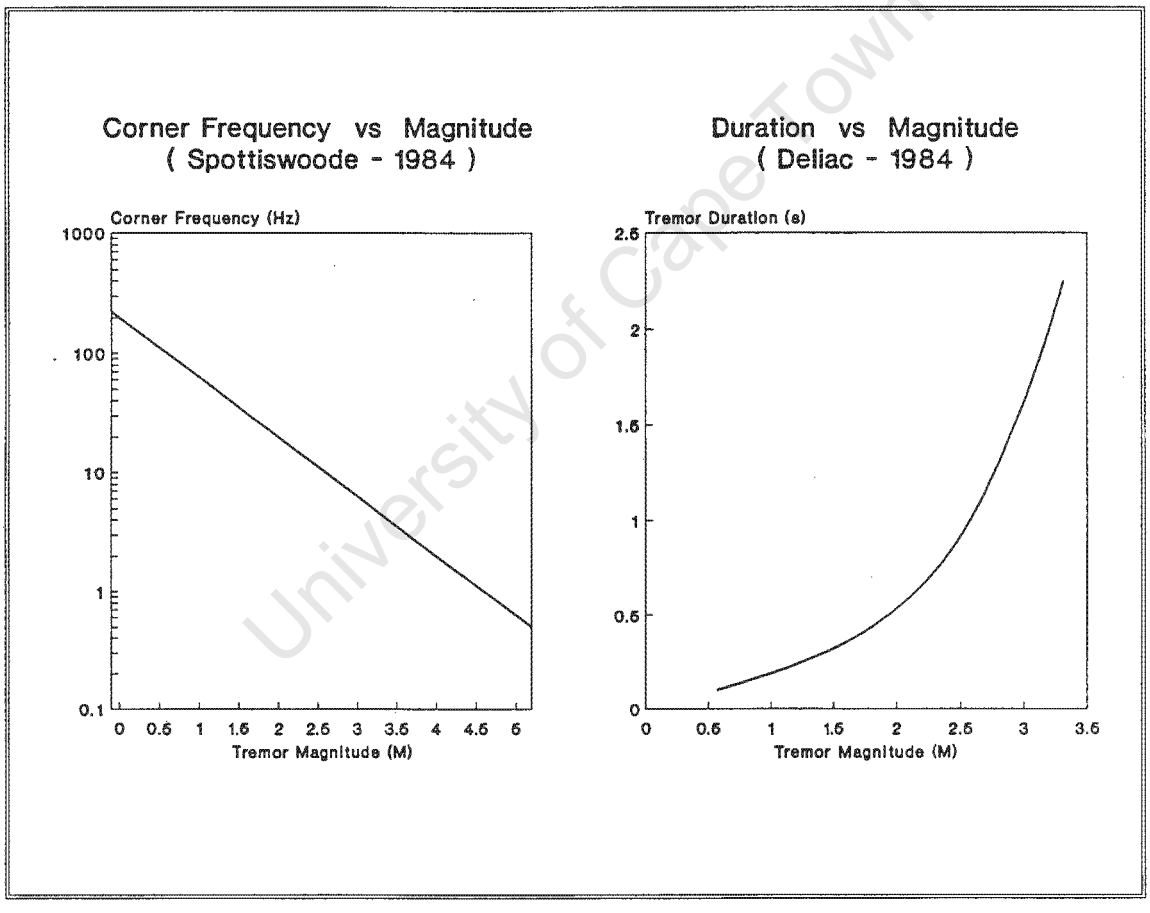

Figure 4.2: Corner frequency and tremor duration for mine tremors of varying magnitude.

The relationships indicated in Figures 4.1 and 4.2 have been established from ground motion parameters of numerous seismic events in South African deep-level gold mines. Characteristics of mine tremors vary widely, and the relations need to be interpreted as generalised estimates rather than definite rules.

4.2 The Response Spectrum Method

The response spectrum method has gained wide acceptance in earthquake engineering design (Gupta [37]). The response spectrum is a plot of the maximum response to a specified load function for all possible single-degree-of-freedom (SDOF) systems. The abscissa of the spectrum is the natural frequency of the SDOF system and the ordinate is the maximum response. Thus by knowing the natural frequency of the system, one can determine the maximum response from a spectral chart.

The SDOF system used in this study to construct response spectra is shown in Figure 4.3.

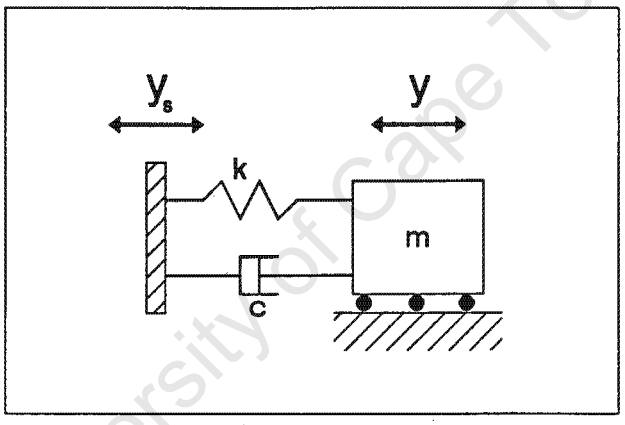

Figure 4.3: SDOF system used to construct response spectrum.

The equation of motion governing the response of the single-degree-of-freedom system is

$$my'' + c(y' - y_s') + k(y - y_s) = 0 \ , \tag{4.1}$$

or in terms of relative displacement (u)

$$mu'' + cu' + ku = -my_s'' \ , \tag{4.2}$$

where y is the displacement of the mass, y_s is the displacement of the base, m, c and k are the mass, damping and spring stiffness respectively and $u = y - y_s$. Using the basic relationships of structural dynamics, $k = m\omega^2$ and $c = 2m\omega\zeta$, Equation 4.2 becomes:

$$u'' + 2\omega\zeta u' + \omega^2 u = -y_s'' \tag{4.3}$$

The natural frequency of the system is defined by the relation:

$$\omega = \sqrt{\frac{k}{m}} \tag{4.4}$$

The response spectrum is constructed by solving Equation 4.1 describing the SDOF system subjected to seismic excitation and recording the maximum response. The analysis is then repeated for a range of natural frequencies of the SDOF system. In this study the differential equation 4.1 is solved by the same explicit time stepping scheme as used by program BLKBEAM.

4.2.1 Tripartite response spectra

It is possible to plot on a single chart using logarithmic scales the maximum response in terms of the absolute acceleration, the relative displacement, and a third quantity known as the relative pseudovelocity. The pseudovelocity is not the same as the actual velocity, but it is closely related and provides for a convenient substitute for the true velocity (Paz [18]). The maximum absolute acceleration, the maximum relative displacement and the maximum pseudovelocity, are known respectively as the spectral acceleration, spectral displacement and spectral velocity.

The spectral displacement S_u is proportional to the spectral acceleration S_a. To demonstrate this, the equation of motion describing a SDOF system (Equation 4.1) is written as

$$my'' + cu' + ku = 0 \ , \tag{4.5}$$

after using the relationship between the relative displacement, and the displacements of the mass and base ($u = y - y_s$). The maximum relative displacement and the maximum absolute acceleration occur when the relative velocity is zero ($u' = 0$), and at that instant Equation 4.5 can be written as

$$my''_{max} + ku_{max} = 0 \ . \tag{4.6}$$

Hence, taking into account Equation 4.4,

$$S_a = |y''_{max}| = \omega^2 S_u \ , \tag{4.7}$$

where ω is the natural frequency and $S_u = u_{max}$. The spectral velocity is defined as:

$$S_v = \omega S_u = \frac{S_a}{\omega} \tag{4.8}$$

The dynamic response of the single-degree-of-freedom system with 0% and 10% damping is computed for a seismic event. The response spectrum for this event is given in Figure 4.4. In this type of plot, because of the relationship relating the spectral velocity to displacement and acceleration, it is possible to draw diagonal scales for the displacement and acceleration, so that, from a single chart, values can be read for the spectral acceleration, spectral velocity and spectral displacements.

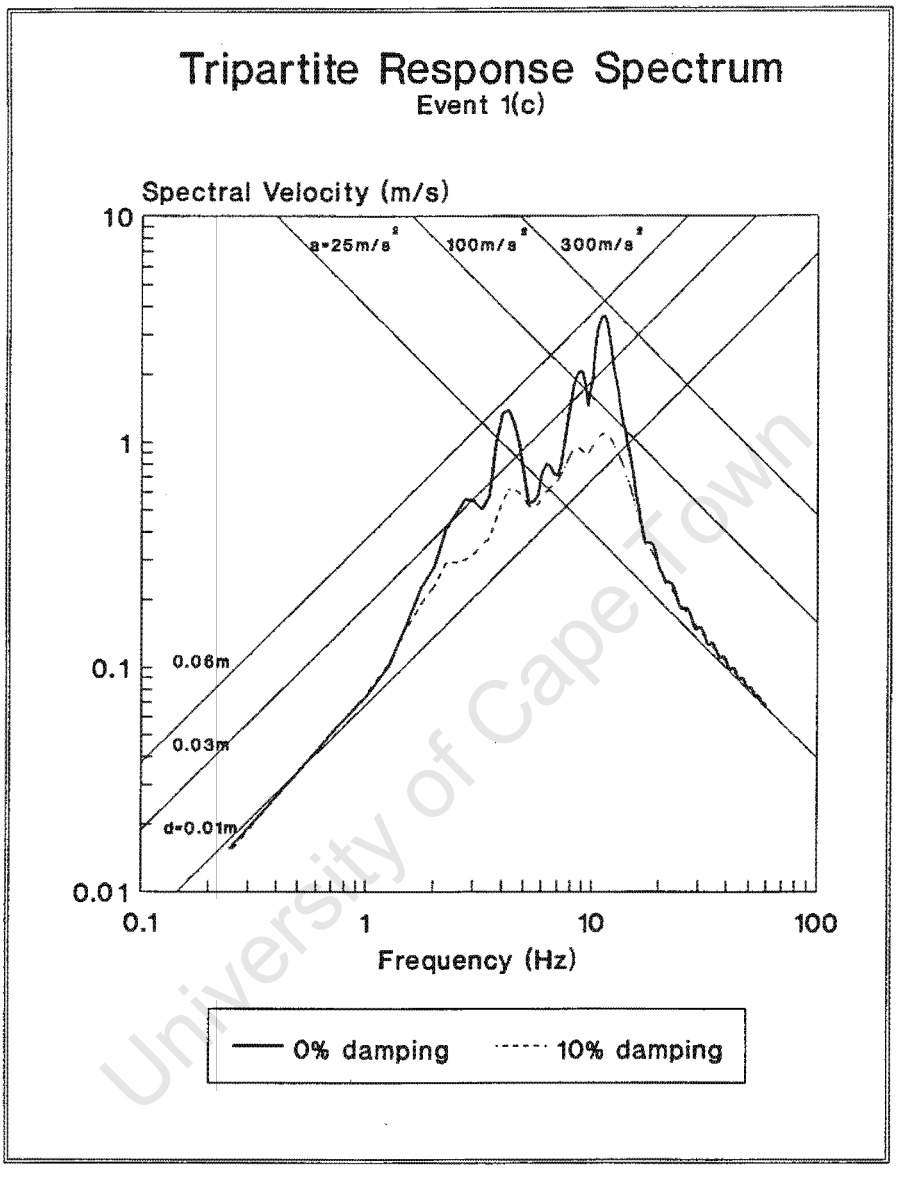

Figure 4.4: Tripartite response spectrum of Event 1(c).

In the low frequency range of a response spectrum the spectral displacement approaches the maximum displacement of the seismic event. In the high frequency range the spectral acceleration is equal to the maximum acceleration of the event. This phenomenon is easily explained considering that the low frequency range is characterised by a low value of spring stiffness, k. As the stiffness becomes progressively smaller, it ceases to transmit any motion to the mass. The total displacement of the mass tends to zero and the relative displacement becomes the displacement of the seismic event. At high frequencies the spring becomes progressively stiffer and hence the acceleration of the mass approaches that of the earthquake.

4.3 Seismic Events used in Numerical Analyses

In the following chapters the response of the hangingwall beam due to seismic excitation is computed for nine different events. Seven of these events were supplied as seismograms by the Chamber of Mines Research Organization [38], the remaining two events are taken from literature by Fernandez *et al.* [39] and McGarr *et al.* [34]. Fernandez processed accelerograms obtained 2 $500m$ from the source of an event which occurred in 1977 in the Klerksdorp gold-field and which registered 5.2 on the Richter scale. To simulate the hangingwall beam behaviour to this event at various distances from the source, the ground motions processed by Fernandez (acceleration-, velocity- and displacement-histories) are scaled by five factors. The scaled events are referred to as Events 1(a)–(e). The tremor documented by McGarr (Event 3) is similarly scaled by three factors. The seven events supplied by COMRO are named according to the number allocated by COMRO.

Details regarding tremor magnitudes as registered on the Richter scale (M_L) , the corner frequencies (F_o), the hypocentral distances (R_o) and the maximum accelerations, velocities and displacements attained by the ground during the event are presented in the following table.

Event No.	M_L	$F_o(Hz)$	$R_o(m)$	$A_{max}(\frac{m}{s^2})$	$V_{max}(\frac{cm}{s})$	$D_{max}(cm)$
1(a)	5.2	11	-	0.25	0.461	0.0109
1(b)[a]	5.2	11	2500	2.45	4.61	0.109
1(c)	5.2	11	-	24.5	46.1	1.09
1(d)	5.2	11	-	123	231	5.5
1(e)	5.2	11	-	245	461	10.9
3(a)[b]	1.45	43	351	1.4	0.596	0.0036
3(b)	1.45	43	-	14	5.96	0.036
3(c)	1.45	43	-	140	59.6	0.36
813	2.11	30	491	1.5	0.239	0.0013
1172	2.57	20	287	4.5	0.641	0.005
939	2.66	170	144	5.4	1.08	0.0067
1020	270	29	210	5.8	2.77	0.0175
1498	3.05	17	99	4.8	1.87	0.028
855	3.06	31	168	3.2	1.02	0.0056
675	3.18	22	264	6.0	2.58	0.033

[a] Actual event documented by Fernandez.

[b] Actual event documented by McGarr.

4.3.1 Fourier Analysis of Seismograms

The traces of the seismograms supplied by COMRO represent ground velocity. The standard method of obtaining ground displacement and acceleration from the velocity histories is to respectively differentiate and integrate the velocity records in the time domain (Fernandez [40]). By representing the velocity history as a Fourier series, the function is easily differentiated and integrated to yield displacement and acceleration signals. A program coded by Paz [18] is utilised to efficiently compute the Fourier series coefficients. Sixty coefficients are proven to be adequate to accurately represent the ground motion histories.

Using the Fourier series, velocity and displacement values of the ground during the event are written to a file at approximately $0.3ms$ intervals. At each time increment during the dynamic analysis `BLKBEAM` accesses this file and, by means of linear interpolation, determines the approximate ground displacement and velocity at that time increment. Errors are introduced by the Fourier series approximation, the time discretisation of the ground motion histories and the linear interpolation. However, these errors are proven to be negligible upon realising no appreciable difference between the ground motion of a seismic event and the motion computed by `BLKBEAM` of the beam node excited by the same event.

4.4 Summary

This chapter has given a broad overview of seismicity in mines. The first section correlated some important tremor parameters to event magnitude as established by various authors. The response spectrum method applied to a single-degree-of-freedom system is briefly reviewed and salient features of the seismic events used by the numerical analyses are listed. To excite the numerical hangingwall beam model by events with a wide range of maximum ground motions, two events are scaled by five and three factors respectively. Thus a total of 15 events are processed with the help of a Fourier series approximation and ground motion histories, discretised by small time intervals, are written to a file. During the dynamic analysis of the hangingwall beam this file specifies the loading history due to the seismic event.

Chapter 5

Seismic Excitation of the Hangingwall

Chapter 5 presents the results obtained by program BLKBEAM simulating the dynamic behaviour of the hangingwall beam during a seismic event. The chapter begins by discussing the concept of normalising the response of a multi-degree-of-freedom (MDOF) system to construct a response spectrum. The single-degree-of-freedom (SDOF) response spectrum is then compared to the normalised response of an elastic beam with no shear fractures and beams with three, four and five shear fractures.

5.1 Normalising Beam Response

Section 4.2 in Chapter 4 illustrated the response spectrum method applied to a SDOF system. A technique is now presented to normalise the response of the MDOF hangingwall beam to construct a response spectrum which is directly comparable to the response spectrum describing a SDOF system.

The equation of motion for a N-degree-of-freedom system can be written as

$$[\mathbf{M}]Y'' + [\mathbf{C}](Y' - Y_s') + [\mathbf{K}](Y - Y_s) = 0 \ , \tag{5.1}$$

where [M], [C] and [K] are mass, damping and stiffness matrices respectively; Y is the displacement vector and Y_s is the displacement vector of the ground motion. By describing the system in terms of relative displacement, $U = Y - Y_s$, the equation of motion becomes:

$$[\mathbf{M}]U'' + [\mathbf{C}]U' + [\mathbf{K}]U = -[\mathbf{M}]Y_s'' \tag{5.2}$$

The mode shapes and natural frequencies of the system are obtained by solving the following eigenvalue problem

$$\left|-\omega^2[\mathbf{M}] + [\mathbf{K}]\right| U = 0 \ , \tag{5.3}$$

where ω is a natural frequency of the structure. The solution of Equation 5.3 gives N frequencies $(\omega_i, i = 1 - N)$ and the corresponding modal vectors $(\phi_i, i = 1 - N)$, N is the number of degrees of freedom of the structure.

The modal vectors can be normalised such that:

$$\phi_i^T[\mathbf{M}]\phi_i = 1 \ , \tag{5.4}$$

$$\phi_i^T[\mathbf{K}]\phi_i = \omega_i^2 \ , \tag{5.5}$$

$$\phi_i^T[\mathbf{C}]\phi_i = 2\omega_i\zeta_i \ , \tag{5.6}$$

where ω_i is the natural frequency in radians per second and ζ_i is the damping ratio, both for mode i.

In the modal superposition method the following transformation is used

$$U = \sum_{i=1}^{N} \phi_i y_i = \sum_{i=1}^{N} U_i \ , \quad U_i = \phi_i y_i \tag{5.7}$$

where y_i is called the normal coordinate. Substitution of Equation 5.7 into Equation 5.2, pre-multiplying by ϕ_i^T, and use of the relations expressed by Equations 5.4 to 5.6 gives

$$y_i'' + 2\omega_i\zeta_i y_i' + \omega_i^2 y_i = -\gamma_i Y_s'' \ . \tag{5.8}$$

The term γ_i is called the participation factor for mode i, and is given by $\gamma_i = \phi_i^T\mathbf{M}$.

In the modal superposition method Equation 5.8 is solved to obtain the time history of the normal coordinates y_i, which with Equation 5.7 gives the history of the relative displacement vector, U.

Here the above concept is used to normalise the response of a MDOF system to a SDOF system. This permits the response spectrum method to directly compare the normalised MDOF beam response with the SDOF system response. Comparing Equation 5.8 with Equation 5.9 from Chapter 4 for a SDOF system,

$$u'' + 2\omega\zeta u' + \omega^2 u = -y_s'' \tag{5.9}$$

it is evident that

$$y_i(t) = \gamma_i u(t) \tag{5.10}$$

when $\omega = \omega_i$ and $\zeta = \zeta_i$. Hence

$$y_{i(max)} = \gamma_i u_{(max)} = \gamma_i S_u(\zeta, \omega) \ , \tag{5.11}$$

where $S_u(\zeta, \omega)$ is the spectral displacement of the SDOF system at a fraction ζ of the critical damping and a frequency ω. Taking Equation 5.7 into account, the maximum displacement vector in the i^{th} mode can be written as:

$$U_{i(max)} = \gamma_i \phi_i S_u(\zeta, \omega) \tag{5.12}$$

Given the displacement vector $U_{i(max)}$, the maximum relative displacement can be determined for any mode of interest.

The participation factor can be interpreted as a measure of the extent a particular mode contributes towards the overall response of a system (Hurty *et al.* [41]). By multiplying the spectral displacement by the first mode participation factor and the modal vector describing the fundamental mode shape, the MDOF system response due to the first mode of vibration can be calculated.

In the following two sections it will be seen that a hangingwall beam excited by a seismic event vibrates predominantly in its first mode of vibration. Thus higher modes do not contribute significantly towards the total system response, (U), and the assumption is made that $U(t) \approx U_1(t)$ and therefore $U_{(max)} \approx U_{1(max)}$. By rearranging Equation 5.12, the spectral displacement of the hangingwall beam can be determined as follows

$$S_u(\zeta, \omega) = \frac{U_{max}}{\gamma_1 \phi_1} \ , \tag{5.13}$$

thus allowing the maximum response of the MDOF beam to be directly compared to the response of a SDOF system.

The technique is applied to an elastic beam (no shear fractures). The first mode participation factor is calculated as $\gamma_1 = 137.0$ and this is multiplied by the maximum value of the normalised first mode eigenvector (due to the shape of the first mode, the maximum response occurs at the centre of the beam). The resulting coefficient ($\gamma_1 \phi_1 = 1.319$), referred to in this study as the normalising coefficient, is constant for all elastic beam lengths investigated.

The maximum response of the beam is divided by the coefficient, thereby reducing the MDOF beam response to the response of a SDOF system. This permits the response spectrum method to describe the response of the hangingwall beam.

5.2 Response of Normalised Elastic Beam

In this section the normalised response spectrum of an elastic beam (no shear fractures) is compared with the SDOF response spectrum. As outlined in Chapter 4, the response spectrum is constructed by determining the maximum system response when excited by a seismic event for various natural frequencies of the structure. To change the natural frequency of a SDOF system the relationship of spring stiffness versus mass is altered. For the MDOF elastic beam, the fundamental frequency of the beam is taken as the abscissa of the spectrum. The fundamental frequency (f_1) is varied by analysing the response of different beam lengths ranging from a halfspan of $4m$ ($f_1 = 82Hz$) to a $35m$ halfspan ($f_1 = 0.4Hz$). During seismic excitation the maximum relative displacement (spectral displacement) occurs at the beam centre. The spectral velocity is determined by the product of the fundamental frequency and the spectral displacement. The response spectrum for the elastic beam, the normalised elastic beam and the SDOF system of Event 1(c) is given in Figure 5.1.

As is clearly indicated by Figure 5.1, the response of the normalised elastic beam is very similar to the response of the SDOF system. This is especially apparent in the range between $3Hz$ and $15Hz$ where the beam response is greatest. Therefore in this range the first mode of vibration of the normalised elastic beam completely describes the beam response. The higher order modes of vibration are not active and the assumption made in the previous section that $U_{(max)} \approx U_{1(max)}$ is therefore justified.

For Event 1(c) the normalised elastic beam response below $2Hz$ and above $20Hz$ deviates slightly from the SDOF system response and higher order modes do contribute marginally towards the overall beam response. However the area of interest of the response spectrum is characterised by maximum spectral velocities which are due to the first mode of vibration only.

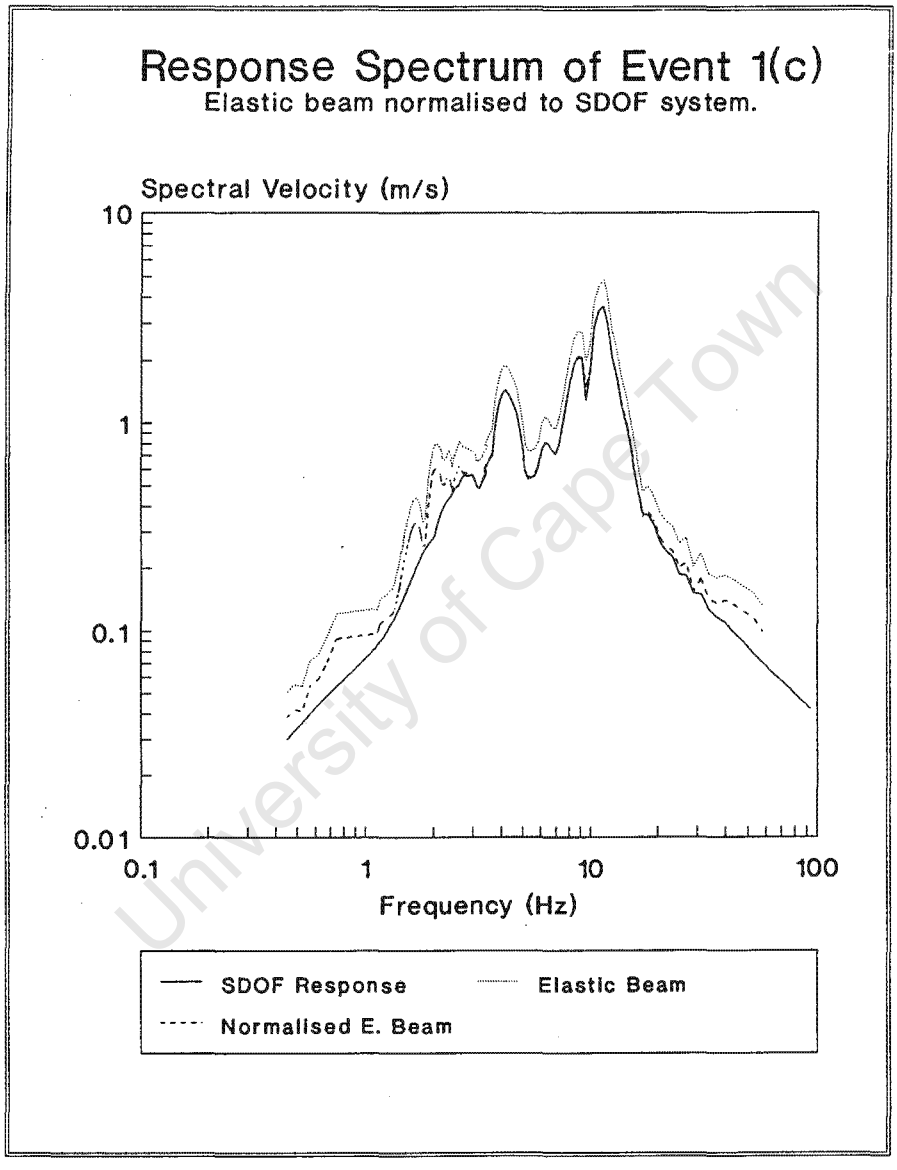

Figure 5.1: Response spectrum of normalised elastic beam.

5.3 Response of Three and Five Shear Fracture Beam

The three and five shear fracture beams are excited by Event 1(c), the response is normalised and the response spectrum is plotted. In this case, the shear fractures divide the beams into equal parts. The beam response is normalised as follows:

1. The spectral displacement is calculated by dividing the maximum response of the fractured hangingwall beam by the normalising coefficient ($\gamma_1\phi_1 = 1.319$) calculated for the elastic beam in Section 5.1.

2. For the elastic beam the abscissa of the spectrum is taken as the fundamental frequency of the beam; the frequency is varied by analysing the beam response at various beam lengths. In the case of the fractured beams the response is plotted such that at each point on the abscissa, the length of the fractured beam is equal to that of the elastic beam. The beam length in a stope is easily measured, therefore correlating frequency to the elastic beam length provides a convenient indicator of the hangingwall beam lengths which are prone to resonance. The spectral velocity of the fractured beams is determined by the product of the fundamental frequency of the elastic beam (at the corresponding beam length) and the spectral displacement at the centre of the fractured beams.

A spectrum comparing the response of the three and five shear fracture beam to the SDOF system and the elastic beam is given by Figure 5.2. The response spectrum reveals two noteworthy details.

The three and five shear fracture beams yield very similar results. This confirms the conclusion reached in Section 5.2 that the beams vibrate principally in their first mode. If the beam vibrates in the third mode of vibration, the three shear fracture model experiences large bending moments in the unfractured sections. These would prise the additional shear fractures of the five shear fracture model open. As the response of the two models is so similar, the assumption is made that the additional shear fractures of the five shear fracture model do not open. Thus the bending moments are small and the beam is primarily vibrating in the first mode.

A second observation is that the shape of the fractured beam response spectrum is essentially the same as that of the SDOF system. The response spectrum is merely shifted towards the higher frequency and spectral velocity range.

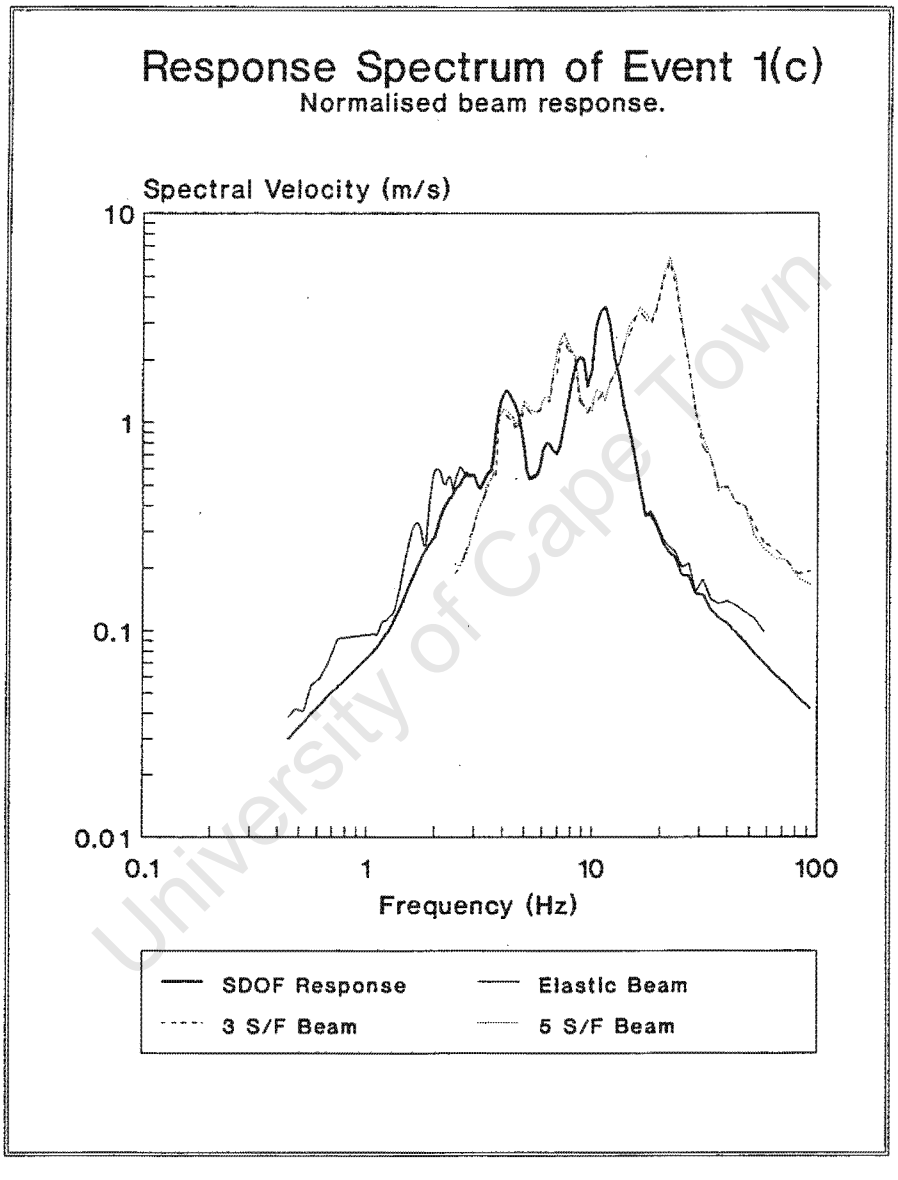

Figure 5.2: Response spectrum of three and five shear fracture beams.

The longest elastic beam analysed has a halfspan of $35m$. The longest halfspan of the fractured beams is limited by the static gravity load the fractured beams can sustain. As only the centre and two outermost shear fractures open under gravity load, the maximum stable halfspan is the same for three and five shear fracture beams. In this study the longest halfspan the fractured beams can support is $24m$ ($2.3Hz$ on the response spectrum). Thus at a halfspan longer than $24m$ the beam fails as a result of selfweight rather than dynamic loading. The maximum response of the fractured beams indicated on the response spectrum occurs at about $18Hz$, where the halfspan is only $7.5m$. The short beam length permits the fractured beam to sustain much higher dynamic loading. However excessive velocities could result in local shearing or crushing failure of the rock and damage to local support. Individual hangingwall blocks could be dislodged and the structural integrity of the complete hangingwall beam jeopardised. This study concentrates on the resonant behaviour of the hangingwall and thus the area of interest on the response spectrum is the high spectral velocity range. Critical beams are referred to as beam lengths exhibiting maximum dynamic response rather than beams buckling as a result of their halfspans exceeding $24m$.

5.4 Response of Four Shear Fracture Beam

In the previous two sections it was shown that the hangingwall beam during seismic excitation vibrates principally in the first mode. Due to the mode shape, the maximum response occurs at the centre of the beam. This leads to a 'worst case scenario' where the shear fractures are positioned such that a block is situated at the centre of the hangingwall beam. The high accelerations and velocities at the beam centre result in the centre block being the most likely part of the hangingwall to be damaged and fall into the stope.

The four shear fracture beam models this case. The response spectrum is constructed by analysing the maximum response of various beam lengths, although the length of the centre block remains constant at 2 metres. The beam is excited by two seismic events, the response is normalised and displayed by Figures 5.3 and 5.4. Figure 5.3 indicates the response due to Event 1(c) and compares the four shear fracture beam response with the SDOF system, the elastic beam and the three shear fracture beam response. Figure 5.4 gives the response of the four shear fracture beam, the SDOF system and the three shear fracture beam excited by Event 3(a). For both events, the four shear fracture beam response is very similar to the three shear fracture beam response. This is due to the fact that the fundamental frequencies of the gravity loaded three and four shear fracture beams at halfspans ranging from $2m$ to $23m$ never deviate by more than 10% from each other. The mean deviation of the two fundamental frequencies is 5.9%. Thus the two beam geometries exhibit similar degrees of resonance throughout the range of beam lengths analysed, and the response spectra are alike.

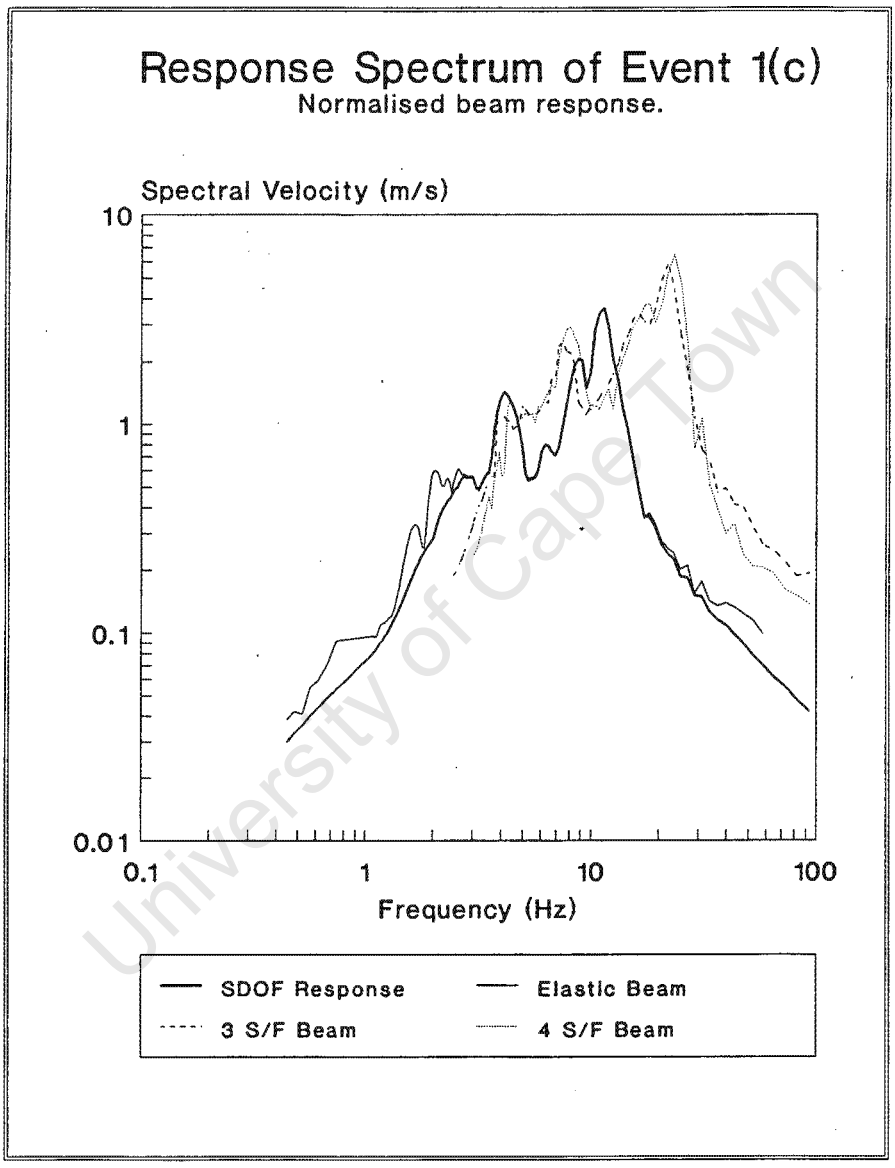

Figure 5.3: Response spectrum the four shear fracture beam excited by Event 1(c).

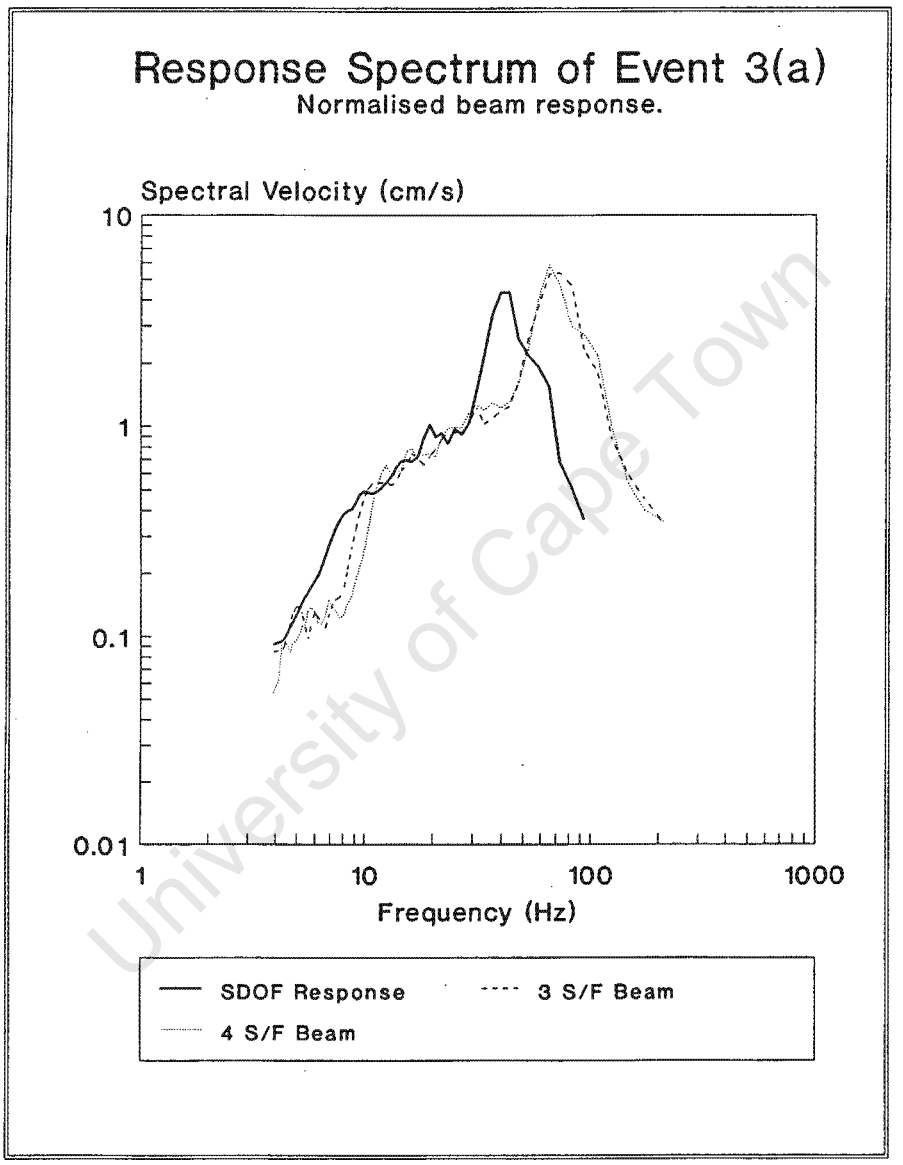

Figure 5.4: Response spectrum the four shear fracture beam excited by Event 3(a).

5.5 Summary

The hangingwall beam response has been normalised, thus allowing the response spectrum method to compare the hangingwall beam response directly with the SDOF system response. This chapter has shown that the hangingwall beam vibrates primarily in its first mode. When comparing the SDOF system response spectrum to the spectrum of a fractured hangingwall beam, it is evident that the shapes of the two spectra are very similar. However, the fractured beam spectrum is shifted to a higher frequency and spectral velocity domain. If the shift is quantified, the SDOF response due to a seismic event could be extrapolated to estimate the response of a hangingwall beam. The following chapter attempts to quantify the spectral shift.

Chapter 6

Shifting the Response Spectrum

In the previous chapter the observation was made that the shape of the normalised fractured beam response spectrum is essentially the same as the single-degree-of-freedom response spectrum. The only marked difference between the two spectra is a shift by the fractured beam spectrum towards the higher frequency and spectral velocity range.

A SDOF response spectrum can be easily constructed for any seismic event. By quantifying the shift, the SDOF spectrum can be extrapolated to obtain the response of a fractured hangingwall beam. Therefore, with minimal computational effort, peak spectral velocities can be estimated for a range of hangingwall beam lengths.

This chapter quantifies the shift of the fractured beam spectrum relative to the SDOF response spectrum. Charts 5.2, 5.3 and 5.4 in Chapter 5 illustrate that the four and five shear fracture beam response is essentially the same as the response of the three shear fracture beam. As the three shear fracture analysis is computationally more efficient, the three shear fracture model is used to plot response spectra and calculate the spectrum shift. Fractured beam response spectra are constructed for various seismic events and compared to the SDOF response spectra, thereby quantifying the shift.

Section 6.1 correlates the frequency of the spectrum abscissa to the beam length. The two subsequent sections determine the frequency and spectral velocity shifts.

6.1 Correlating Frequency to Beam Length

The response spectrum abscissa is scaled according to frequency. As described in Section 5.2, the abscissa of the elastic beam response spectrum is chosen as the fundamental frequency of the elastic beam at various beam lengths. Therefore the abscissa can be

interpreted as beam length. The response of the fractured beam is evaluated at various beam lengths and is plotted such that, at each point on the abscissa, the length of the fractured beam is equal to that of the elastic beam.

A chart relating the fundamental frequency of the elastic beam to the beam halfspan is presented in Figure 6.1. Such a chart is required to determine critical hangingwall beam lengths which are prone to resonance when excited by a seismic event. This is accomplished by determining the frequency corresponding to the maximum spectral velocity as governed by the response spectrum. Using Figure 6.1, the frequency is easily converted to beam halfspan. At this critical beam length resonance induces the largest velocities and damage to the hangingwall beam is most likely.

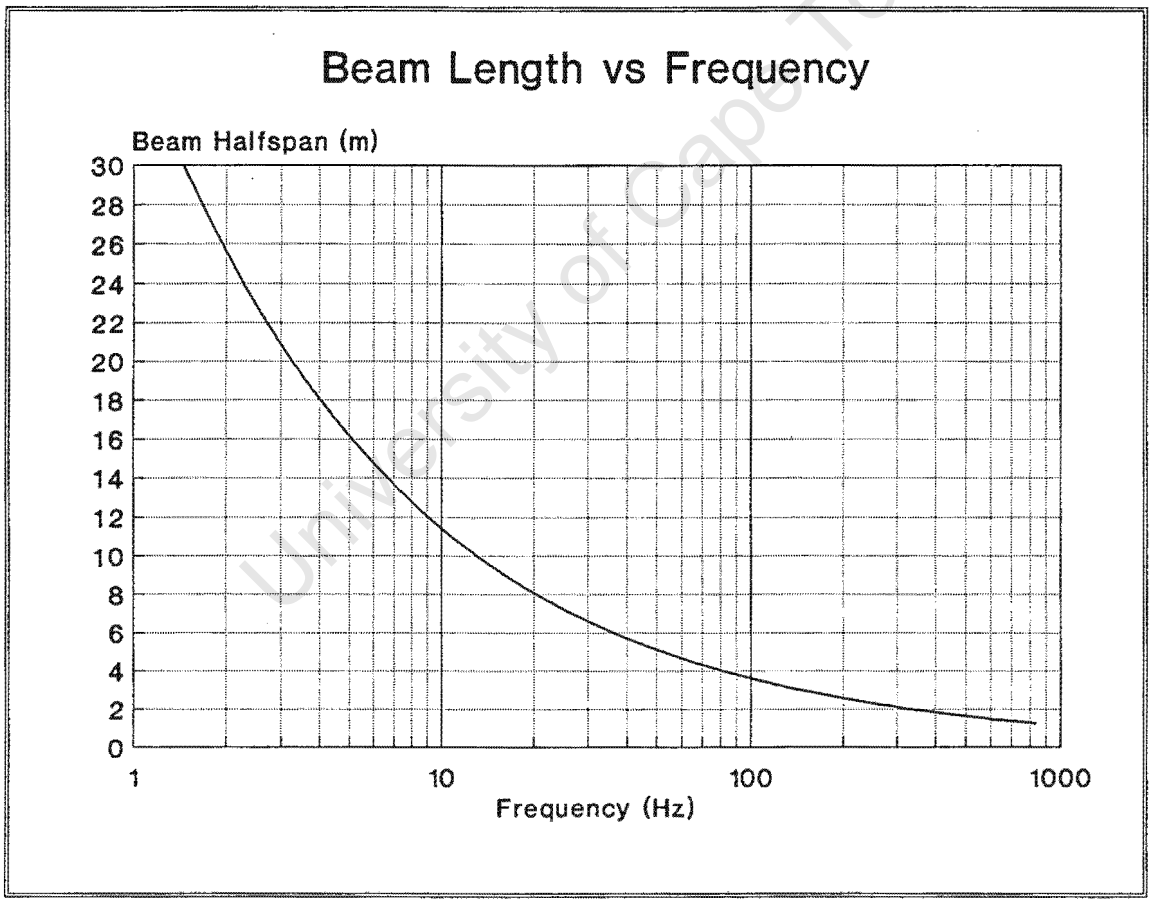

Figure 6.1: Graph relating frequency to beam halfspan.

6.2 Quantifying the Frequency Shift

The fractured beam response spectrum is shifted to a higher frequency range when compared with the SDOF spectrum. This section attempts to quantify the frequency shift.

For small seismic events the relationship between the frequency of the SDOF spectrum and the frequency of the shifted response spectrum presented by the chart in Figure 6.2 is valid. As the seismic event is small, the excited hangingwall beam does not deviate significantly from its gravity loaded equilibrium position. Thus the shift is determined by the difference of the fundamental frequency of the elastic beam compared to the fundamental frequency of the gravity loaded fractured beam. This difference is quantified and presented graphically in Figure 6.2.

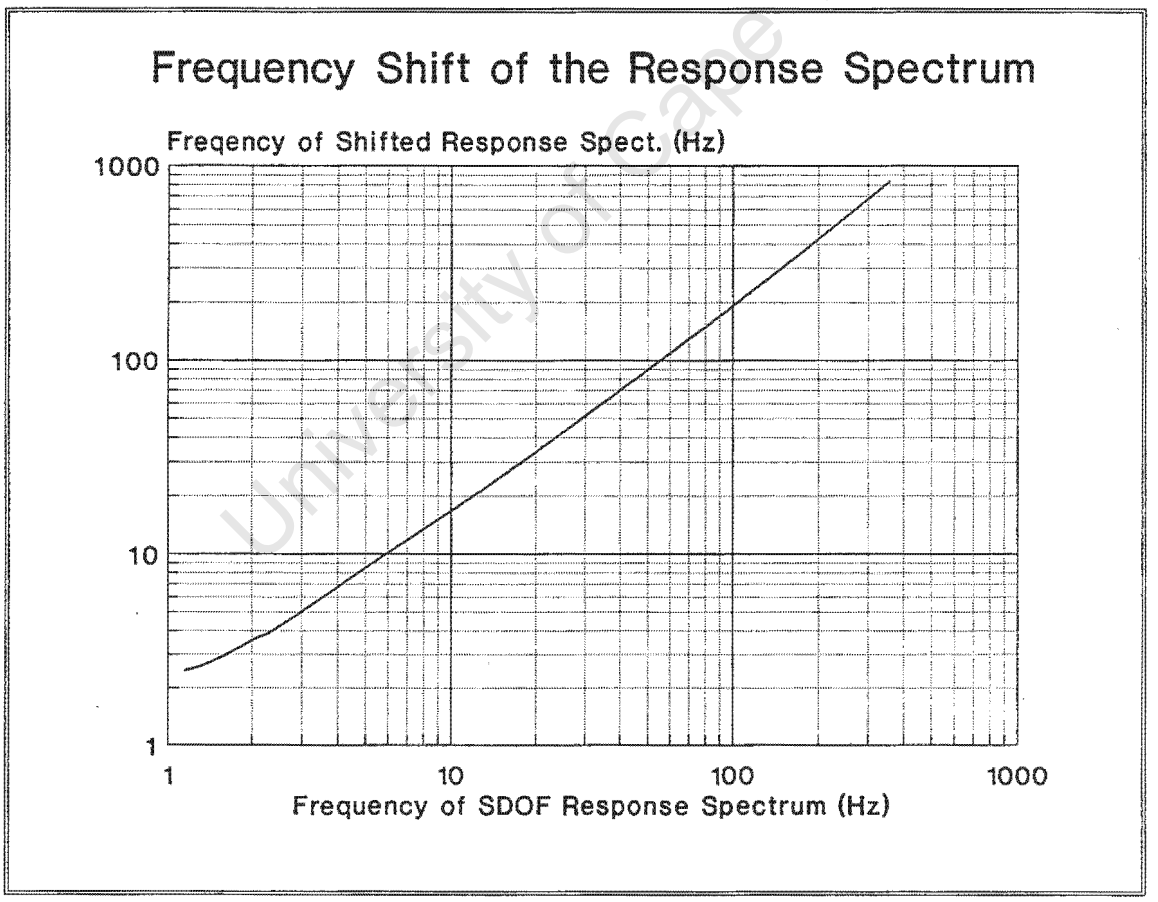

Figure 6.2: Frequency shift for small seismic events.

However, as the magnitude of the seismic event increases, the fractured beam displaces further from its gravity loaded position. The frequency of the shifted response spectrum

determined from Figure 6.2 needs to be multiplied by a further shift factor, presented in Figure 6.3. The shift factor is plotted versus a wide range of maximum earthquake velocities. The factor is empirically determined by calculating the frequency shift of 15 events with 0% damping and 12 events with 10% damping.

As expected, for small earthquakes the shift factor tends to 1 and the frequency shift presented in Figure 6.2 is adequate. As the event magnitude increases, the frequency shift needs to be multiplied by the escalating shift factor.

This is intuitively obvious when considering the linear dependence of the fundamental frequency of the fractured beam on the centre deflection of the beam. As the beam is excited by more severe events, the maximum centre deflection increases and the minimum fundamental frequency decreases. Thus the difference between the fundamental frequencies of the elastic and fractured beam is increased, and the frequency shift is amplified.

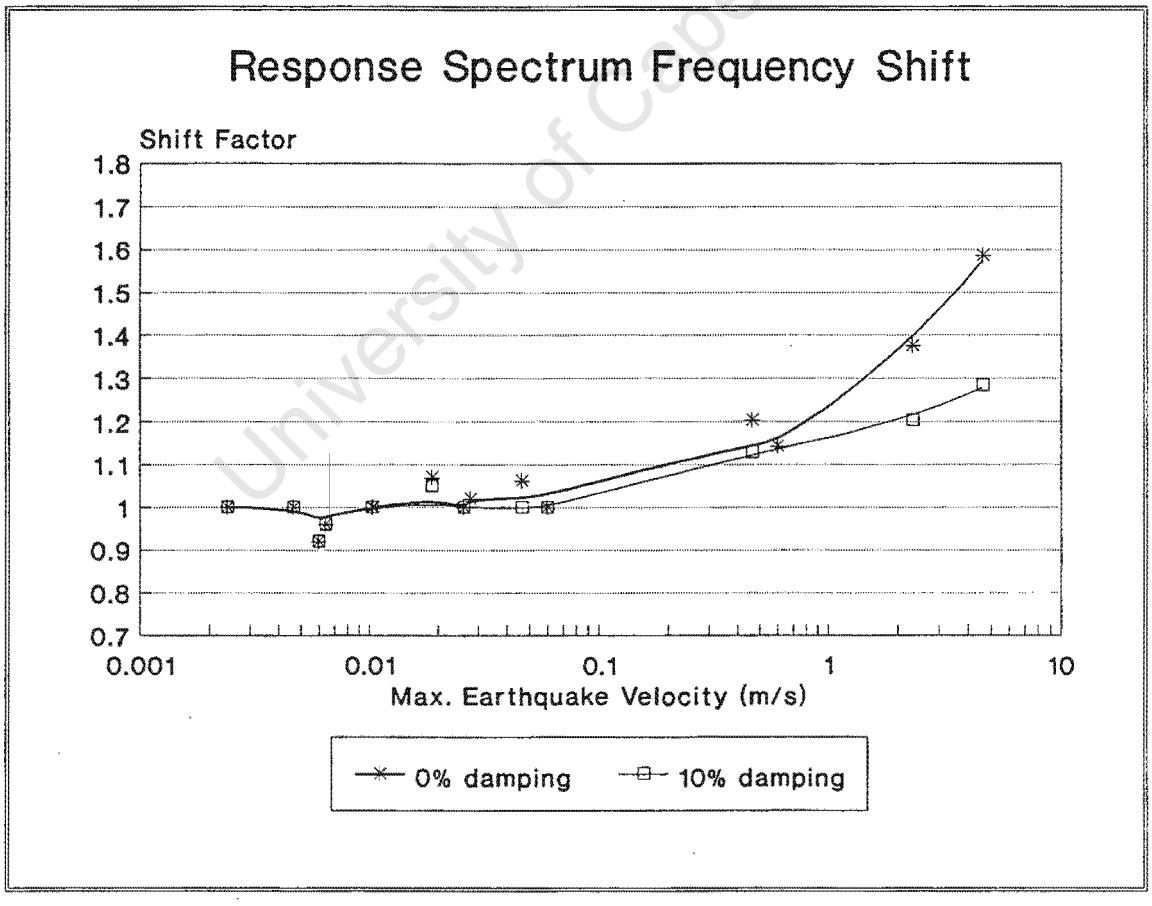

Figure 6.3: Frequency shift factor for a range of maximum event velocities.

6.3 Quantifying the Spectral Velocity Shift

The response spectrum is not only shifted in the frequency domain, but also in the spectral velocity domain. The velocity shift is determined for 15 different events for 0% damping and 12 events for 10% damping. The following graph illustrates the shift factor for a wide range of maximum earthquake velocities. By multiplying the spectral velocity of an undamped SDOF system response spectrum by the shift factor calculated for a 0% and 10% damped hangingwall beam, the approximate spectral velocity of the respectively damped fractured hangingwall beam can be determined.

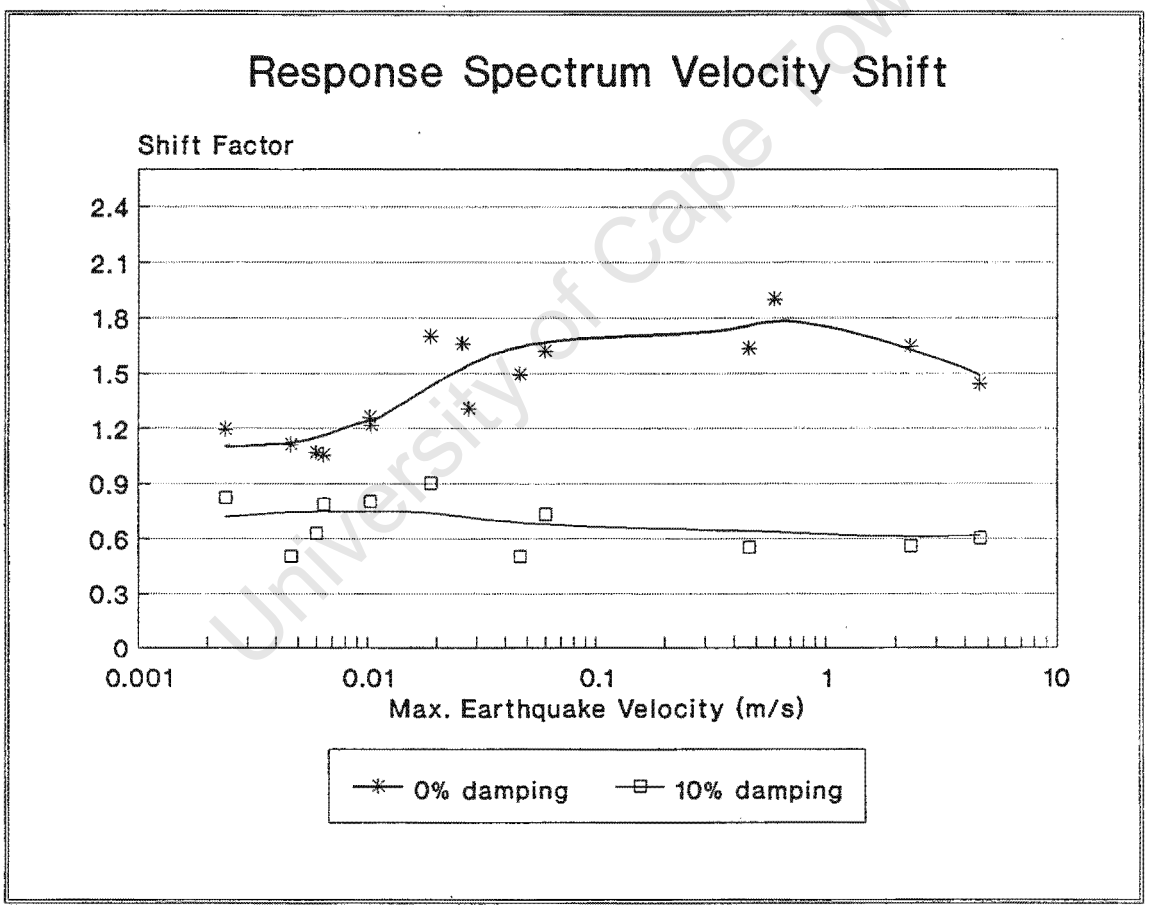

Figure 6.4: Graph quantifying the response spectrum velocity shift.

The maximum velocity attained by rock during a seismic event is generally considered to be the most reliable ground motion parameter to measure the severity of a mine tremor (Wagner [42]). Using the spectral velocity shift factor, the maximum spectral velocity of a fractured hangingwall beam during a seismic event can be approximated.

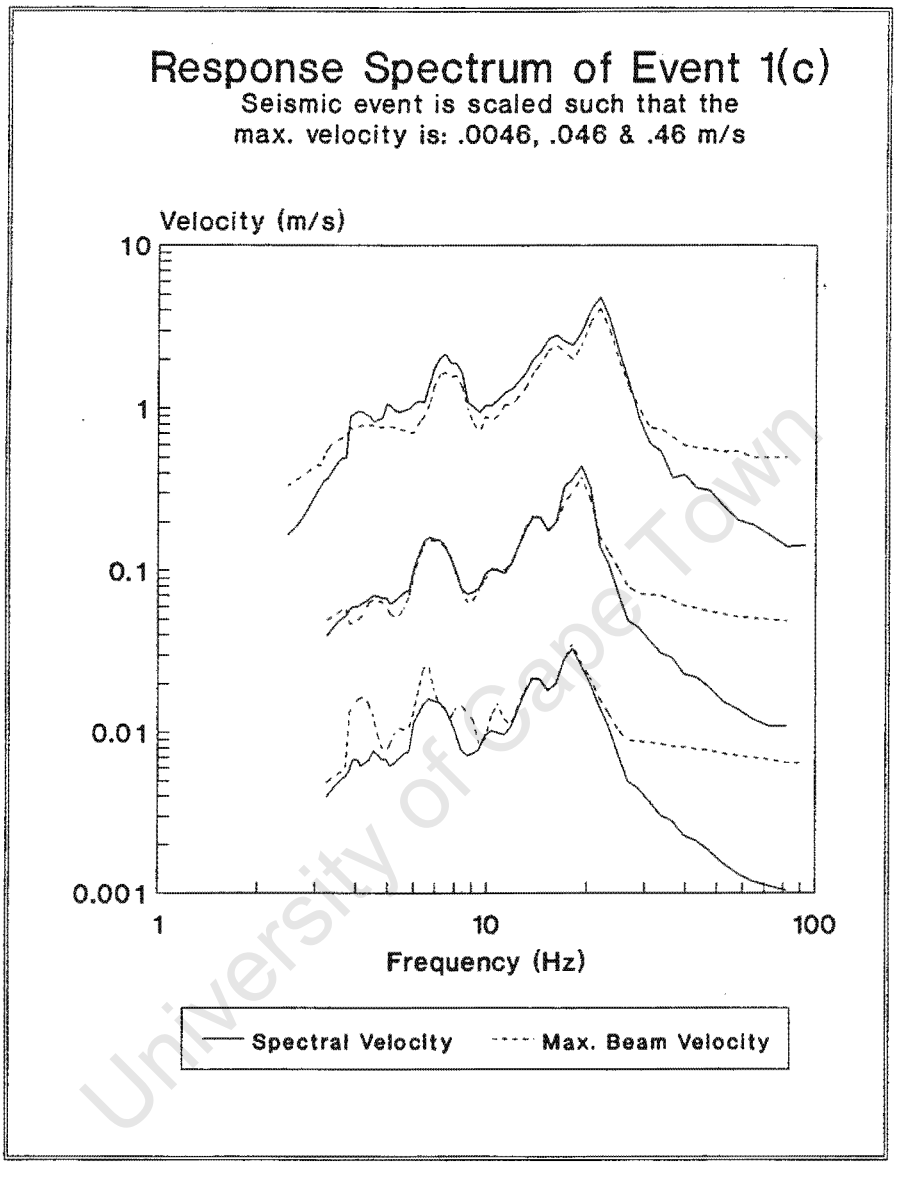

Figure 6.5: The difference between the spectral and actual hangingwall velocity.

Figure 6.5 compares the spectral velocity with the actual velocity of a fractured hangingwall beam when excited by Event 1(c). In order to make a direct comparison the spectral velocity has not been divided by the normalising coefficient ($\gamma_1\phi_1 = 1.319$). To obtain the comparison for a wide range of seismic magnitudes, Event 1(c) is scaled by three factors such that the maximum event velocity is 0.0046, 0.046 and 0.46 m/s. It is apparent that, in the area of interest of the response spectrum, the actual velocity of the beam compares favourably with the spectral velocity. This holds for a wide range of velocities and the maximum spectral velocity is thus an excellent gauge of the damage potential of a seismic event.

6.4 Summary

The graphs presented in this chapter allow beam lengths to be related to the frequency scaled on the response spectrum abscissa, and frequency and spectral velocity shifts to be estimated. The spectral shifts are quantified by comparing the response spectrum of the fractured hangingwall beam to the response spectrum of a SDOF system for 12–15 seismic events of varying magnitudes. An efficient technique has now been developed to extrapolate a SDOF response spectrum to estimate the response of a fractured hangingwall beam.

Chapter 7

Response of Hangingwall Supported by Backfill

Stope support can either be applied at particular points as in the case of conventional support, or it can be continuous as in the case of backfill. The South African mining industry used backfill as a stope supporting medium as early as 1910. Backfill was then successfully employed at relatively shallow depths. However, as mining depth increased, seismicity became a major problem and, due to a poor appreciation of the mechanics of backfill, the use of backfill was discontinued in the 1940s (Kirsten *et al.* [43]). It has recently been reintroduced with the objective of reducing seismicity and enhancing stope safety.

Backfill can improve stope safety by providing both local and regional support. Local support is defined as the effect of backfill on the stability of the hangingwall between the backfill and the stope face. An understanding of local support offered by backfill is required to optimize the conventional support used in the working area. Regional support of backfill influences the behaviour of the rock mass surrounding the excavation area. It has been shown that the regional support provided by backfill can reduce the number and size of seismic events.

The most important attributes of backfill are the continuity of support and the exponential increase in stiffness when subjected to compression. Various authors have concluded that, in these two respects, conventional support cannot provide the stability of which backfill is capable.

Gürtunca *et al.* [44] presented the results obtained from a rock-engineering monitoring program carried out at West Driefontein gold mine. Dewatered and classified tailings had been used as backfills for local and regional support. The underground observation showed less rockburst damage in backfilled stopes than in unfilled stopes. He also determined

closure rates to be significantly lower in filled stopes compared with unfilled stopes.

Kirsten and Stacey [45] showed that, as regional support offered by backfilled stopes reduces closure when compared with conventionally supported stopes, seismic activity in the vicinity of backfilled stopes is reduced. They also postulated that the partial transmission of seismic energy through backfill can be interpreted as a stabilizing criterion and that hangingwall beam vibrations are reduced by the damping characteristics of backfill. These three aspects are a consequence of the regional support provided by backfill and can reduce the motions attained by the hangingwall during seismic events.

In another paper Kirsten *et al.* [43] emphasised the importance of backfill preventing the falling out of potentially unstable blocks in the filled areas. This insures the structural integrity of the complete hangingwall beam and therefore increases the hangingwall stability above the working area.

In a study by Goldbach [46] it was shown that backfill reduces the ground motion of seismic events. In particular he determined, by means of a spectral analysis, that backfill had reduced the length of unsupported stope beams from $30m$ for a conventionally supported stope to $10m$ for a backfilled stope. A shorter beam resonates at higher frequencies where, for large seismic events, less seismic energy is present. Goldbach also noticed that seismic events dissipated four times faster in a backfilled stope than in an unfilled stope. This was concluded to be due to the efficient transmission of seismic energy as a consequence of the reduced beam length and the closing of hangingwall fractures by large vertical backfill stresses.

Klokow [47] claimed reduced accident rates (up to 60%) and rockburst damage in extensively backfilled stopes.

A study by Hemp *et al.* [48] investigated the seismicity at three different sites during mining with and without backfill. An attempt was made to evaluate the efficacy of backfill as a regional support in reducing seismicity. The investigation highlighted the difficulty of assessing backfill performance because of the influence geological inconsistencies have on seismicity. Nevertheless, the results from this study indicated that in some cases the seismicity had been reduced by backfilling the stopes.

Gay *et al.* [49] studied the seismicity of filled and unfilled stopes in West Driefontein gold mine. They concluded that, although more seismic events occurred in the backfilled stope than in the conventionally supported stope, the seismic events were smaller in magnitude. In filled stopes the seismic energy was released at a more uniform rate, whilst the energy release rate of unfilled stopes was irregular, with periods of relatively little seismicity interspersed by larger events. Again it was noted that more reliable data are required as inconsistent geology could have influenced the results.

Lenhart [50] concluded that backfill does not reduce seismicity when placed in stopes

excavated close to faults or dykes. However, the high vertical stresses generated by backfill were found to reduce the load on stabilizing pillars, thus preventing the edges of the pillars from exceeding the critical shear stress that would ultimately lead to foundation failure.

The work by the various authors has indicated that in general backfilled stopes experience less seismic activity. Further, the stability of the hangingwall beam is improved and hence stope safety is enhanced. This chapter attempts to quantitatively assess the superior stability of backfill supported hangingwall beams. The following section illustrates the numerical model used by the analyses. Sections 7.2 and 7.3 present the response of the hangingwall beams supported by dewatered and cemented backfills.

7.1 Numerical Model of Backfill Supported Hangingwall

Previous response spectra were constructed by determining the maximum displacement at the beam centre for beam halfspans varying from $3m$ to $23m$. In these analyses the shear fractures divided the beam into blocks of equal length.

The five shear fracture model is used to represent the backfill supported hangingwall. In backfill analyses the unfilled stope length remains constant and the hangingwall beam section representing the ceiling of the unfilled stope is represented by the two outermost, unfractured beam blocks. The total hangingwall beam length is varied by changing the length of the two inner blocks which are supported by backfill. The beam geometry is indicated in Figure 7.1.

The backfill is modelled by non-linear springs assuming backfill stress-strain characteristics in compression and zero stiffness in tension. As two beam blocks are supported by backfill, and each block of the five shear fracture model is discretised by two elements, the backfill springs are only applied to the five centre nodal points.

An important attribute of backfill is the substantial vertical stresses generated by the tailings when compressed by the overlying rock mass. As the stope closes, the hangingwall thus tends to be clamped between the backfill and the overlying rock strata. In the numerical model a force is applied to the three centre nodes to model the compression and hence the stope closure. The backfill immediately adjacent to the unfilled stope is not compressed as it is assumed the backfill in this region has just been inserted. Therefore stope closure in this region has not yet strained the backfill.

The compression, referred to in Figure 7.1 as *closure pressure*, is adjusted at the centre of the hangingwall beam for each beam length analysed, such that the closure rate at the beam centre is $10mm$ per metre of face advance. This is the closure rate of a typical deep-

the stope closure is assumed to be zero before any backfill is placed. This assumption is necessary to model the correct strain rate of the tailings as the stope is filled. Thus the total closure rate is calculated according to the length of the backfill supported beam section ($10mm$ per metre of backfilled stope).

Snyman *et al.* [51] used the finite element method to calculate the vertical backfill stress at various distances from the stope face. The closure pressure at nodes adjacent to the centre node is taken as 0.6 times the central closure pressure to obtain a vertical stress distribution which agrees with the results of Snyman.

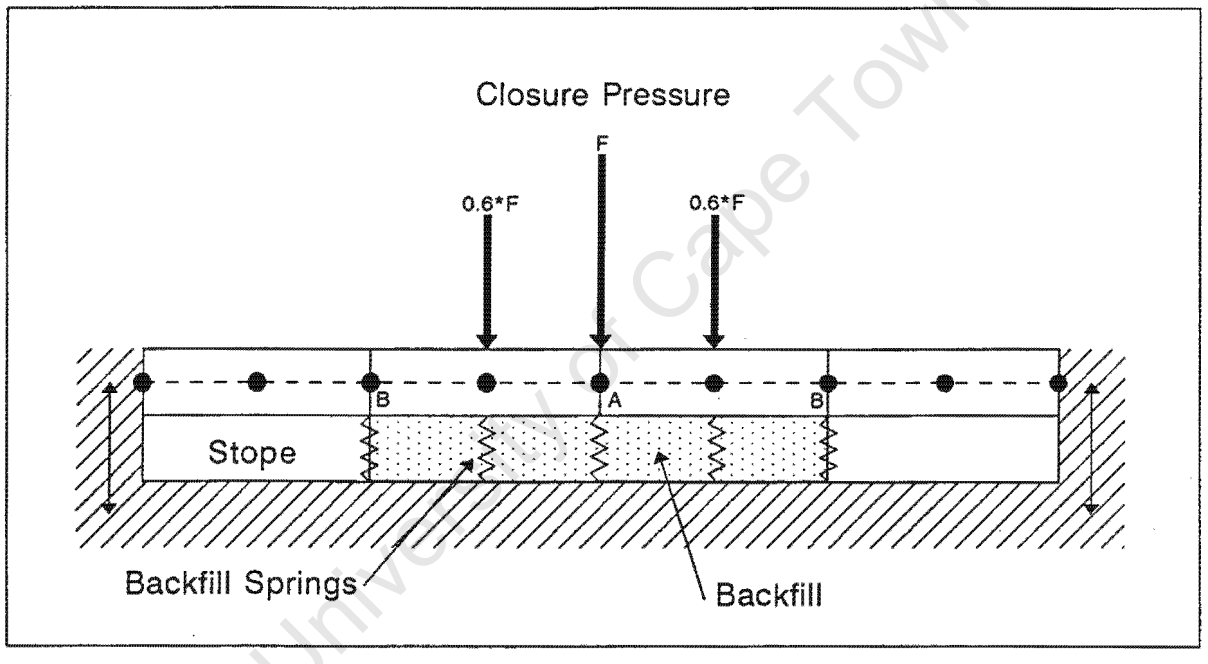

Figure 7.1: Beam model of backfill supported hangingwall.

The proposed model, although extremely simplified, will indicate trends regarding the global response of the backfill supported hangingwall beam. To determine the effect on local response (dynamic hangingwall behaviour between the face and the backfill), the five shear fracture model needs to be extended to incorporate additional shear fractures in the unsupported beam sections. However, this investigation is limited to the global behaviour of the five shear fracture model.

It is generally realised that the stress-strain behaviour of backfill has a marked effect on the dynamic hangingwall beam behaviour. To evaluate the performance of two types of backfill, the next two sections present the response of the hangingwall beam supported by comparatively soft dewatered tailings and much stiffer cemented tailings.

7.2 Hangingwall Response with Dewatered Tailings

This section determines the response of the hangingwall beam supported by dewatered tailings. The stress-strain relationship for dewatered tailings as proposed by Adams *et al.* [52], Roberts *at al.* [3] and Kirsten *et al.* [43] is given in the following figure.

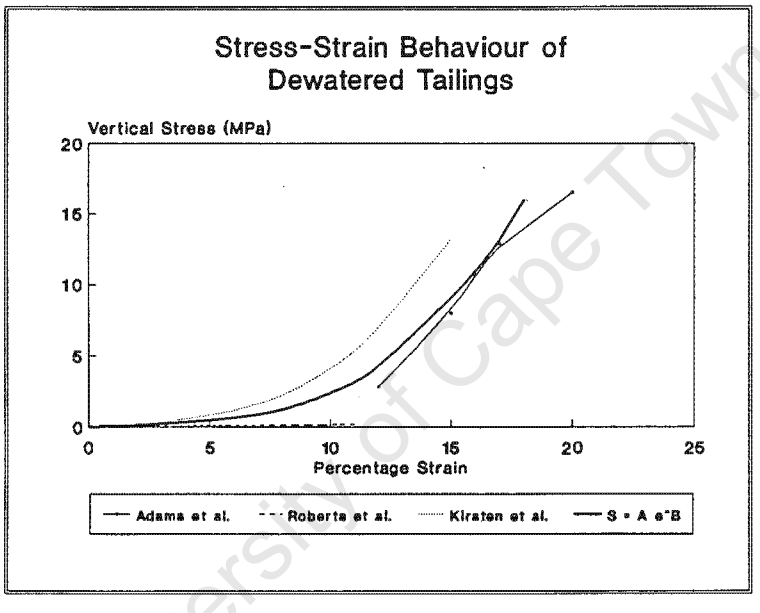

Figure 7.2: Stress-strain relationships of dewatered tailings as determined by Adams, Roberts and Kirsten. The mean used in this study is represented by the wide, solid line.

The stress-strain relationship used for this study is a mean of the relations determined by Adams *et al.*, Roberts *et al.* and Kirsten *et al.*, and is given by the following equation.

$$\sigma = 4500\epsilon^{3.3}$$

The hangingwall beam is excited by Event 1(c) and the response is determined for unfilled stope lengths of $4m$, $6m$ and $8m$. The following response spectrum compares the normalised response of the supported beams with the three shear fracture unsupported beam.

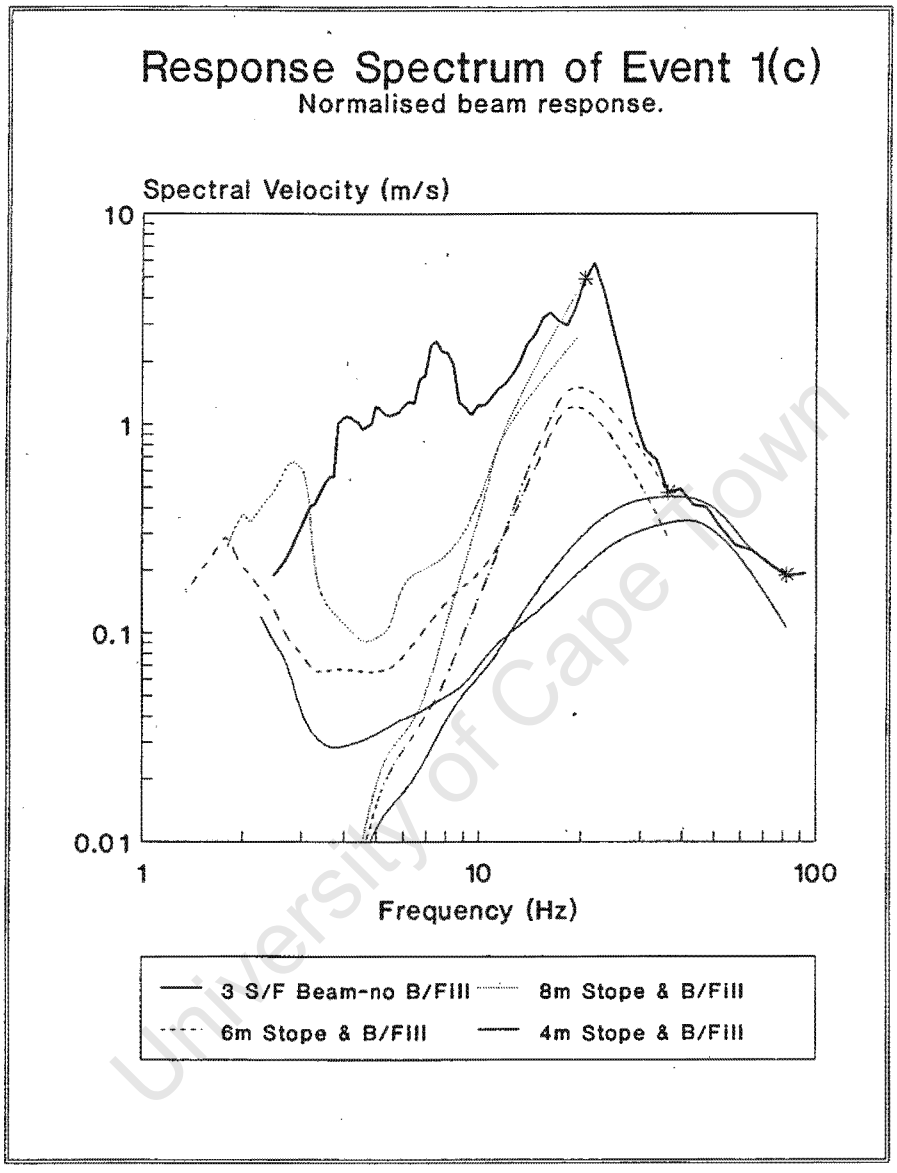

Figure 7.3: Response spectrum of hangingwall beam supported by dewatered tailings.

For each supported beam case, the maximum relative displacement is determined at two nodes: at the hangingwall beam centre (referred to as node A in Figure 7.1) and at the node positioned at the transition between backfill and the unfilled stope (referred to as node B). The points marked on the response spectrum by the stars indicate the maximum response of unsupported $4m$, $6m$ and $8m$ halfspan beams.

In all three cases, the response at node A for short backfilled sections is larger than the response of node B. This is because of the small stope closure associated with short beam lengths. At low strains, the backfill is soft and has not been sufficiently compressed to

restrain the motion of node A effectively. As the length of the backfilled stope section advances, the stope closure increases and the backfill is compressed, generating high vertical stresses such that node A is clamped and relative motion tends to zero. The maximum response occurs now at node B. For Event 1(c) the relative motion of node B decreases to a local minimum at approximately $4Hz$ before increasing again to a peak between $1Hz$ and $2Hz$. This last peak is probably due to resonating effects of the unsupported beam sections.

Two important conclusions can be drawn from Figure 7.3.

1. The effect of the exponential increase in backfill stiffness of dewatered tailings is apparent. For small stope closures the backfill is not compressed sufficiently to restrain the hangingwall beam motions effectively.

2. As the length of the unsupported stope increases, the hangingwall beam response escalates. Therefore, to reduce the hangingwall beam resonance effectively, the backfill needs to be placed as close to the stope face as possible. Short unfilled stope lengths are particularly important in the case of hangingwall beams supported by only a short section of backfill. This is because the backfill supporting the small beam sections is only compressed slightly by the low strains associated with small stope closure. Due to the exponential stress-strain behaviour of dewatered tailings, the low strain cannot generate sufficient vertical stresses to effectively pin the hangingwall beam.

   For Event 1(c) maximum seismic energy occurs at a frequency which excites an unsupported hangingwall with a halfspan of $7.5m$. Thus the backfill supported beam modelling an $8m$ unfilled stope exhibits large spectral velocities when analysed with only short beam sections supported by backfill. The response is only efficiently reduced after the total length on the supported beam sections exceeds about $7m$ (measured at a frequency of about $10Hz$).

Although stiff fills are required to reduce the size and number of seismic events (Kirsten *et al.* [43]), the actual developments in industry have taken place around relatively soft, hydraulically placed fills. This resulted from the urgent need to improve safety and stability of the working areas, and from successful application of softer tailings in early trials.

The limitations of soft fills due to shrinkage are apparent in this study. The response of hangingwall beams is not efficiently reduced when supported by backfill which does not generate substantial vertical stresses.

7.3 Hangingwall Response with Cemented Tailings

Unlike dewatered tailings, the shrinkage of cemented tailings is negligible. The in situ stress-strain behaviour of cemented tailings has been determined by COMRO and stresses of up to $2.3MPa$ were measured after only 2% strain (COMRO [53]). This is a markedly stiffer response than that exhibited by dewatered tailings analysed in the previous section. According to the stress-strain behaviour of cemented backfill documented by COMRO, the stress-strain relationship can be reasonably accurately represented as a linear function. In Figure 7.4 the stress-strain relationship of cemented tailings is compared to the behaviour of dewatered tailings. The much stiffer behaviour of cemented backfill at low strains is evident.

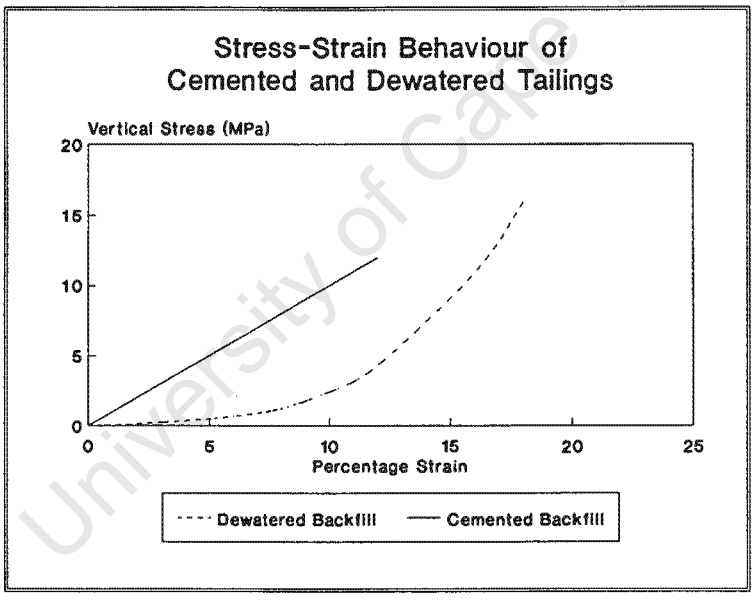

Figure 7.4: Stress-strain relationship of cemented and dewatered tailings used in numerical analyses.

As in the previous section, the backfill supported hangingwall model is excited by Event 1(c). The response is determined for unfilled stope lengths of $4m$, $6m$ and $8m$. The response of the supported beams is compared to the three shear fracture beam response and is given in Figure 7.5.

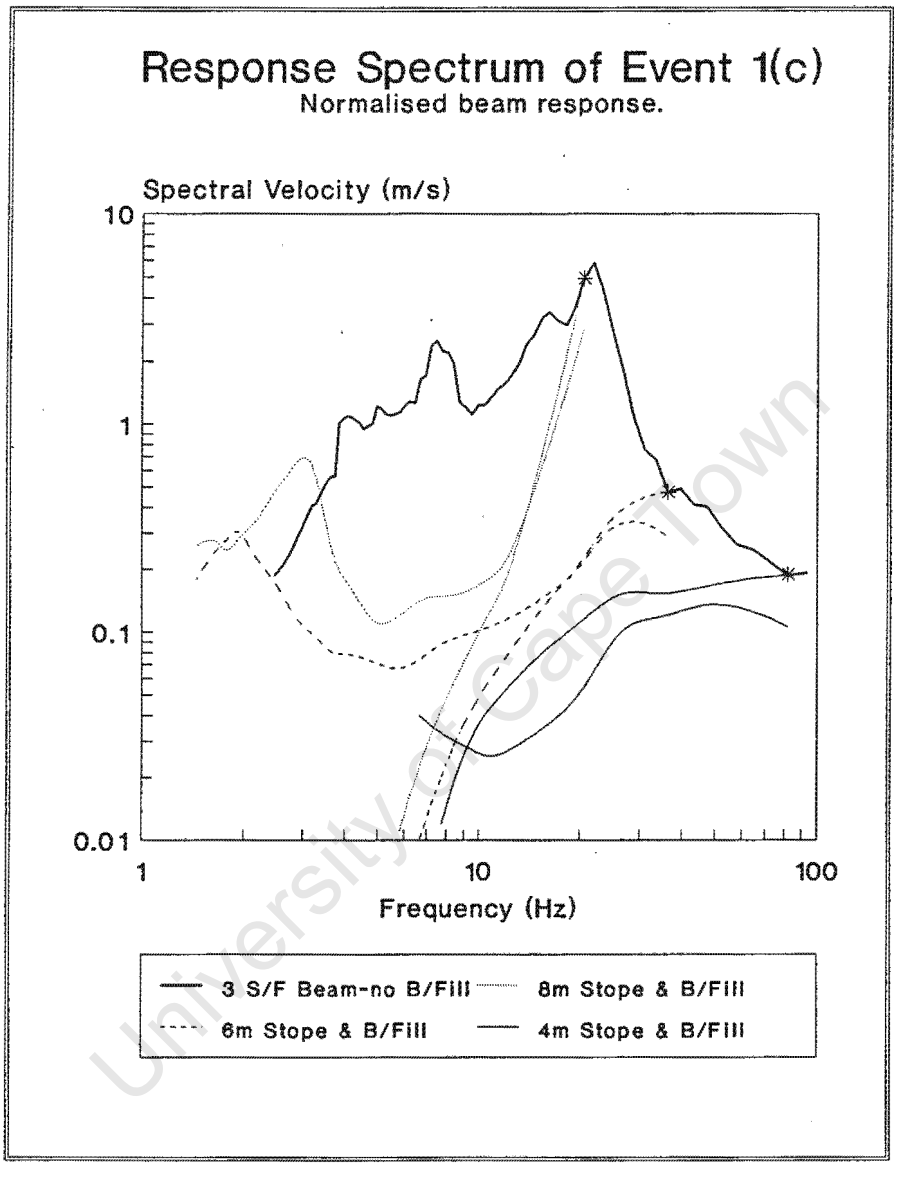

Figure 7.5: Response spectrum of hangingwall supported by cemented tailings.

By comparing the response of the hangingwall supported by cemented tailings with the hangingwall supported by dewatered tailings, the stiffer cemented backfill behaviour at low strains is evident. High vertical stresses generated by even small degrees of stope closure constrain the motions of the beam centre node appreciably.

The response of node B is also reduced for small stope closure. As the lengths of the supported beam sections increase, the response of node B supported by cemented fills becomes very similar to the response of the same node supported by dewatered tailings. This is due to the ability of both backfill types generating high vertical stresses at large

strains, thereby pinning the beam centre.

7.4 Summary

This chapter has compared the response of the hangingwall beam supported by two types of backfill, namely comparatively soft backfill consisting of dewatered tailings and much stiffer backfill consisting of cemented tailings. The beams are excited by a seismic event and the response is described with the aid of a response spectrum.

Two conclusions can be reached from backfill analyses. Firstly, the support provided by backfill is more effective when the fills are placed close to the stope face. Secondly, when the tailings are strained less than approximately 7%, support offered by the stiffer cemented backfills is superior to the support rendered by softer, dewatered tailings.

The backfill analyses presented in this chapter indicate trends. To gain a greater understanding of backfill performance, it is recommended that a finer mesh model be adopted in order to apply backfill springs to more nodes. Additional shear fractures are required in the hangingwall block representing the hangingwall beam above the unfilled stope section. This would permit the assessment of local support provided by backfill.

Chapter 8

Design Recommendations and Conclusions

This chapter commences by giving a short review of the work done in this investigation. Subsequent sections propose hangingwall beam design recommendations and draw conclusions in view of the findings of the report.

The objective of this study was to analyse the global response of the hangingwall beam during seismicity. To evaluate the global response, an insight into the resonating behaviour of the hangingwall beam is required. Localised failure, such as shearing or crushing of rock at the shear fractures, is not considered in this investigation.

A finite element program was developed to determine the response of the hangingwall beam excited by a seismic event. The maximum beam response is normalised, thus allowing the response spectrum method to describe the maximum response of the hangingwall beam. The response spectrum is a valuable tool to indicate, for a specific seismic event, the maximum beam response for a wide range of beam lengths. It is therefore straightforward to assess the critical hangingwall beam length which, due to resonance, exhibits the maximum response.

Unlike the construction of the hangingwall beam response spectrum, the assembly of a SDOF response spectrum is computationally cheap and a general practice in earthquake engineering. Chapter 6 has shown that the SDOF response spectrum can easily be extrapolated to accurately predict the response of the hangingwall beam. Thus the seismologist can apply the empirical rules developed in Chapter 6 and extrapolate the SDOF response spectrum to predict critical beam lengths prone to resonance and maximum hangingwall beam motions.

The response of the hangingwall supported by two types of backfill was investigated

in Chapter 7. The response was found to be considerably reduced when the backfill is packed close to the stope face. At small strains, the stiffer cemented tailings provided superior support than offered by the softer dewatered tailings.

8.1 Hangingwall Beam Design Recommendations

This investigation has proposed a method to extrapolate a SDOF response spectrum to the response spectrum of the hangingwall beam. The following list suggests a procedure to obtain the maximum hangingwall beam response given the ground motion histories of a seismic event.

1. The ground motion histories of a seismic event are processed to obtain the response spectrum describing a SDOF system with 0% damping. Establishing the response spectrum is standard practice in earthquake engineering and can be accomplished with the help of a personal computer.

2. The SDOF response spectrum is now shifted according to the empirical rules defined in Chapter 6.

   - Frequency shift: The response spectrum is shifted to the higher frequency range by moving each point defining the spectrum to the frequency stipulated by the chart in Figure 6.2. If the maximum event velocity exceeds 0.05m/s, the new frequency to which each response spectrum point is shifted needs to be multiplied by the shift factor. The shift factor is defined in Figure 6.3 and is given for a hangingwall damped by 0% and 10%.
   - Velocity shift: The spectral velocity of the SDOF response spectrum is multiplied by the shift factor given by Figure 6.4. The shift factor is defined for a 0% and 10% damped hangingwall beam and is given for a wide range of maximum earthquake velocities.

3. The maximum spectral velocity of the shifted response spectrum indicates the critical beam length which, for the event analysed, is most prone to resonance and therefore experiences the largest velocities. Using Figure 6.1 the frequency with the maximum spectral velocity can be converted to halfspan length, thereby establishing the critical beam length.

4. The spectral velocity displayed by the shifted response spectrum represents normalised spectral velocity. To determine the actual spectral velocity, the velocity indicated by the shifted response spectrum needs to be multiplied by the normalising factor (normalising factor: $\gamma_1\phi_1 = 1.319$). The actual spectral velocity has been

shown to be representative of the true beam velocity and is therefore an excellent indicator of the damage potential of a seismic event. Velocities in excess of $2m/s$ are generally considered particularly damaging.

Up to this stage, only unsupported hangingwall beams were investigated. Chapter 7 formulates a simple numerical model to analyse the performance of two types of backfill consisting of dewatered tailings and cemented tailings. In this study the beam response is markedly reduced when backfill is placed close to the face. Kirsten and Stacey [54] recommended backfill to be placed not further than $5m$ away from the stope face. For Event 1(c) analysed in Chapter 7 a fill-to-face lag of less than $5m$ would reduce the maximum hangingwall beam motions considerably. Thus, in view of the proposal by Kirsten and Stacey and results of the numerical backfill analyses, it is recommended that a fill-to-face lag of less than $5m$ be maintained. It is further recommended that the superior support offered by cemented tailings be utilised, rather than the support provided by the softer, dewatered fills.

Spottiswoode determined a relationship between corner frequency and event magnitude (Figure 4.2). The relationship is used to predict the critical beam length prone to resonance for a range of event magnitudes. This is accomplished by shifting the corner frequency for various event magnitudes according to the relation expressed by the chart in Figure 6.2. The shift factor is determined from the peak event velocities as predicted by Spottiswoode (Figure 4.1) at hypocentral distances of $50m$ and $100m$. The shifted corner frequency is multiplied by the shift factor to determine the correct critical beam lengths for various event magnitudes. Critical beam lengths are calculated for 0% and 10% damped hangingwall beams. Figure 8.1 displays the relationship between the critical beam length and event magnitude.

For small seismic events, the maximum event velocity is less than $0.05m/s$ and the shift factor is 1. Therefore the four cases presented in Figure 8.1 converge to the same line as the event magnitude decreases. For larger events, the maximum event velocity – and therefore the shift factor – increases and thus the lines representing the four cases diverge. The corner frequency of the event exciting the hangingwall beam with the highest velocities (hypocentral distance=$50m$, 0% damping case) is shifted the most; hence the critical beam length prone to resonance for this case is shorter than predicted by the other three cases.

However, although the maximum event velocities at a $50m$ hypocentral distance are twice the velocities of the $100m$ hypocentral distance case, the critical beam length does not vary significantly. For example, the difference in critical beam lengths excited by a magnitude 4 event is on average only 4% when comparing the 0% and 10% damping cases. Below an event magnitude of 3, the critical beam lengths predicted by the four cases can be considered to be equal.

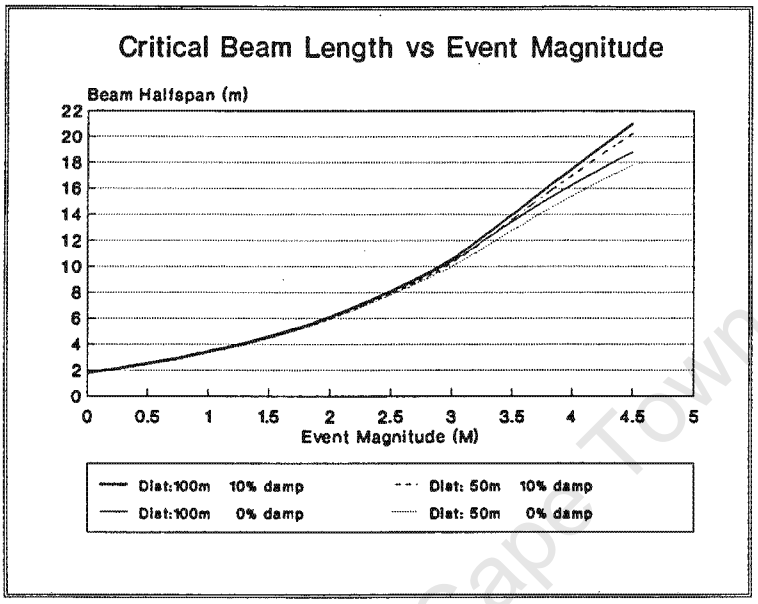

Figure 8.1: Relationship between critical beam length and event magnitude. The relation is given for four cases: $100m$ hypocentral distance with 0% and 10% damping and $50m$ hypocentral distance with 0% and 10% damping.

McGarr [33] concluded that tremors of magnitude greater than 2.5 generally cause appreciable underground damage. In an attempt to enhance stope safety, design criteria can be stipulated to safeguard against resonance of hangingwall beams during seismic events of magnitude 2.5 or greater. Utilising Figure 8.1 it is evident that, to limit resonance, the hangingwall beam halfspan must be less than $8m$ long.

8.2 Conclusions

This study entailed the numerical modelling of the isolated hangingwall beam during a seismic event. In spite of the simplified and idealised nature of the numerical hangingwall beam model, the following broad conclusions can be drawn regarding the dynamic behaviour of the hangingwall during seismicity.

1. Empirical rules have been developed to extrapolate the response spectrum describing a SDOF system to accurately predict the response spectrum of the hangingwall beam. The hangingwall response spectrum can be utilised to estimate critical beam

lengths prone to resonance and the spectral velocities attained by the hangingwall at various beam lengths. The spectral velocity is a valuable indicator regarding the damage potential of a seismic event.

2. To curb hangingwall beam resonance during seismic events with a magnitude of 2.5 or larger, it is recommended that the maximum hangingwall halfspan is limited to $8m$.

3. Cemented tailings provide superior support to the support offered by comparatively soft dewatered tailings. This is particularly apparent when the backfill has been strained less than 7%.

4. Backfill can significantly reduce the hangingwall beam motions by placing the tailings close to the stope face. A fill-to-face lag not exceeding $5m$ is recommended.

The finite element model analysed in this study is discretised by 8 beam elements along the length of the hangingwall beam. The discretisation is sufficiently refined to accurately model the global response of the unsupported hangingwall. However, to evaluate the efficacy of support, it is desirable to model the hangingwall beam with as many elements as are computationally viable. This permits the support stiffness provided by backfill and conventional support to be applied at added nodes, thereby creating a more realistic numerical model than analysed in this investigation. Further, when evaluating backfill it is recommended that at least one additional shear fracture be incorporated in the hangingwall beam section over the unfilled stope.

In view of these findings it is recommended that future work be undertaken to extend the numerical model to include additional elements and shear fractures. The extended model would facilitate a detailed comparison of the dynamic response of a backfill with a conventionally supported hangingwall.

Bibliography

[1] R. HEUNIS. The development of rock-burst control strategies for South African gold mines. *J. S. Afr. Inst. Min. Metall.*, **80**(4):139–149, April 1980.

[2] H. WAGNER. Support requirements for rockburst conditions. In N.C. Gay and E.H. Wainwright, editors, *Proceedings of the 1st International Congress on Rockbursts and Seismicity in Mines*, pages 209–218, SAIMM, Johannesburg, 1982.

[3] M.K. ROBERTS and R.K. BRUMMER. Support requirements in rockburst conditions. *J. S. Afr. Inst. Min. Metall.*, **88**(3):97–104, March 1988.

[4] M.F. SNYMAN and J.B. MARTIN. *The influence of horizontal and vertical discontinuities near a deep tabular excavation in rock.* Technical Report 181, CERECAM, University of Cape Town, March 1992.

[5] R.K. BRUMMER. *Fractures and deformation at the edges of tabular gold mining excavations.* PhD thesis, Randse Afrikaanse Universiteit, 1987.

[6] W.H. EVANS. The strength of undermined strata. *Trans. Inst. Mining and Metallurgy*, **50**:475–500, 1941.

[7] B.H.G. BRADY and E.T. BROWN. *Rock Mechanics for Underground Mining.* George Allen and Unwin, 1985.

[8] N.A. de VILLIERS. *Beam models for the hangingwall of deep, tabular excavations in stratified rock.* MSc (Eng) thesis, University of Cape Town, 1989.

[9] K. SEPHER and B. STRIMPSON. Roof deflections and sag in jointed, horizontally bedded strata – a numerical study. *Rock Mechanics and Rock Engineering*, **21**:207–218, 1988.

[10] M.J. PENDER. Prefailure joint dilatancy and the behaviour of a beam with vertical joints. *Rock Mechanics and Rock Engineering*, **18**:253–266, 1985.

[11] P.C. JOUGHIN. *Analysis of the dynamic behaviour of the stope hangingwall in a deep mine.* MSc (Eng) thesis, University of Cape Town, 1989.

[12] J.F. HALL and M.J. DOWLING. Response of jointed arches to earthquake excitation. *Earthquake Eng. Struct. Dyn.*, **13**(6):779–798, Nov.–Dec. 1985.

[13] G.L. FENVES, S. MOJTAHEDI, and R.B.REIMER. Effect of contraction joints on earthquake response of an arch dam. *J. of Struct. Eng.*, **118**(4):1039–1055, April 1992.

[14] N.W. NEWMARK and E. ROSENBLUETH. *Fundamentals of Earthquake Engineering.* Prentice-Hall (INC.), 1971.

[15] *An Introduction to ABAQUS/Explicit.* Hibbitt, Karlsson and Sorensen, Inc.

[16] *ABAQUS Users Manual.* Hibbitt, Karlsson and Sorensen, Inc.

[17] D.J. DAWE. *Matrix and Finite Element Displacement Analysis of Structures.* Claredon Press, 1984.

[18] M. PAZ. *Structural Dynamics, Theory and Computation.* Van Nostrand Reinhold Company, 1980.

[19] K.J. BATHE and E.L. WILSON. *Numerical Methods in Finite Element Analysis.* Prentice Hall, 1976.

[20] R.D. COOK, D.S. MALKUS, and M.E. PLESHA. *Concepts and Applications of Finite Element Analysis.* John Wiley and Sons, third edition, 1989.

[21] D.S. BURNETT. *Finite Element Analysis.* Addison-Wesley Publishing Company, 1986.

[22] N.G.W. COOK. Seismicity associated with mining. *Eng. Geology*, **10**:99–122, 1976.

[23] A. McGARR. Violent deformation of rocks near deep-level, tabular excavations—seismic events. *Bull. Seism. Soc. of America*, **61**(5):1453–1466, October 1971.

[24] A. McGARR. Analysis of peak ground motion in terms of a model of inhomogeneous faulting. *J. Geophys. Research*, **86**(B5):3901–3912, May 1981.

[25] N.G.W. COOK. The basic mechanics of rockbursts. In *Symposium on Rock Mechanics and Strata Control in Mines*, pages 56–66, J. S. Afr. Inst. Min. Metall., Johannesburg, April–June 1963.

[26] G.J. POTGIETER and C. ROERING. The influence of geology on the mechanisms of mining-associated seismicity in the Klerksdorp gold-field. In N.C. Gay and E.H. Wainwright, editors, *Proceedings of the* 1^{st} *International Congress on Rockbursts and Seismicity in Mines*, pages 45–49, SAIMM, Johannesburg, 1982.

[27] W.D. ORTLEPP. Rockbursts in South African gold mines: a phenomenological view. In N.C. Gay and E.H. Wainwright, editors, *Proceedings of the 1st International Congress on Rockbursts and Seismicity in Mines*, pages 165–178, SAIMM, Johannesburg, 1982.

[28] A.J. ROURKE and C. ROERING. Source mechanism studies of mine-induced seismic events in a deep-level gold mine. In N.C. Gay and E.H. Wainwright, editors, *Proceedings of the 1st International Congress on Rockbursts and Seismicity in Mines*, pages 51–55, SAIMM, Johannesburg, 1982.

[29] H.E.F. van ANTWERPEN and M.G. SPENGLER. The effect of mining related seismicity on excavations at East Rand Proprietary Mines, Limited. In N.C. Gay and E.H. Wainwright, editors, *Proceedings of the 1st International Congress on Rockbursts and Seismicity in Mines*, pages 235–243, SAIMM, Johannesburg, 1982.

[30] J.F. CURTIS. Rockburst phenomena in the gold mines of the Witwatersrand. *Inst. of Mining and Metall.*, **90**(Series A):163–176, October 1981.

[31] S.M. SPOTTISWOODE. Source mechanisms of mine tremors at Blyvooruitzicht Gold Mine. In N.C. Gay and E.H. Wainwright, editors, *Proceedings of the 1st International Congress on Rockbursts and Seismicity in Mines*, pages 29–37, SAIMM, Johannesburg, 1982.

[32] N.C. JOUGHIN. *The measurement and analysis of earth motion resulting from underground rock failure.* PhD thesis, University of Witwatersrand, 1961.

[33] A. McGARR. Some applications of seismic source studies to assessing underground hazard. In N.C. Gay and E.H. Wainwright, editors, *Proceedings of the 1st International Congress on Rockbursts and Seismicity in Mines*, pages 199–207, SAIMM, Johannesburg, 1982.

[34] A. McGARR, R.W.E. GREEN, and S.M. SPOTTISWOODE. Strong ground motion of mine tremors: some implications for near-source ground motion parameters. *Bull. Seism. Soc. of America*, **71**(1):295–319, February 1981.

[35] S.M. SPOTTISWOODE and J.M. CHURCHER. The effect of backfill on the transmission of seismic energy. In *Backfill in South African Mines*, pages 203–217, SAIMM, Johannesburg, 1988.

[36] E.P. DELIAC and N.C. GAY. The influence of stabilizing pillars on seismicity and rockbursts at ERPM. In N.C. Gay and E.H. Wainwright, editors, *Proceedings of the 1st International Congress on Rockbursts and Seismicity in Mines*, pages 257–263, SAIMM, Johannesburg, 1982.

[37] A.K. GUPTA. *Response Spectrum Method.* Blackwell Scientific Publications, 1990.

[38] D. HEMP. Documentation for seven seismic events. June 1992. Supplied by COMRO.

[39] L.M. FERNANDEZ and P.K. VAN DER HEEVER. Ground movement and damage accompanying a large seismic event in the Klerksdorp district. In N.C. Gay and E.H. Wainwright, editors, *Proceedings of the* 1^{st} *International Congress on Rockbursts and Seismicity in Mines*, pages 193–197, SAIMM, Johannesburg, 1982.

[40] L.M. FERNANDEZ. Frequency domain processing of strong motion accelerograms. *Geological Survey (Seismological Series)*, **15**, 1984.

[41] W.C. HURTY and M.F. RUBINSTEIN. *Dynamics of Structures.* Prentice-Hall (INC.), 1964.

[42] H. WAGNER. Discussion session 4 — Rockburst Damage. In N.C. Gay and E.H. Wainwright, editors, *Proceedings of the* 1^{st} *International Congress on Rockbursts and Seismicity in Mines*, page 220, SAIMM, Johannesburg, 1982.

[43] H.A.D. KIRSTEN and T.R. STACEY. Stress-displacement behaviour of fractured rock around a deep tabular stope of limited span. *J. S. Afr. Inst. Min. Metall.*, **89**(2):47–58, February 1989.

[44] R.G. GÜRTUNCA and D.J. ADAMS. A rock-engineering monitoring programme at West Driefontein gold mine. *J. S. Afr. Inst. Min. Metall.*, **91**(12):423–433, December 1991.

[45] H.A.D. KIRSTEN and T.R. STACEY. Hangingwall behaviour in tabular stopes subjected to seismic events. *J. S. Afr. Inst. Min. Metall.*, **88**(5):163–172, May 1988.

[46] O.D. GOLDBACH. *Ground motion studies in a backfilled stope at West Driefontein.* Technical Report 24/91, COMRO, October 1991.

[47] J.W. KLOKOW. Potential of new support and mining methods to reduce rock related accidents. *Mine Safety Digest*, **1**:6–8, January 1992.

[48] D.A. HEMP and O.D. GOLDBACH. *The influence of backfill on seismicity.* Technical Report 39/90, COMRO, September 1990.

[49] N.C. GAY, A.J. JAGER, and P.S. PIPER. Quantitative evaluation of fill performance in South African gold mines. In *Backfill in South African Mines*, SAIMM, Johannesburg, 1988.

[50] W.A. LENHART. Seismicity associated with deep-level mining at Western Deep Levels Limited. *J. S. Afr. Inst. Min. Metall.*, **92**(5):113–120, May 1992.

[51] M.F. SNYMAN, G.P. MITCHELL, and J.B. MARTIN. *The numerical simulation of excavations in deep level mining.* Technical Report 164, CERECAM, University of Cape Town, June 1991.

[52] D.J. ADAMS, R.G. GÜRTUNCA, and A.P. SQUELCH. The three-dimensional in situ behaviour of backfill materials. In *Paper presented at the* 7^{th} *International Congress on Rock Mechanics*, Aachen, Germany, 1991.

[53] COMRO. *Annual report 1991.* Technical Report, COMRO, 1991.

[54] H.A.D. KIRSTEN and T.R. STACEY. Destabilising effects of seismic disturbances on fractured rock surrounding tabular stopes. In *Proceedings of the* 2^{nd} *International Congress on Rockbursts and Seismicity in Mines*, pages 541–554, University of Minnesota, Minnesota, 1988.

Appendix A

Code of Program BLKBEAM

APPENDIX A. CODE OF PROGRAM BLKBEAM

```
      Program BLKBEAM
c*************************************************************
c                  B E A M  S O L U T I O N
c                       point masses
c
c                    FIVE  SHEAR  FRACTURES
c
c                      EXPLICIT SOLUTION
c
c*************************************************************
c
      implicit real * 8 (A-H,O-Z)
      dimension EK(30,30),EFK(30),EM(30,30),EFF(30),FG(30),CG(30,30)
      dimension UD(30,4),UV(30),UA(30),CL(30,30)
      dimension SK(30,30),ST(30,30),GGK(30,30),UX(30)
      dimension GK(30,30),TTT(30,30),GGKK(30,30),ID(30),CCGG(30,30)
      dimension X(30,30),EIGV(30),D(30),DMAX(12),VMAX(12),AMAX(12)
      dimension ISP(5),ZETASP(5),Q(1000,2)
c
c*************************************************************
c
c---  Logical unit number of output file:
      LUN = 70
c
c---  Length of unsupported region of stope:
      BLUN = 4.00
c
c---  Specify scanning data
      BLMIN =  4
      BLMAX =  30.0
c---  No. of beam lengths in interval to be sampled:
      BLINTER =  52

c---  Enter damping ratio: ZETA
       ZETALD = 0.10
c
c
c---  specify seismic data
c---  Enter amplitude of ground motion:
      AMP = 0.0
c
c---  Enter max. time to be analysed:
      TQMAX = 1.5
c
c*************************************************************
c*************************************************************
c
c---  Specify material properties and H/B dimensions
      E = 70.0D9
      DM = 2700 * 1.00
c
      DBL = (BLMAX - BLMIN)/BLINTER
c
c
      BL = BLMIN
c
c
c---  Open seismic data file
      open(19,file='TQUAKE1.DAT',status='old')
c
```

```
      read(19,*)NDATA
      read(19,*)
      do 101 I = 1,NDATA
        read(19,*)Q(I,1),Q(I,2)
101   continue
c
      close(19)
c
c
c---  L O O P   over beam length domain:
c

3     continue
c
      BL = DBL + BL
c
c---  Specify length of centre beam segment:
      BLEND = BL - BLUN
c
c
c      HERZ = DW + HERZ
c      W = HERZ * 2*3.141592654
c
c---  specify time stepping data
      DT = 0.0
      T = 0.0
c
c---  set initial conditions
c
c
      U5MAX = 0.0
      U11MAX = 0.0
      U3STAT = 0.0
      U5STAT = 0.0
      U9STAT = 0.0
      U11STAT = 0.0
      COUNT = 1
      TDUMAX = 0.0
      UOM = 0.0
      NJAC = 0
      ICRASH = 0
      NN = 1
      IFLAG = 0
      IAFLAG = 0
      TEQ = 10.0
      HERZM = 0.0
      HMIN = 100000.0
c
      do 5 I=1,11
       do 5 J=1,4
          UD(I,J) = 0.0
5     continue
c
c
      do 201 I = 1,12
        DMAX(I) = 0.0
        VMAX(I) = 0.0
        AMAX(I) = 0.0
201   continue
c
c---  Specify nodal coordinates:
      UX(1) = 0
```

```
      UX(2) = (BL-BLEND) * 0.5
      UX(3) = 0
      UX(4) = (BL-BLEND)
      UX(5) = 0
      UX(6) = (BL-BLEND)
      UX(7) = 0
      UX(8) = (BL-BLEND) + BLEND*0.5
      UX(9) = 0
      UX(10) = BL
      UX(11) = 0
c
c---  L O O P   over time domain
c

10    continue

c
c---  Zero global stiffness matrix:
      do 120 I = 1,30
      do 120 J = 1,30
120    GGK(I,J) = 0.0
c
c
c---  Damping fractions as beam is loaded
      ZETA = 0.60
      ZETAEX = 1.0
c
c
c---  Calculate time required for beam to be in equilibrium:
      if ( T.gt.0.01 .and. TEQ.eq.10 ) then
        TOLA = 0.00001
        TOLV = 0.0000001
        if ( DABS(UA(11)).lt.TOLA .and. DABS(UV(11)).lt.TOLV ) TEQ=T
      endif
c
c
c
c
      TMAX = TEQ+TQMAX
c
c
      call CHECKSP(UD,ISP,ZETASP,IFLAG,BL,T,DT)
c
c---  Specify the ground motion:
c      UOM = AMP * DSIN(W*T)
c
c---  Find max. displacement of DOF 11&5 when beam is in equil.
      if (T.lt.TEQ) U11STAT = UD(11,1)
      if (T.lt.TEQ) U9STAT  = UD(9,1)
      if (T.lt.TEQ) U5STAT  = UD(5,1)
      if (T.lt.TEQ) U3STAT  = UD(3,1)
c
c---  Specify earthquake motion:
      if ( T.gt.TEQ ) then
111     continue
        if( (T-TEQ).ge.Q(NN,1) .and. (T-TEQ).lt.Q( (NN+1),1) )then
          UOM = ( (T-TEQ) -Q(NN,1))*(Q((NN+1),2)-Q(NN,2))/
     $          (Q((NN+1),1)-Q(NN,1)) + Q(NN,2)
        else
          NN = NN+1
          goto 111
        endif
```

```
        ZETA = ZETALD
        ZETAEX = 1.00
      endif
c
c
      call ASSELEM(UD,GGK,UX,E,UOM,BL,BLEND)
c
      call APPLYBC(GGK,ISP,N,GGKK,UD,UOM,BLEND)
c
      if ( NJAC.eq.0 )then
        call EIGEN(N,DM,BL,BLEND,ISP,GGKK,HERZM,HMIN,LUN)
        NJAC = NJAC+1
      endif
c
c
      if (TEQ.eq.T) then
        open(UNIT=LUN,STATUS='UNKNOWN')
        do 1021 I = 1,100000
1021      read(LUN,*,END=1111)
1111    continue
        write(LUN,*)'ISP(1/3/2)/H-min=',ISP(1),ISP(3),ISP(2),HMIN
        close(LUN)
      endif
c
c
      DT = 1 / (5.5*HERZM)
c
      call MADAFO(GGKK,N,ISP,ZETASP,DM,BL,ZETA,ZETAEX,UOM,
     $ BLUN,T,TEQ,SK,CL,EM,FG,NSOL,UD,HERZM,HMIN,BLEND,CSUP)
c
      call SOLVE(SK,CL,EM,FG,DT,T,NSOL,UD,UV,UA,ISP,CSUP,UOM)
c
      call OUTPUT(UD,UV,UA,ZETA,AMP,ISP,UOM,T,TMAX,LUN,
     $ HERZ,U5MAX,U11MAX,ICRASH,U5STAT,U11STAT,BL,TEQ,HMIN,BLEND,
     $ U3STAT,U9STAT)
c
c
c---  check if analysis complete
      if ( T.lt.TMAX. and. ICRASH.ne.1 ) goto 10
c
      if (BL.lt.BLMAX) goto 3
c
c
c
c
      end
c*************************************************************
c*************************************************************
      subroutine CHECKSP(UD,ISP,ZETASP,IFLAG,BL,T,DT)
c*************************************************************
c
c     This routine determines if the shear planes are open
c     and checks if the increment needs to be recycled.
c
c*************************************************************
      implicit real*8(A-H,O-Z)
      dimension UD(30,4),ISP(5),ZETASP(5)
c---  Check if shear planes are closed:
c
c
      IRCYCLE = 0
c
```

```
c
c---  First shear plane:
      ISP(1) = 1
c
c---  Must increment be recycled ??
      if ( UD(1,1).lt.0.0 ) then
        ISP(1) = 0
        IRCYCLE = 1
      endif
C
c
c---  Second shear plane:
      ISP(2) = 1
c
c---  Must increment be recycled ??
      if ( UD(10,1).gt.0.0 ) then
        ISP(2) = 0
        IRCYCLE = 1
      endif
c
c---  Third centre shear plane:
c
c--- Check only every second time increment if centre shear plane can
open:
c
c
      if (ISP(3).eq.0) then
        ICOUNT = ICOUNT+1
        if (ICOUNT.gt.2) ICOUNT = 0
        if (ICOUNT.lt.2) then
          ISP(3) = 0
        else
          ISP(3) = 1
        endif
        goto 1100
      endif
c
      ISP(3) = 1
c
1100  continue
c
c
      if ( UD(4,1).gt.UD(6,1) ) then
        ISP(3) = 0
        IRCYCLE = 1
      endif
c
c---  First increment: set ISP(3)=0 to calculate max. e-value.
      if (IFLAG.eq.0) then
        ISP(1) = 1
        ISP(2) = 1
        ISP(3) = 0
        IFLAG = 1
      endif
c
      if ( IRCYCLE.eq.1) then
         T = T - DT*0.99
        do 100 I = 1,11
          UD(I,1) = UD(I,2)
          UD(I,2) = UD(I,3)
          UD(I,3) = UD(I,4)
100       continue
```

```
      endif
c
c
c      ISP(1) = 0
c      ISP(3) = 0
c
c     ISP(2) = 0
c
      return
      end
c*************************************************************
c
      subroutine ASSELEM(UD,GGK,UX,E,UOM,BL,BLEND)
c*************************************************************
c
c     This routine calculates the element matrices and
c     assembles them into the global stiffness matrix.
c
c*************************************************************
      implicit real*8(A-H,O-Z)
      dimension UD(30,4),UX(30),EK(6,6),GGK(30,30)
c
c
      ZIOP = 0.0090
      ZICL = 0.011
c
      NEXSKIP = 0
      NSKIP = 0
c
      NELESP = 0
c---  Number of super elements to loop over:
      NSUP = 2
200   continue
      NELESP = NELESP + 1
c---  Loop over super elements:
      if (NELESP.le.NSUP) then
c
c
      NELE  = 0
c---  Specify number of elements to loop over
      NE = 4
100   continue
      NELE = NELE + 1
c:---  Loop over all elements in super element:
       if (NELE.le.NE) then
c
C
c---  The first element:
      if (NELE.eq.1) then
c
        if (NELESP.eq.1) then
          if ( UD(3,1).ge.(-UOM) ) then
c---        Beam hinges at base.
            DX = (UD(1,1)-0)
            DY = -0.5
          else
c---        Beam hinges at top.
            DX = (UD(1,1)-0)
            DY = 0.5
          endif
          ZI = ZICL * 10**( -5000*DABS(UD(1,1)) ) + ZIOP*0.5
        endif
```

```
c
        if (NELESP.eq.2) then
          if ( (UD(5,1)+UD(7,1)).ge.(UD(3,1)+UD(9,1)) ) then
c---        Beam hinges at top.
            DX = (  UD(6,1) - (UD(4,1)+UD(6,1))*0.5  )
            DY = 0.5
          else
c---        Beam hinges at base.
            DX = (  UD(6,1) - (UD(4,1)+UD(6,1))*0.5  )
            DY = -0.5
          endif
          ZI = ZICL * 10**( -5000*DABS(UD(6,1)-UD(4,1)) ) + ZIOP
        endif
c
        DL = (DX*DX + DY*DY)**0.5
        CO = DX/DL
        SI = DY/DL
        EL = 0.5
        goto 222
      endif
c
c
c---  The last element
      if (NELE.eq.NE) then
c
        if (NELESP.eq.2) then
          if ( UD(11,1).ge.UD(9,1) ) then
c---        Beam hinges at top.
            DX = (0-UD(10,1))
            DY = (-0.5)
          else
c---        Beam hinges at base.
            DX = (0-UD(10,1))
            DY = (0.5)
          endif
          ZI = ZICL * 10**( -5000*DABS(UD(10,1)) ) + ZIOP
        endif
c
        if (NELESP.eq.1) then
          if ( (UD(5,1)+UD(7,1)).ge.(UD(3,1)+UD(9,1)) ) then
c---        Beam hinges at top.
            DX = (  (UD(4,1)+UD(6,1))*0.5  -  UD(4,1)  )
            DY = -0.5
          else
c---        Beam hinges at base.
            DX = (  (UD(4,1)+UD(6,1))*0.5  -  UD(4,1)  )
            DY =  0.5
          endif
         ZI = ZICL * 10**( -5000*DABS(UD(4,1)-UD(6,1)) ) + ZIOP
        endif

        DL = (DX*DX + DY*DY)**0.5
        CO = DX/DL
        SI = DY/DL
        EL = 0.5
        goto 222
      endif
c
c---  Centre beam properties:
      if (NELESP.eq.1) then
c
        if (NELE.eq.2) then
```

```
          DX = ( UD(2,1)+UX(2) ) - ( UD(1,1)+UX(1) )
          DY = ( UD(3,1) - (-UOM) )
        else if (NELE.eq.3) then
          DX = ( UD(4,1)+UX(4) ) - ( UD(2,1)+UX(2) )
          DY = ( UD(5,1) - UD(3,1) )
        endif
c
        EL = (BL-BLEND) * 0.5
      endif
c
c
      if (NELESP.eq.2) then
c
        if (NELE.eq.2) then
          DX = ( UD(8,1)+UX(8) ) - ( UD(6,1)+UX(6) )
          DY = ( UD(9,1) - UD(7,1) )
        else if (NELE.eq.3) then
          DX = ( UD(10,1)+UX(10) ) - ( UD(8,1)+UX(8) )
          DY = ( UD(11,1) - UD(9,1) )
        endif
c
        EL = (BLEND) * 0.5
      endif
c
      DL = (DX*DX + DY*DY)**0.5
      CO = DX/DL
      SI = DY/DL
c      EL = BL*0.25
      ZI = 0.08333333333333
c
222   continue
c:
c---  assemble terms in element stiffness matrices:
      do 20 I = 1,6
      do 20 J = 1,6
20    EK(I,J) = 0.0
c
      EK(1,1) = E*CO*CO/EL + 12*E*ZI*SI*SI/EL**3
      EK(2,1) = (E/EL-12*E*ZI/EL**3)*CO*SI
      EK(3,1) = -6*E*ZI*SI/EL**2
      EK(4,1) = -EK(1,1)
      EK(5,1) = -EK(2,1)
      EK(6,1) =  EK(3,1)
c
      EK(2,2) = E*SI*SI/EL+12*E*ZI*CO*CO/EL**3
      EK(3,2) = 6*E*ZI*CO/EL**2
      EK(4,2) = -EK(2,1)
      EK(5,2) = -E*SI*SI/EL-12*E*ZI*CO*CO/EL**3
      EK(6,2) =  EK(3,2)
c
      EK(3,3) = 4*E*ZI/EL
      EK(4,3) = -EK(3,1)
      EK(5,3) = -EK(3,2)
      EK(6,3) = 2*E*ZI/EL
c
      EK(4,4) = EK(1,1)
      EK(5,4) = EK(2,1)
      EK(6,4) = -EK(3,1)
c
      EK(5,5) = EK(2,2)
      EK(6,5) = -EK(3,2)
c
```

```
      EK(6,6) = EK(3,3)
c
c
      do 400 I = 1,6
        do 400 J = 1,6
          EK(I,J) = EK(J,I)
400   continue
c
c
c      write(*,*)'nskip=',NSKIP
      NEXSKIP = 0
c --- Assemble terms in global stiffness matrix:
      if ( NELESP.eq.2 .and. NELE.eq.1 ) then
        do 133 I = 1,6
          do 133 J = 1,6
            if (I.le.2) II = I + NSKIP
            if (J.le.2) JJ = J + NSKIP
            if (I.gt.2) II = I + NSKIP + 1
            if (J.gt.2) JJ = J + NSKIP + 1
            GGK(II,JJ) = GGK(II,JJ) + EK(I,J)
133     continue
        NEXSKIP = 1
c
      else
c
        do 122  I = 1,6
          do 122 J = 1,6
          II = I + NSKIP
          JJ = J + NSKIP
          GGK(II,JJ) = GGK(II,JJ) + EK(I,J)
122     continue
      endif
c---  Close loop over elements
      NSKIP = NSKIP + 3 + NEXSKIP
      goto 100
      endif
c---  Close loop over super-elements
      goto 200
      endif
c
c     do 111 I = 1,35
c111    write(*,*)'GGK=',I,GGK(I,I)
c
      return
      end
c*************************************************************
c
      subroutine APPLYBC(GK,ISP,N,GGKK,UD,UOM,BLEND)
c*************************************************************
c
c     This routine applies the essential boundary conditions,
c     shifts the entries in the stiffness matrix and calls
c     the static condensation routine.
c
c*************************************************************
      implicit real*8(A-H,O-Z)
      dimension GK(30,30),ISP(5),ID(30),ST(30,30),GGKK(30,30)
      dimension EM(30,30),CG(30,30),TTT(30,30),UD(30,4)
c
c
c
c---  Apply the essential boundary conditions
```

```
      GK(1,1)  =  0.0
      GK(26,26) = 0.0
c
c
c---  B.C. if S/P 1 is closed:
c
      if ( ISP(1).eq.0 ) then
        GK(4,4) = 0.0
        GK(6,6) = 0.0
      endif
c
c---  B.C. if S/P 2 is closed:
      if ( ISP(2).eq.0 ) then
        GK(23,23) = 0.0
        GK(25,25) = 0.0
      endif
c
c
c
c---  Total DOF's before any BC's are applied:
      MTOT = 28
c
c
c---  Prepare matrix for the static condensation - swop row-columns:
c---  Independant DOF:
      M = MTOT
      do 325 I = 1,MTOT
        do 325 J = 1,MTOT
        ST(I,J) = GK(I,J)
325    continue
c
c---  Independant DOF's:
      ID(1)  = 2
      ID(2)  = 3
      ID(3)  = 6
      ID(4)  = 9
      ID(5)  = 12
      ID(6)  = 13
      ID(7)  = 14
      ID(8)  = 15
      ID(9)  = 16
      ID(10) = 19
      ID(11) = 22
      ID(12) = 25
      ID(13) = 27
      ID(14) = 28
      NCR = 14
c---  Dependant DOF's:
      ID(15) = 1
      ID(16) = 5
      ID(17) = 4
      ID(18) = 7
      ID(19) = 8
      ID(20) = 10
      ID(21) = 11
      ID(22) = 17
      ID(23) = 18
      ID(24) = 20
      ID(25) = 21
      ID(26) = 23
      ID(27) = 24
      ID(28) = 26
```

```
c---  Swop rows:
      do 126 I = 1,MTOT
        do 126 J = 1,MTOT
          GK(J,I) = ST( ID(J) , I )
126   continue
c
      do 235 I = 1,MTOT
        do 235 J = 1,MTOT
        ST(I,J) = GK(I,J)
235    continue
c
c---  Swop column:
      do 127 I = 1,MTOT
        do 127 J = 1,MTOT
          GK(I,J) = ST( I, ID(J) )
127    continue
c
c
      if (ISP(3).eq.0) then
c---    Row-Column operation if the centre shear fracture is closed:
c---    Want DOF's:   (20) = (22)     &     (5) = (10)
c
c---    1. DOF(20) = DOF(22)
c---    Column operator:
        do 147 I = 1,MTOT
          GK(I,20) = GK(I,20) + GK(I,22)
147     continue
c---    Zero column:
        do 148 I = 1,MTOT
            GK(I,22) = 0.0
148     continue
c
c---    Row operation
        do 149 I = 1,MTOT
          GK(20,I) = GK(20,I) + GK(22,I)
149     continue
c---    Zero row:
        do 150 I = 1,MTOT
           GK(22,I) = 0.0
150     continue
c
c
c---    1. DOF(5) = DOF(10)
c---    Column operator:
        do 157 I = 1,MTOT
          GK(I,5) = GK(I,5) + GK(I,10)
157     continue
c---    Shift matrix values:
        do 158 I = 1,MTOT
            GK(I,10) = 0.0
158     continue
c
c---    Row operation
        do 159 I = 1,MTOT
          GK(5,I) = GK(5,I) + GK(10,I)
159     continue
c---    Shift matrix values:
        do 160 I = 1,MTOT
            GK(10,I) = 0.0
160     continue
c
      endif
```

```
c
c---   Eliminate redundant DOF:
650    continue
       do 700 I = 1,MTOT
         if ( GK(I,I).eq.0.0 ) then
           MTOT = MTOT - 1
c---   Shift rows
           do 710 II = I,MTOT
             do 710 JJ = 1,MTOT+1
               GK(II,JJ) = GK(II+1,JJ)
710        continue
c---   Shift columns
           do 720 II = I,MTOT
             do 720 JJ = 1,MTOT+1
               GK(JJ,II) = GK(JJ,II+1)
720        continue
c
           do 730 K = I,MTOT
             ID(I) = ID(I+1)
730        continue
c
           if ( I.le.NCR) NCR = NCR - 1
c
           goto 650
         endif
700    continue
c
c
c
c---   Call static condensation routine:
c
c
       ND = MTOT
       NCRR = NCR
       call CONDES(ND,NCRR,GK,EM,CG,TTT,GGKK)
c
       N = MTOT - NCR - 1
c
c      write(*,*)'N= - MTOT= - NCR=',N,MTOT,NCR
c
       return
       end
c*************************************************************
c
c
       subroutine EIGEN(N,DM,BL,BLEND,ISP,GGKK,HERZM,HMIN,LUN)
c*************************************************************
c
c      This routine forms the mass matrix and
c      calls the Eigenvalue routine.
c
c*************************************************************
       implicit real*8(A-H,O-Z)
       dimension EM(30,30),ISP(5),GGKK(30,30),SK(30,30)
       dimension D(30),EIGV(30),X(30,30),HERZ(30)
c
c
c---   Determine the mass matrix:
       do 745 I = 1,11
         do 745 J = 1,11
         EM(I,J) = 0.0
745    continue
```

```
c
c
      EM(1,1) = (BL-BLEND)*0.5*0.5  *  DM
      EM(2,2) = (BL-BLEND)*0.5      *  DM
      EM(3,3) = EM(2,2)
      EM(4,4) = ( (BL-BLEND)*0.5*0.5 + BLEND*0.25 )  *  DM * 0.5
      EM(5,5) = EM(4,4)
      EM(6,6) = EM(4,4)
      EM(7,7) = EM(4,4)
      EM(8,8) = BLEND * 0.5 * DM
      EM(9,9) = EM(8,8)
      EM(10,10) = BLEND * 0.25 * DM
      EM(11,11) = EM(10,10)
c
c      do 1992 I = 1,11
c        write(*,*)'em=',EM(I,I)
c1992  continue
c
c
      if ( ISP(1).eq.0 ) then
        do 45 I = 1,10
          EM(I,I) = EM(I+1,I+1)
45      continue
        EM(11,11) = 0.0
      endif
c
c      do 1993 I = 1,11
c        write(*,*)'em=',EM(I,I)
c1993  continue
c
c
c
      if (ISP(3).eq.0 .and. ISP(1).eq.1) then
        EM(6,6) = EM(7,7)
        EM(7,7) = EM(8,8)
        EM(8,8) = EM(9,9)
        EM(9,9) = EM(10,10)
        EM(10,10) = EM(11,11)
        EM(11,11) = 0.0
      endif
c
      if (ISP(3).eq.0 .and. ISP(1).eq.0) then
        EM(5,5) = EM(6,6)
        EM(6,6) = EM(7,7)
        EM(7,7) = EM(8,8)
        EM(8,8) = EM(9,9)
        EM(9,9) = EM(10,10)
        EM(10,10) = EM(11,11)
        EM(11,11) = 0.0
      endif
c
c      do 1994 I = 1,11
c        write(*,*)'em=',EM(I,I)
c1994  continue
      if (ISP(2).eq.0) then
        EM(N,N) = EM(N+1,N+1)
        EM(N+1,N+1) = 0.0
      endif
c
c      write(*,*)'n=',N
c      do 1995 I = 1,11
c        write(*,*)'em=',EM(I,I)
```

```
c1995  continue
c---  Apply final boundary condition - specify ground motion of end
node:
      do 30 I = 1,N
        do 30 J = 1,N
        SK(I,J) = 0.0
c
30    continue
      do 33 I = 1,N
        do 33 J = 1,N
        SK(I,J) = GGKK(I+1,J+1)
33    continue
c
c     do 555 I = 1,N
c55   write(*,*)'sk=',I,SK(I,I),EM(I,I)
c---  Calculate the eigen values
      do 84 I = 1,30
      D(I) = 0
      EIGV(I) = 0
      do 84 J = 1,30
        X(I,J) = 0
84    continue
c
      IFPR = 0
      call JACOBI(SK,EM,X,EIGV,D,N,IFPR,HERZ,LUN)
c
c---  Get largest natural frequency:
      do 50 I = 1,N
        if ( HERZ(I).gt.HERZM ) HERZM = HERZ(I)
        if ( HERZ(I).lt.HMIN ) HMIN = HERZ(I)
50    continue
c
      open(LUN,access='SEQUENTIAL',status='UNKNOWN')
c
      do 1222 I = 1,100000
1222    read(LUN,*,END=1212)
1212  continue
c       .
      write(LUN,*)'*******************************'
      write(LUN,*)'Beam length=',BL,'B-END=',BLEND
      write(*,*)'Beam length=',BL,'B-END=',BLEND
      write(LUN,1000)HMIN,HERZM
c      do 55 I = 1,N
c        write(lun,1000)HERZ(I)
c55    continue
1000  format(2f10.3)
c
      close(LUN)
c
      return
      end
c*************************************************************


      subroutine MADAFO(GGKK,N,ISP,ZETASP,DM,BL,ZETA,ZETAEX,UOM,
     $ BLUN,T,TEQ,SK,CL,EM,FG,NSOL,UD,HERZM,HMIN,BLEND,CSUP)
c*************************************************************
c
c     This routine forms the mass, damping and force matrix.
c
c*************************************************************
      implicit real*8(A-H,O-Z)
      dimension SK(30,30),SSK(30,30),GGKK(30,30),ISP(5),ZETASP(5)
```

APPENDIX A. CODE OF PROGRAM BLKBEAM

```
      dimension CG(30,30),EM(30,30),CL(30,30),FG(30),UD(30,4)
      dimension FFG(30),FFGG(30),CSUP(30)
c
c
c---  No. of DOF's solved for:
      NSOL = 11
c
      do 333 I = 1,NSOL
        do 333 J = 1,NSOL
        SK(I,J) = 0.0
        SSK(I,J) = 0.0
333    continue
c
      do 330 I = 1,N
        do 330 J = 1,N
        SK(I,J) = GGKK(I+1,J+1)
        SSK(I,J) = GGKK(I+1,J+1)
330    continue
c
c
c---  Shift entries in stiffness matrix:
      if ( ISP(1).eq.0 ) then
        do 405 I = 2,NSOL
          do 405 J = 2,NSOL
            SK(I,J) = SSK(I-1,J-1)
405     continue
        do 407 I = 1,NSOL
            SK(I,1) = 0.0
            SK(1,I) = 0.0
407     continue
      endif
c
      do 222 I = 1,NSOL
        do 222 J = 1,NSOL
          SSK(I,J) = 0.0
          SSK(I,J) = SK(I,J)
222   continue
c
      if (ISP(3).eq.0) then
        do 455 I = 7,NSOL
          do 455 J = 7,NSOL
            SK(I,J) = SSK(I-1,J-1)
455     continue
c
        do 465 I = 1,6
          do 465 J = 6,NSOL-1
            SK(I,J+1) = SSK(I,J)
            SK(J+1,I) = SSK(J,I)
465     continue
c
        do 457 I = 1,NSOL
            SK(I,6) = 0.0
            SK(6,I) = 0.0
457     continue
      endif
c
c
      if ( ISP(2).eq.0 ) then
        do 410 I = 1,NSOL-2
            SK(11,I) = SK(10,I)
            SK(10,I) = 0.0
            SK(I,11) = SK(I,10)
```

```
            SK(I,10) = 0.0
410       continue
          SK(11,11) = SK(10,10)
          SK(10,10) = 0.0
          SK(10,11) = 0.0
          SK(11,10) = 0.0
        endif
c
c
c---    Determine entries in mass matrix:
        do 747 I = 1,NSOL
          do 747 J = 1,NSOL
          EM(I,J) = 0.0
747     continue
c
c
        EM(1,1) = (BL-BLEND)*0.5*0.5  *  DM
        EM(2,2) = (BL-BLEND)*0.5      *  DM
        EM(3,3) = EM(2,2)
        EM(4,4) = ( (BL-BLEND)*0.5*0.5 + BLEND*0.25 )  *  DM * 0.5
        EM(5,5) = EM(4,4)
        EM(6,6) = EM(4,4)
        EM(7,7) = EM(4,4)
        EM(8,8) = BLEND * 0.5 * DM
        EM(9,9) = EM(8,8)
        EM(10,10) = BLEND * 0.25 * DM
        EM(11,11) = EM(10,10)
c
c
c---    Detemine entries in capacity matrix:
c---    Calculate spectral damping coefficients:
        PI = 3.141592654
        W1 = 2*PI*HMIN
        W2 = 2*PI*HERZM
c---    Damping coefficients for the beam:
        ALPHA = 2*(ZETA*W2-ZETA*W1)/(W2*W2-W1*W1)
        BETA  = 2*W1*W2*(ZETA*W2-ZETA*W1)/(W2*W2-W1*W1)
c
c---    Calculate damping coefficients for shear fractures:
        ALPHAEX = 2*(ZETAEX*W2-ZETAEX*W1)/(W2*W2-W1*W1)
        BETAEX  = 2*W1*W2*(ZETAEX*W2-ZETAEX*W1)/(W2*W2-W1*W1)
c
c
c---    form global capacity matrix ( Raleigh damping ):
        do 58 I=1,NSOL
          do 58 J=1,NSOL
          CG(I,J) = ALPHA*SK(I,J) + BETA*EM(I,J)
58      continue
c
c
c---    Extra damping at shear fracture:
        CG(1,1) = CG(1,1) + ALPHAEX*SK(1,1) + BETAEX*EM(1,1)
        if ( UD(1,1).le.0.0) then
          CG(1,1) = CG(1,1) * 10
        endif
c
        CG(4,4) = CG(4,4) + ALPHAEX*SK(4,4) + BETAEX*EM(4,4)
        CG(6,6) = CG(6,6) + ALPHAEX*SK(6,6) + BETAEX*EM(6,6)
c
        CG(10,10) = CG(10,10) + ALPHAEX*SK(10,10) + BETAEX*EM(10,10)
        if ( UD(10,1).ge.0.000) then
          CG(10,10) = CG(10,10) * 10
```

```
      endif
c
c
c
c
      if (ISP(1).eq.0) EM(1,1) = 0.0
      if (ISP(2).eq.0) EM(10,10) = 0.0
      if (ISP(3).eq.0) then
        EM(6,6) = 0.0
        EM(4,4) = 2*EM(4,4)
      endif
c
c---  Zero lumped capacity matrix:
      do 49 I=1,NSOL
        do 49 J=1,NSOL
        CL(I,J) = 0.0
49    continue
c
c---  Lump the capacity matrix:
      do 59 I=1,NSOL
        do 59 J=1,NSOL
        CL(I,I) = CL(I,I) + CG(I,J)
59    continue
c
c
c---  Determine entries in force vector:
      do 60 I = 1,NSOL
      FG(I) = 0.0
      FFG(I) = 0.0
60    continue
c
c---  Gravity load:
      do 65 I = 1,5
        FG(I*2+1) =  EM(I*2+1,I*2+1) * 10
65    continue
c
c
c
c---  Call subroutine to implement support forces:
      call SUPPORT(UOM,FG,UD,BLEND,BL,T,TEQ,BLUN)
c
c
      GGKK(N+2,1) = 0.0
      GGKK(N+3,1) = 0.0
c
      do 666 I = 1,NSOL
        FFG(I) = GGKK(I+1,1)
666   continue
c
c---  Apply earthquake motion
      if (ISP(1).eq.0) then
        do 200 I = 1,NSOL-1
          FFG( I+1 ) = GGKK( (I+1),1 )
200     continue
        FFG(1) = 0.0
      endif
c
      do 777 I = 1,NSOL
        FFGG(I) = FFG(I)
777   continue
c
      if (ISP(3).eq.0) then
```

```
        do 300 I = 6,NSOL-1
          FFG(I+1) = FFGG(I)
300     continue
        FFG(6) = 0.0
      endif
c
      if (ISP(2).eq.0) then
          FFG(11) = FFG(10)
          FFG(10) = 0.0
      endif
c
c---  Current force values:
      do 166 I = 1,NSOL
         FG(I)=FG(I) - FFG(I)*(-UOM)
166   continue
c
      return
      end
c*************************************************************
c
      subroutine SUPPORT(UOM,FG,UD,BLEND,BL,T,TEQ,BLUN)
c*************************************************************
c
c     This routine implements the stope support.
c
c*************************************************************
      implicit real*8(A-H,O-Z)
c
      dimension FG(30),UD(30,4)
c
c
c
c---  Calculate backfill strain at DOF 11:
      STRAIN11 = UD(11,1) - (-UOM)
c
c---  Calculate backfill strain at DOF 9:
      STRAIN9  = UD(9,1) - (-UOM)
c
c---  Calculate backfill strain at DOF 7:
      STRAIN7  = UD(7,1) - (-UOM)
c
c
      if ( STRAIN11.lt.0.0 ) then
       STRAIN11 = 0.0
      endif
c
      if ( STRAIN9.lt.0.0 ) then
        STRAIN9 = 0.0
      endif
c
      if ( STRAIN7.lt.0.0 ) then
        STRAIN7 = 0.0
      endif
c
c---  Stiffness of backfill - dewatered tailings:
c---  'BACKK' is in KPa - take as support per square metre.
c
c---   Dewatered Tailings:
c      BACKK11 = 4500000 * ( STRAIN11**(3.30)  )
c      BACKK9  = 4500000 * ( STRAIN9**(3.30)  )
c      BACKK7  = 4500000 * ( STRAIN7**(3.30)  )
c
```

APPENDIX A. CODE OF PROGRAM BLKBEAM

```
c---   Cemented Tailings:
       BACK11 =  100000 * STRAIN11
       BACKK9  = 100000 * STRAIN9
       BACKK7  = 100000 * STRAIN7
c
      BACKK11 = BACKK11 * ( BL ) * 0.25
      BACKK9  = BACKK9  * ( BL ) * 0.50
      BACKK7  = BACKK7  * ( BL ) * 0.25
c
c
c---  Stipulate force compressing the backfill  in KPa
c---  Compress B-fill such that:
c---  Rate of stope closure = 10mm per metre of face advance:
      if (T.ge.TEQ) goto 2300
c
          BLCL = BL
c
      C2Q11 = DABS( (BLCL*0.01) - UD11P )
      C1Q11 = DABS( (BLCL*0.01) - UD(11,1) )
c
      C2Q9  = DABS( 1.0*(BLCL*0.01)  -  UD9P )
      C1Q9  = DABS( 1.0*(BLCL*0.01)  -  UD(9,1) )
c
c
      if ( C2Q11.lt.0.00001 .and. C1Q11.lt.0.00001 ) goto 2323
      COMPF11 = COMPF11 + ( (BLCL*0.01)-UD(11,1) ) * 100
      UD11P = UD(11,1)
2323  continue
c
c
2300  continue
c
      COMPF9 = COMPF11 * 2 * 0.6
c
c---  Resulting force (in Pa) acting at DOF 11 (downwards is positive):
      RESF11 = (COMPF11 - BACKK11) * 1000
c
c---  Resulting force (in Pa) acting at DOF 9 (downwards is positive):
      RESF9 = (COMPF9 - BACKK9) * 1000
c
c---  Resulting force (in Pa) acting at DOF 7 (downwards is positive):
      RESF7 = ( - BACKK7) * 1000
c
c---  Update force vector:
      FG(11) = FG(11) + RESF11
      FG(9) = FG(9) + RESF9
      FG(7) = FG(7) + RESF7
c
c
c
      return
      end
c*************************************************************
c
      subroutine SOLVE(SK,CL,EM,FG,DT,T,NSOL,UD,UV,UA,ISP,CSUP,UOM)
c*************************************************************
c
c     This routine solves the system of equations
c     by the explicit central difference method.
c
c*************************************************************
      implicit real*8(A-H,O-Z)
```

APPENDIX A. CODE OF PROGRAM BLKBEAM

```
      dimension SK(30,30),CL(30,30),EM(30,30),FG(30),ISP(5)
      dimension EFF(30),EFK(30),UD(30,4),UV(30),UA(30),CSUP(30)
c
c
c---  assemble terms in effective force matrix:
c
      do 74 I=1,NSOL
        EFF(I) = FG(I)
c
        if ( SK(I,I).eq.0.0 ) then
          EFF(I) = 0.0D0
          goto 73
        endif
c
        do 70 J=1,NSOL
         EFF(I) = EFF(I) - (SK(I,J)-2/(DT*DT)*EM(I,J))*UD(J,1) -
     $            ( 1/(DT*DT)*EM(I,J)-1/(2*DT)*CL(I,J) )*UD(J,2)
70      continue
73      continue
c        write(*,*)'eff(i) & DT',I,EFF(I),DT
74    continue
c
c---  assemble effective stiffness vector:
      do 75 I=1,NSOL
        EFK(I) = 1/(DT*DT)*EM(I,I) + 1/(2*DT)*CL(I,I)
75    continue
c
      do 90 I=1,NSOL
        UD(I,4) = UD(I,3)
        UD(I,3) = UD(I,2)
        UD(I,2) = UD(I,1)
90    continue
c
c---  calculate new displacements:
      do 80 I=1,NSOL
        if ( EFK(I).eq.0.0D0 ) then
          UD(I,1) = 0.0D0
          goto 888
        endif
        UD(I,1) = EFF(I)/EFK(I)
888     continue
80    continue
c
      if (ISP(3).eq.0) then
        UD(6,1) = UD(4,1)
      endif
c
c---  Calculate new velocities:
      do 82 I = 1,NSOL
        UV(I) = ( UD(I,1) - UD(I,3) ) / (2*DT)
82    continue
c
c---  Calculate new accelerations:
      do 83 I = 1,NSOL
        UA(I) = ( UD(I,1) - 2*UD(I,2) + UD(I,3) ) / (DT*DT)
83    continue
c
c---  Next time step:
      T = T + DT
c
      return
      end
```

APPENDIX A. CODE OF PROGRAM BLKBEAM

```
c************************************************************
c
      subroutine OUTPUT(UD,UV,UA,ZETA,AMP,ISP,UOM,T,TMAX,LUN,
     $ HERZ,U5MAX,U11MAX,ICRASH,U5STAT,U11STAT,BL,TEQ,HMIN,BLEND,
     $ U3STAT,U9STAT)
c************************************************************
c
c     This routine supplies the output.
c
c************************************************************
      implicit real*8(A-H,O-Z)
      dimension UD(30,4),UV(30),UA(30),ISP(5)
      dimension DMX(12),VMX(12),AMX(12)
      dimension DMAX(12),VMAX(12),AMAX(12)

c
      ICRASH = 0
c
c---  No output if increment will be recycled
      if (T.lt.TMAX) then
        if ( UD(10,1).gt.0.0 .or. UD(1,1).lt.0.0 .or.
     $       UD(4,1).gt.UD(6,1)  ) return
      endif
c
c
c
c
c---  OUTPUT TO FILE:
c
c
      ICOUNT = 0
      if(ICOUNT.eq.13) then
        ICOUNT = 1
        write(*,1391)T,UOM,-UD(11,1),-UD(7,1),-UD(5,1),-UD(3,1)
1391    format(6F10.6)
      endif
c
      ICOUNT = ICOUNT + 1
c
c
c---  Check if beam has crashed:
      if ( (UD(11,1)+UOM).gt.1.2 ) then
        goto 200
      endif
c
      if ( (UD(5,1)+UOM).gt.1.2 ) then
        goto 200
      endif
c
c
c---  Determine max. displ. ,vel. & accel. of DOF(11)
      if ( T.le.(TEQ+0.05) ) goto 2222
        if ( DABS(UD(11,1)-U11STAT) .gt. DMAX(11) ) then
          DMAX(11)=DABS( UD(11,1)-U11STAT )
          DMX(11) = UD(11,1)
        endif
c
        if ( DABS(UV(11)) .gt. VMAX(11) ) then
          VMAX(11)=DABS( UV(11) )
          VMX(11) = UV(11)
        endif
c
```

```
        if ( DABS(UA(11)) .gt. AMAX(11) ) then
          AMAX(11)=DABS( UA(11) )
          AMX(11) = UA(11)
        endif
c
c---  Calculate the max. kinetic energy of centre block:
c---  Calculate average speed of block:
      VAV = ( UV(11)+UV(9)+UV(7) ) / 3.00
      EKIN = 0.5 * (2700*BLEND) * VAV**2
      if ( EKIN.gt.EKINMAX ) then
        EKINMAX = EKIN
        TEKINMAX = T
      endif
c
c
c
2222  continue
c
c---  UMAX1 is the max. deflection of the beam from its equilibrium
position.
      UMAX1 = UD(11,1) - U11STAT
      if ( DABS(UMAX1).gt.U11MAX ) then
         U11MAX = DABS(UMAX1)
         TDUMAX = T
      endif
c
c
      if ( T.le.(TEQ) ) goto 1011
c
c---  Determine the absolute min displacement:
      if (UD(11,1).gt.UMIN) UMIN = UD(11,1)
c
c---  Determine the max relative displacement
      UUDD=UD(11,1)-U11STAT
      if ( DABS(UUDD-(-UOM)).gt.URLMAX ) URLMAX=DABS(UUDD+UOM)
c
      PI = 3.141592654
      UVSP = 2*PI*HMIN * URLMAX
      UASP = (2*PI*HMIN)**2 * URLMAX
c
c
c---  Calculate shear force at centre shear fracture:
      DY = UD(7,1) - UD(5,1)
      SHFORCE = 70.0D9 * DY
      if (T.le.TEQ) SHFEQ = SHFORCE
c
c---  Calculate largest shear force during earthquake:
      if (T.gt.TEQ) then
        if ( DABS(SHFORCE).gt.DABS(SHMAX) ) then
          SHMAX = SHFORCE
          SHT = T
        endif
      endif
c
c
c
c---  Calculate max. relative deflection at UD(11,1) & UD(5,1) & UD(3,1)
c
c---  Relative displacement form gravity loaded position:
      U11EQ = UD(11,1) - U11STAT
      if ( U11EQ.gt.0.0 ) then
        if ( (U11EQ-(-UOM)) .gt. UD11MAX ) UD11MAX = U11EQ-(-UOM)
```

```
      endif
      if ( DABS(U11EQ-(-UOM)) .gt. U11ABSM ) then
        U11ABSM = DABS(U11EQ-(-UOM))
        UD11MIN = U11EQ-(-UOM)
      endif
c
c---  Relative displacement form gravity loaded position:
      U5EQ = UD(5,1) - U5STAT
      if ( U5EQ.gt.0.0 ) then
        if ( (U5EQ-(-UOM)) .gt. UD5MAX ) UD5MAX = U5EQ-(-UOM)
      endif
      if ( DABS(U5EQ-(-UOM)) .gt. U5ABSM ) then
        U5ABSM = DABS(U5EQ-(-UOM))
        UD5MIN = U5EQ-(-UOM)
      endif
c
c---  Relative displacement form gravity loaded position:
      U3EQ = UD(3,1) - U3STAT
      if ( U3EQ.gt.0.0 ) then
        if ( (U3EQ-(-UOM)) .gt. UD3MAX ) UD3MAX = U3EQ-(-UOM)
      endif
      if ( DABS(U3EQ-(-UOM)) .gt. U3ABSM ) then
        U3ABSM = DABS(U3EQ-(-UOM))
        UD3MIN = U3EQ-(-UOM)
      endif
c
c
c
1011  continue
c
c---  check if analysis complete
      if (T.lt.TMAX) return
c
200   continue
c
      SHT = SHT - TEQ
      TEKINMAX = TEKINMAX - TEQ
c
      open(LUN,access='SEQUENTIAL',status='UNKNOWN')
      do 133 I = 1,100000
133     read(LUN,*,END=1505)
1505  continue
      if (T.lt.TMAX) write(LUN,*)'Beam crashed!!'
      if (T.ge.TMAX) write(LUN,*)'Analysis complete'
c
      write(LUN,1085)U11MAX,TDUMAX-TEQ,ZETA,U11STAT,BL
1085  format(1X,5HUMAX=,F7.5,2X,6HTUMAX=,F6.3,2X,5HZETA=,F4.2,2X,
     $       8HU11STAT=,F7.5,1X,3HBL=,F5.2)
c
      write(LUN,1091)DMX(11),VMX(11),AMX(11),TEQ,UMIN
1091  format(1X,6HDMX11=,F7.5,1X,6HVMX11=,F10.5,1X,6HAMX11=,F12.5,
     $       1X,5HTEQ=,F7.4,1X,5HUMIN=,F6.4)
      write(LUN,*)'max rel DISPL.=',URLMAX
      write(LUN,*)'spectral vel.=',UVSP
      write(LUN,*)'spectral accel.=',UASP
      write(LUN,*)'s/force at equil=',SHFEQ
c      write(LUN,*)'max. shear force & time=',SHMAX,SHT
c      write(LUN,*)'max. kinetic energy & time=',EKINMAX,TEKINMAX
      write(LUN,5558)U11STAT,U9STAT,U5STAT,U3STAT
      write(LUN,5555)UD11MIN,UD11MAX,(UD11MAX*HMIN*2*PI)
      write(LUN,5556)UD5MIN,UD5MAX,(UD5MAX*HMIN*2*PI)
      write(LUN,5557)UD3MIN,UD3MAX,(UD3MAX*HMIN*2*PI)
```

APPENDIX A. CODE OF PROGRAM BLKBEAM

```
      write(LUN,*)'***********************************'
c
5555  format(1X,11HN11 MrelUD=,F11.8,1X,8HPOSrelU=,F11.8,1X,2HV=,F9.6)
5556  format(1X,11HN 5 MrelUD=,F11.8,1X,8HPOSrelU=,F11.8,1X,2HV=,F9.6)
5557  format(1X,11HN 3 MrelUD=,F11.8,1X,8HPOSrelU=,F11.8,1X,2HV=,F9.6)
5558  format(1X,8HU11STAT=,F10.6,1X,7HU9STAT=,F10.6,1X,7HU5STAT=,
     $       F9.6,1X,7HU3STAT=,F9.6)
      close(LUN)
c
c
c        write(LUN,1085)UMAX1,TDUMAX,ZETA,AMP,HERZ,TRANS1,TRANS2
c1085    format(1X,4HUMX=,F7.5,1X,5HTUMX=,F6.3,1X,3HZT=,F4.2,1X,
c     $         4HAMP=,F7.5,1X,5HHERZ=,F8.5,1X,6HTR1/2=,F6.2,1X,F6.2)
c
c         write(LUN,1091)DMX(9),VMX(9),AMX(9)
c1091     format(1X,5HDMX9=,F7.5,2X,5HVMX9=,F10.5,2X,5HAMX9=,F12.5)
c         write(LUN,*)
c      close(LUN)
c
c
c---  Reset variables:
      COUNT = 1
      ICRASH = 1
      U5MAX = 0.0
      U11MAX = 0.0
c
      U11ABSM = 0.0
      U5ABSM = 0.0
      U3ABSM = 0.0
c
      UD11MAX = 0.0
      UD11MIN = 0.0
      UD5MAX = 0.0
      UD5MIN = 0.0
      UD3MAX = 0.0
      UD3MIN = 0.0
c
      UMIN = 0.0
      URLMAX = 0.0
      TDUMAX = 0.0
      SHMAX = 0.0
      EKINMAX = 0.0
      DMAX(11) = 0.0
      VMAX(11) = 0.0
      AMAX(11) = 0.0
c
c
      return
      end
c
c**************************************************************************
      SUBROUTINE CONDES(ND,NCR,SK,SM,SC,T,GGKK)
c**************************************************************************
c
c     Static condensation routine - developed by Paz.
c
c**************************************************************************
      IMPLICIT REAL*8(A-H,O-Z)
      DIMENSION SK(30,30),SM(30,30),T(30,30),TT(30),SC(30,30)
      DIMENSION GGKK(30,30)
c
c
```

APPENDIX A. CODE OF PROGRAM BLKBEAM

```
c---  Calculate the reduced stiffness matrix and the transformation
matrix:
c
c
c
      NL = ND-NCR
      DO 9 K=1,NCR
      IF (DABS(SK(K,K)).GT.1.D-10) GOTO5
      WRITE (6,202) K
202   FORMAT ('                          PIVOT TOO SMALL',I10)
      GOTO 99
5     KP1 = K+1
      DO 6 J=KP1,ND
6     SK(K,J) = SK(K,J)/SK(K,K)
      SK(K,K) = 1.
      DO 9 I=1,ND
      IF (I.EQ.K.OR.SK(I,K).EQ.0) GOTO 9
      DO 8 J=KP1,ND
8     SK(I,J) = SK(I,J) - SK(I,K) * SK(K,J)
      SK(I,K) = 0.0
9     CONTINUE
      DO 30 I = 1,NCR
      DO 30 J = 1,NL
      JJ = J+NCR
30    T(I,J) = -SK(I,JJ)
      DO 40 I=1,NL
      II = I+NCR
      DO 50 J = 1,NL
50    T(II,J) = 0.0
      T(II,I) = 1.0
40    CONTINUE
      DO 20 I = 1,NL
      DO 20 J = 1,NL
      II = I + NCR
      JJ = J + NCR
20    SK(I,J) = SK(II,JJ)
c      WRITE(6,169)
c169   FORMAT(1HO,5X,'THE REDUCED STIFFNESS MATRIX IS'/)
c      DO 80 I = 1,NL
c80    WRITE(6,190) (SK(I,J),J=1,NL)
c      WRITE(6,170)
c170   FORMAT(/6X,'THE TRANSFORMATION MATRIX IS'/)
c      DO 81 I = 1,ND
c81    WRITE(6,190) (T(I,J),J = 1,NL)
c190   FORMAT (6E14.6)
c
c
      do 300 I = 1,NL
        do 300 J = 1,NL
        GGKK(I,J) = SK(I,J)
300   continue
c
c
99    return
      end
c*************************************************************************
      SUBROUTINE JACOBI(A,B,X,EIGV,D,N,IFPR,HERZ,LUN)
c*************************************************************************
c
c      Eigen value and vector extraction routine - developed by Bathe.
c
c*************************************************************************
```

APPENDIX A. CODE OF PROGRAM BLKBEAM

```
      IMPLICIT REAL*8(A-H,O-Z)
c     ABS(X) = DABS(X)
c     SQRT(X) = DSQRT(X)
      DIMENSION A(30,30),B(30,30),X(30,30),EIGV(30),D(30),HERZ(30)
c
c
      IOUT=6
      RTOL = 1.D-12
      NSMAX=15
c---  Initialise matrices:
      do 10 I = 1,N
      IF(A(I,I).GT.0. .AND. B(I,I).GT.0.)GOTO 4
      WRITE(IOUT,2020)
      STOP
4     D(I) = A(I,I)/B(I,I)
10    EIGV(I) = D(I)
      DO 30 I = 1,N
      DO 20 J = 1,N
20    X(I,J) = 0.0
30    X(I,I) = 1.0
      IF (N.EQ.1) RETURN
c
c---  Initialize sweep counter
      NSWEEP = 0
      NR = N-1
40    NSWEEP = NSWEEP + 1
      IF (IFPR.EQ.1)WRITE(IOUT,2000)NSWEEP
c
c---  Check if off-diagonal element is large
c
      EPS = (0.01**NSWEEP)**2
      DO 210 J = 1,NR
      JJ = J+1
      DO 210 K = JJ,N
      EPTOLA = (A(J,K)*A(J,K))/(A(J,J)*A(K,K))
      EPTOLB = (B(J,K)*B(J,K))/(B(J,J)*B(K,K))
      IF ((EPTOLA.LT.EPS).AND.(EPTOLB.LT.EPS)) GOTO 210
c
c---  If zeroing is required, calculate the rotation matrix:
      AKK=A(K,K)*B(J,K)-B(K,K)*A(J,K)
      AJJ=A(J,J)*B(J,K)-B(J,J)*A(J,K)
      AB=A(J,J)*B(K,K)-A(K,K)*B(J,J)
      CHECK=(AB*AB+4.*AKK*AJJ)/4.
      IF (CHECK)50,60,60
50    WRITE(IOUT,2020)
      stop
60    SQCH=DSQRT(CHECK)
      D1=AB/2.+SQCH
      D2=AB/2.-SQCH
      DEN=D1
      IF (DABS(D2).GT.DABS(D1))DEN=D2
      IF(DEN)80,70,80
70    CA=0.
      CG=-A(J,K)/A(K,K)
      GOTO 90
80    CA=AKK/DEN
      CG=-AJJ/DEN
c
c---  Generalized rotation to zero the present off-diagonal element
90    IF(N-2)100,190,100
100   JP1 = J+1
      JM1 = J - 1
```

```
      KP1 = K+1
      KM1 = K-1
      IF(JM1-1)130,110,110
110   DO 120 I = 1,JM1
      AJ=A(I,J)
      BJ=B(I,J)
      AK=A(I,K)
      BK=B(I,K)
      A(I,J)=AJ+CG*AK
      B(I,J)=BJ+CG*BK
      A(I,K)=AK+CA*AJ
120   B(I,K)=BK+CA*BJ
130   IF (KP1-N)140,140,160
140   DO 150 I = KP1,N
      AJ=A(J,I)
      BJ=B(J,I)
      AK=A(K,I)
      BK=B(K,I)
      A(J,I)=AJ+CG*AK
      B(J,I)=BJ+CG*BK
      A(K,I)=AK+CA*AJ
150   B(K,I)=BK+CA*BJ
160   IF (JP1-KM1)170,170,190
170   DO 180 I = JP1,KM1
      AJ=A(J,I)
      BJ=B(J,I)
      AK=A(I,K)
      BK=B(I,K)
      A(J,I) = AJ+CG*AK
      B(J,I) = BJ + CG*BK
      A(I,K) = AK+CA*AJ
180   B(I,K) = BK+CA*BJ
190   AK=A(K,K)
      BK=B(K,K)
      A(K,K) = AK+2.*CA*A(J,K)+CA*CA*A(J,J)
      B(K,K) = BK+2.*CA*B(J,K)+CA*CA*B(J,J)
      A(J,J) = A(J,J)+2.*CG*A(J,K)+CG*CG*AK
      B(J,J) = B(J,J)+2.*CG*B(J,K)+CG*CG*BK
      A(J,K) = 0.
      B(J,K) = 0.
c
c---  Update the eigenvector matrix:
      DO 200 I = 1,N
      XJ = X(I,J)
      XK = X(I,K)
      X(I,J) = XJ+CG*XK
200   X(I,K) = XK+CA*XJ
210   continue
c
c---  Update the eigenvalues
      DO 220 I = 1,N
      IF (A(I,I).GT.0. .AND. B(I,I).GT.0.) GOTO 220
      WRITE(IOUT,2020)
      STOP
220   EIGV(I) = A(I,I)/B(I,I)
      IF (IFPR.EQ.0) GOTO 230
      WRITE(IOUT,2030)
      WRITE(IOUT,2010) (EIGV(I),I=1,N)
c
c---  Check for convergence:
230   DO 240 I = 1,N
      TOL = RTOL*D(I)
```

```
      DIF = DABS(EIGV(I) - D(I))
      IF (DIF.GT.TOL) GOTO 280
240   CONTINUE
c
c---  Check off-diagonal terms to see if another sweep is required:
      EPS = RTOL**2
      DO 250 J = 1,NR
      JJ = J+1
      DO 250 K = JJ,N
      EPSA=(A(J,K)*A(J,K))/(A(J,J)*A(K,K))
      EPSB=(B(J,K)*B(J,K))/(B(J,J)*B(K,K))
      IF ((EPSA.LT.EPS).AND.(EPSB.LT.EPS)) GOTO 250
      GOTO 280
250   CONTINUE
c
c---  Fill out bottom triangle of resultant matrices:
255   DO 260 I = 1,N
      DO 260 K = 1,N
      A(J,I) = A(I,J)
260   B(J,I) = B(I,J)
      DO 270 J = 1,N
      BB = DSQRT(B(J,J))
      DO 270 K = 1,N
270   X(K,J) = X(K,J)/BB
      DO 400 I = 1,N
400   HERZ(I) = DSQRT(EIGV(I))/(2*3.141593)
c     RETURN
c
c---  Update matrix and start new sweep:
c      WRITE(6,1990)
      DO 1991 LI = 1,N
c1991  WRITE(6,2010) (X(LI,LJ),LJ=1,N)
1991  write(*,*)
1990  FORMAT(/10X,'EIGENVECTORS',/)
c      WRITE(6,*)
c      WRITE(LUN,2040) NSWEEP
c      WRITE(LUN,2010) (HERZ(I),I=1,N)
      RETURN
280   DO 290 I = 1,N
290   D(I)=EIGV(I)
      IF (NSWEEP.LT.NSMAX) GOTO 40
      GOTO 255
2000  FORMAT(/,    ' SWEEP=',I2)
2010  FORMAT(1H ,5X,6F14.3/)
2020  FORMAT (25HO***ERROR SOLUTION STOP   /)
c    1        30H MATRICES NOT POSITIVE DEFINITE   )
2030  FORMAT(25H CURRENT EIGENVALUES ARE:/)
2040  FORMAT(45H CONVERGED NATURAL FREQUENCIES :   Sweep no.:,I2)
      END
c*************************************************
```

Appendix B

Courses Completed

APPENDIX B. COURSES COMPLETED

Courses completed in partial fulfilment of the M. Sc. degree:

Course		Date	Credits
CAM500Z	Applied Mechanics A	1991	3
CAM501Z	Applied Mechanics B	1991	3
CAM502Z	An Introduction to Finite Elements	1991	3
CAM503Z	Finite Element Analysis	1991	4
CAM504Z	Engineering Software Design and Development	1991	3
CIV504S	Structural Dynamics	1991	3
MAT402F	Materials Selection and Failure Analysis	1991	3

Course Credits: 22
Thesis Credits: 20
Total: 42

Minimum credit requirement for the M.Sc. degree: 40 credits